



HAL
open science

Fast Marching methods for Curvature Penalized Shortest Paths

Jean-Marie Mirebeau

► **To cite this version:**

Jean-Marie Mirebeau. Fast Marching methods for Curvature Penalized Shortest Paths. 2017. hal-01538482v1

HAL Id: hal-01538482

<https://hal.science/hal-01538482v1>

Preprint submitted on 13 Jun 2017 (v1), last revised 9 Nov 2017 (v3)

HAL is a multi-disciplinary open access archive for the deposit and dissemination of scientific research documents, whether they are published or not. The documents may come from teaching and research institutions in France or abroad, or from public or private research centers.

L'archive ouverte pluridisciplinaire **HAL**, est destinée au dépôt et à la diffusion de documents scientifiques de niveau recherche, publiés ou non, émanant des établissements d'enseignement et de recherche français ou étrangers, des laboratoires publics ou privés.

Fast Marching methods for Curvature Penalized Shortest Paths

Jean-Marie Mirebeau*

June 13, 2017

Abstract

We introduce numerical schemes for computing distances and shortest paths with respect to several planar paths models, featuring curvature penalization and data-driven velocity: the Dubins car, the Euler/Mumford elastica, and a two variants of the Reeds-Shepp car. For that purpose, we design monotone and causal discretizations of the associated Hamilton-Jacobi-Bellman PDEs, posed on the three dimensional domain $\mathbb{R}^2 \times \mathbb{S}^1$. Our discretizations involves sparse, adaptive and anisotropic stencils on a cartesian grid, built using techniques from lattice geometry. A convergence proof is provided, in the setting of discontinuous viscosity solutions. The discretized problems are solvable in a single pass using a variant of the Fast-Marching algorithm. Numerical experiments illustrate applications of our schemes in motion planning and image segmentation.

1 Introduction

In this paper, we develop numerical schemes for computing distance maps and globally minimal paths with respect to data driven costs depending on the local path position, orientation, and curvature. We address a variety of models including two variants of the Reeds-Shepp car [RS90, DMMP16], the Euler-Mumford elastica [Eul44, CMC16], and the Dubins car [Dub57]. Their qualitative features differ widely: depending on the model, minimal paths may or may not be smooth, and the associated distance may or may not be continuous. For that purpose, we discretize generalized eikonal equations, also called first order static Hamilton-Jacobi-Bellman PDEs, with a unified approach relying on a common tool from lattice geometry, also considered in [Mir17]. Our discretizations are monotone and causal, hence can be solved using the fast marching algorithm/dynamic programming principle, with complexity $\mathcal{O}(N \ln N)$ complexity where N is the number of points in the discrete domain. Applications to motion planning control problems and medical image segmentation tasks are in the works, see §5 and [MD17].

In the models of interest to us, the cost of a smooth path $\mathbf{x} : [0, T] \rightarrow \mathbb{R}^2$, parametrized at unit speed, takes the form

$$\int_0^T \alpha(\mathbf{x}(s), \dot{\mathbf{x}}(s)) \mathcal{C}(|\ddot{\mathbf{x}}(s)|) ds. \quad (1)$$

Our objective is to numerically compute globally minimal paths, given a source and target point and orientation, and regarding the control time T as a free parameter. We denoted by $\alpha : \mathbb{R}^2 \times \mathbb{S}^1 \rightarrow]0, \infty]$ a continuous cost function, depending on the path position and orientation,

*University Paris-Sud, CNRS, University Paris-Saclay, 91405, Orsay, France
This work was partly supported by ANR research grant MAGA, ANR-16-CE40-0014

usually data driven in applications. The path curvature $|\ddot{\mathbf{x}}(s)|$ is penalized using a second cost function $\mathcal{C} : \mathbb{R} \rightarrow \mathbb{R}_+$, for which we consider the three following instantiations

$$\mathcal{C}^{\text{RS}}(\kappa) := \sqrt{1 + |\xi\kappa|^2}, \quad \mathcal{C}^{\text{EM}}(\kappa) := 1 + |\xi\kappa|^2, \quad \mathcal{C}^{\text{D}}(\kappa) := \begin{cases} 1 & \text{if } |\xi\kappa| \leq 1, \\ +\infty & \text{otherwise.} \end{cases} \quad (2)$$

The costs \mathcal{C}^{RS} , \mathcal{C}^{EM} and \mathcal{C}^{D} correspond respectively to the Reeds-Shepp car, the Euler-Mumford elastica, and the Dubins car models. The parameter $\xi > 0$ has the dimension of a length and should be interpreted as a typical radius of curvature. Our approach easily extends to models where $\xi : \mathbb{R}^2 \times \mathbb{S}^1 \rightarrow]0, \infty[$ is a continuous positive function of the path position and orientation, similarly to the cost α . The Reeds-Shepp car (with or without reverse gear), the Euler-Mumford elastica and the Dubins car are classical path models involving increasingly strong penalizations of curvature. Their qualitative properties are strikingly distinct, as illustrated on Figure 1 and discussed below.

- The Reeds-Shepp cost $\mathcal{C}^{\text{RS}}(\kappa) = \sqrt{1 + |\xi\kappa|^2}$ is used to model slow vehicles, typically wheelchairs. Following [DMMP16] we consider the two models based on this cost, referred to as the *Reeds-Shepp reversible* (RS \pm , as originally considered in [RS90]) and *Reeds-Shepp forward* (RS+) models, and where the vehicle respectively may, or may not, shift into reverse gear. Minimal paths for the reversible and forward models distinguish themselves by the presence of *cusps* and of *in place rotations* of the path orientation, respectively, see Figure 1. The latter happen at the path endpoints and sometimes at the corners of obstacles, and are admissible since the curvature cost \mathcal{C}^{RS} only grows linearly asymptotically. See [DMMP16] for a discussion and the description of a semi-lagrangian PDE discretization of the Reeds-Shepp models, which is different from the one considered in this paper¹.
- The Euler-Mumford cost $\mathcal{C}^{\text{EM}} = 1 + |\xi\kappa|^2$ has the physical interpretation, when the data driven cost is identically constant $\alpha \equiv 1$ and the final time T is fixed, of the bending energy of an elastic bar [Eul44]. The relevance of this model for image processing and segmentation was first outlined in [Mum94]. Contrary to earlier works of the author [CMC15], the PDE discretization introduced in this paper for this model obeys a causality property which makes the Fast-Marching algorithm applicable.
- The Dubins cost \mathcal{C}^{D} penalizes euclidean path length, unless curvature exceeds the threshold ξ^{-1} , in which case the path is rejected, see (2). Minimal (relaxed) paths for this cost are known, when $\alpha \equiv 1$, to be concatenations of straight lines and of circular segments of radius ξ^{-1} . This description is used in [BCL94] to design exact polynomial time solvers for the minimal Dubins path problem, in the presence of smooth obstacles. In contrast, our PDE approach is approximate by nature, but it can accommodate non-constant costs α , and can easily be extended to variants of the model involving e.g. position dependent bounds on the radius of curvature or additional state variables.

In order to describe our numerical methods, we need to introduce some notations. Our implementation of curvature penalization requires to lift paths into the configuration space $\mathbb{M} := \mathbb{R}^2 \times \mathbb{S}^1$ of positions and orientations. Other strategies were previously proposed in the literature, see Remark 1.2. In the following, we use the identification $\mathbb{S}^1 \cong \mathbb{R}/(2\pi\mathbb{Z})$, and denote

¹The Reeds-Shepp models are in this paper mostly discussed for comparison with the Euler-Mumford and Dubins models, since our numerical results in the Reeds-Shepp case are actually quite similar to [DMMP16], despite the distinct discretization.

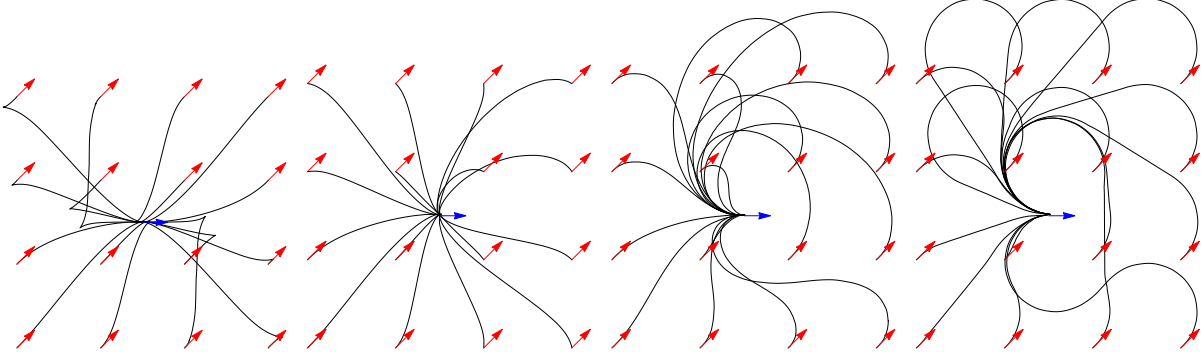


Figure 1: Globally minimal paths for the Reeds-Shepp reversible model ($\xi = 0.3$), Reeds-Shepp forward model ($\xi = 0.3$), Euler-Mumford elastica model ($\xi = 0.2$), and Dubins model ($\xi = 0.2$), with uniform cost $\alpha \equiv 1$. Seed point $(1/2, 1/2, 0) \in \mathbb{R}^2 \times \mathbb{S}^1$, tip points $(k/3, l/3, \pi/4)$, $k, l \in \{0, \dots, 3\}$. (Discretization parameters: $\varepsilon = 0.1$, angular resolution $2\pi/60$.)

points of the configuration space by $\mathbf{p} = (\mathbf{x}, \theta) \in \mathbb{M}$. The tangent space to $\mathbb{M} := \mathbb{R}^2 \times \mathbb{S}^1$ is independent of the base point, and denoted $\mathbb{E} := \mathbb{R}^2 \times \mathbb{R}$. Vectors are denoted $\dot{\mathbf{p}} = (\dot{\mathbf{x}}, \dot{\theta}) \in \mathbb{E}$, and co-vectors $\hat{\mathbf{p}} = (\hat{\mathbf{x}}, \hat{\theta}) \in \mathbb{E}^*$. The unit vector of orientation $\theta \in \mathbb{S}^1$ is denoted $\mathbf{n}(\theta) := (\cos \theta, \sin \theta)$.

A (local) metric on \mathbb{M} is a function $\mathcal{F} : \mathbb{M} \times \mathbb{E} \rightarrow [0, \infty]$, which is convex and 1-homogeneous in its second argument. The cost functions $\mathcal{C} = \mathcal{C}^{\text{RS}}, \mathcal{C}^{\text{EM}}, \mathcal{C}^{\text{D}}$ define three metrics $\mathcal{F} = \mathcal{F}^{\text{RS}+}, \mathcal{F}^{\text{EM}}, \mathcal{F}^{\text{D}}$ by homogenization as follows: for all $\mathbf{p} = (\mathbf{x}, \theta) \in \mathbb{M}$ and all $\dot{\mathbf{p}} = (\dot{\mathbf{x}}, \dot{\theta}) \in \mathbb{E}$

$$\mathcal{F}_{\mathbf{p}}(\dot{\mathbf{p}}) = \begin{cases} \|\dot{\mathbf{x}}\| \mathcal{C}(|\dot{\theta}|/\|\dot{\mathbf{x}}\|) & \text{if } \dot{\mathbf{x}} = \|\dot{\mathbf{x}}\| \mathbf{n}(\theta), \\ +\infty & \text{otherwise.} \end{cases} \quad (3)$$

with the additional convention that $\mathcal{F}_{\mathbf{p}}(0) = 0$. A fourth metric $\mathcal{F}^{\text{RS}\pm}$, corresponding to the Reeds-Shepp model *with* reverse gear, is defined like $\mathcal{F}^{\text{RS}+}$ up to the constraint which is replaced with the unsigned collinearity requirement $\dot{\mathbf{x}} = \langle \dot{\mathbf{x}}, \mathbf{n}(\theta) \rangle \mathbf{n}(\theta)$. We prove in §B that (3) does indeed define a convex lower semi-continuous function w.r.t. $\dot{\mathbf{p}}$, as this it is not entirely obvious from the definition.

The length of a Lipschitz path $\gamma : [0, 1] \rightarrow \mathbb{R}^2 \times \mathbb{S}^1$, w.r.t. a metric \mathcal{F} , is defined as

$$\text{length}_{\mathcal{F}}(\gamma) := \int_0^1 \alpha(\gamma(t)) \mathcal{F}_{\gamma(t)}(\dot{\gamma}(t)) dt, \quad (4)$$

where $\alpha : \mathbb{M} \rightarrow]0, \infty[$ is a continuous cost function, previously mentioned and fixed throughout this paper. A *bounded* domain $\Omega \subseteq \mathbb{M}$ is fixed throughout the paper, and to each (local) metric \mathcal{F} is associated a pseudo-distance $d_{\mathcal{F}}$ defined for all $\mathbf{p}, \mathbf{q} \in \bar{\Omega}$ by

$$d_{\mathcal{F}}(\mathbf{p}, \mathbf{q}) := \inf \{ \text{length}_{\mathcal{F}}(\gamma); \gamma \in \text{Lip}([0, 1], \bar{\Omega}), \gamma(0) = \mathbf{p}, \gamma(1) = \mathbf{q} \}. \quad (5)$$

Note that one may have $d_{\mathcal{F}}(\mathbf{p}, \mathbf{q}) \neq d_{\mathcal{F}}(\mathbf{q}, \mathbf{p})$, or $d_{\mathcal{F}}(\mathbf{p}, \mathbf{q}) = \infty$. For the metrics $\mathcal{F}^{\text{RS}+}, \mathcal{F}^{\text{RS}\pm}, \mathcal{F}^{\text{EM}}$ and \mathcal{F}^{D} considered in this paper, the infimum (5) is attained whenever $d_{\mathcal{F}}(\mathbf{p}, \mathbf{q}) < \infty$, see Appendix A of [CMC15] or Appendix A of [DMMP16]. The objective of this paper is to numerically solve the following optimal control problem: find the shortest path from the domain boundary $\partial\Omega$ to any point in Ω . The value function $u : \bar{\Omega} \rightarrow [0, \infty]$ for this problem reads for all $\mathbf{q} \in \bar{\Omega}$

$$u(\mathbf{q}) := \inf_{\mathbf{p} \in \partial\Omega} d_{\mathcal{F}}(\mathbf{p}, \mathbf{q}). \quad (6)$$

The function u associated to the Reeds-Shepp *reversible* metric is continuous, thanks to the sub-Riemannian nature of this model, which is thus locally controllable by Chow's theorem [Mon06]. In contrast, the function u can be discontinuous along $\partial\Omega$ for non locally controllable models, such as the Reeds-Shepp *forward*, Euler-Elastica and Dubins models. In fact, u may even be discontinuous in the interior of Ω , in the Dubins case, as well as in the Reeds-Shepp for some domain shapes, see Proposition 3.3. See Figure 14 page 42 for the level lines of u .

Despite its potential discontinuities, the function $u : \bar{\Omega} \rightarrow \mathbb{R}$ is a (discontinuous) viscosity solution to a generalized eikonal equation: for all $\mathbf{p} \in \Omega$

$$\mathcal{H}_{\mathbf{p}}(du(\mathbf{p})) = \frac{1}{2}\alpha(\mathbf{p})^2, \quad (7)$$

and $u(\mathbf{p}) = 0$ for all $\mathbf{p} \in \partial\Omega$. See [BCD97] and §3.2 for details, including the appropriate relaxation of the boundary conditions. This PDE involves the Hamiltonian $\mathcal{H} : \mathbb{M} \times \mathbb{E}^* \rightarrow [0, \infty[$ of the model, which is defined as the Legendre-Fenchel conjugate of the Lagrangian $\mathcal{L} : \mathbb{M} \times \mathbb{E} \rightarrow [0, \infty]$. For all $\mathbf{p} \in \mathbb{M}$ and $\hat{\mathbf{p}} \in \mathbb{E}^*$

$$\mathcal{H}_{\mathbf{p}}(\hat{\mathbf{p}}) := \sup_{\dot{\mathbf{p}} \in \mathbb{E}} \langle \hat{\mathbf{p}}, \dot{\mathbf{p}} \rangle - \mathcal{L}_{\mathbf{p}}(\dot{\mathbf{p}}), \quad \text{where } \mathcal{L}_{\mathbf{p}}(\dot{\mathbf{p}}) := \frac{1}{2}\mathcal{F}_{\mathbf{p}}(\dot{\mathbf{p}})^2. \quad (8)$$

The explicit expressions of the hamiltonians $\mathcal{H}^{\text{RS}\pm}$, $\mathcal{H}^{\text{RS}+}$, \mathcal{H}^{EM} and \mathcal{H}^{D} associated to the models of interest are provided in §2, where we also provide monotone and causal discretizations of the Hamilton-Jacobi-Bellman PDE (7). Our PDE discretizations rely on small, sparse and strongly anisotropic stencils, see Figure 3. They are designed using the following result, which proof relies on Voronoi's first reduction, a tool from discrete geometry characterizing the interaction of a positive quadratic form with an additive lattice [Sch09]. Similar techniques are used for anisotropic diffusion PDEs in [FM13], for Monge-Ampere equations in [Mir16], and for eikonal PDEs associated to Riemannian, sub-Riemannian and Rander metrics in [Mir17].

The next proposition, proved in §4, shows how the positive part of a linear form $\hat{\mathbf{p}} \mapsto \langle \hat{\mathbf{p}}, \dot{\mathbf{n}} \rangle_+$ can be approximated using positive parts of linear forms $\hat{\mathbf{p}} \mapsto \langle \hat{\mathbf{p}}, \dot{\mathbf{e}} \rangle_+$ associated to *integral* vectors $\dot{\mathbf{e}} \in \mathbb{Z}^d$. Here and in the rest of this paper, we denote $a_+ := \max\{a, 0\}$ and $a_- := \max\{-a, 0\}$, for any $a \in \mathbb{R}$. This result allows in our numerical schemes to approximate the directional derivative $\langle du(\mathbf{p}), \dot{\mathbf{n}} \rangle_+$ at a point $\mathbf{p} \in \mathbb{M}$ using finite differences of the form $\frac{1}{h}(u(\mathbf{p}) - u(\mathbf{p} - h\dot{\mathbf{e}}))_+$, where $h > 0$ is the discretization grid scale.

Proposition 1.1. *Let $d \in \{2, 3\}$, let $\dot{\mathbf{n}} \in \mathbb{R}^d$, and let $\varepsilon \in]0, 1]$. Then there exists non-negative weights $\rho_{\dot{\mathbf{e}}}^\varepsilon(\dot{\mathbf{n}})$, $\dot{\mathbf{e}} \in \mathbb{Z}^d$, such that for all $\hat{\mathbf{p}} \in \mathbb{R}^d$*

$$\langle \hat{\mathbf{p}}, \dot{\mathbf{n}} \rangle_+^2 \leq \sum_{\dot{\mathbf{e}} \in \mathbb{Z}^d} \rho_{\dot{\mathbf{e}}}^\varepsilon(\dot{\mathbf{n}}) \langle \hat{\mathbf{p}}, \dot{\mathbf{e}} \rangle_+^2 \leq \langle \hat{\mathbf{p}}, \dot{\mathbf{n}} \rangle_+^2 + \varepsilon^2 \|\dot{\mathbf{n}}\|^2 \|\hat{\mathbf{p}}\|^2.$$

Furthermore the support $\{\dot{\mathbf{e}} \in \mathbb{Z}^d; \rho_{\dot{\mathbf{e}}}^\varepsilon(\dot{\mathbf{n}}) > 0\}$ has at most 3 elements in dimension $d = 2$ (resp. 6 elements in dimension $d = 3$), and is contained in a ball of radius $C_{\text{WS}}/\varepsilon$, where C_{WS} is an absolute constant. In addition $\sum_{\dot{\mathbf{e}} \in \mathbb{Z}^d} \rho_{\dot{\mathbf{e}}}^\varepsilon(\dot{\mathbf{n}}) \|\dot{\mathbf{e}}\|^2 = \|\dot{\mathbf{n}}\|^2(1 + (d-1)\varepsilon^2)$.

In practice, we usually choose the relaxation parameter $\varepsilon = 1/10$ and obtain a support which is 5 or 6 pixels wide, see Figure 3. Our numerical method thus belongs to the category of *Wide-Stencil* schemes (hence the subscript to the constant C_{WS}). Further details on the discretization of (7) using Proposition 1.1 are presented in §2.

Once the solution u to (7) is computed, minimal paths from $\partial\Omega$ to any given $\mathbf{q} \in \Omega$, are extracted as solutions to the following ODE (solved backwards in time)

$$\dot{\gamma}(t) = d\mathcal{H}_{\gamma(t)}(du(\gamma(t))), \quad (9)$$

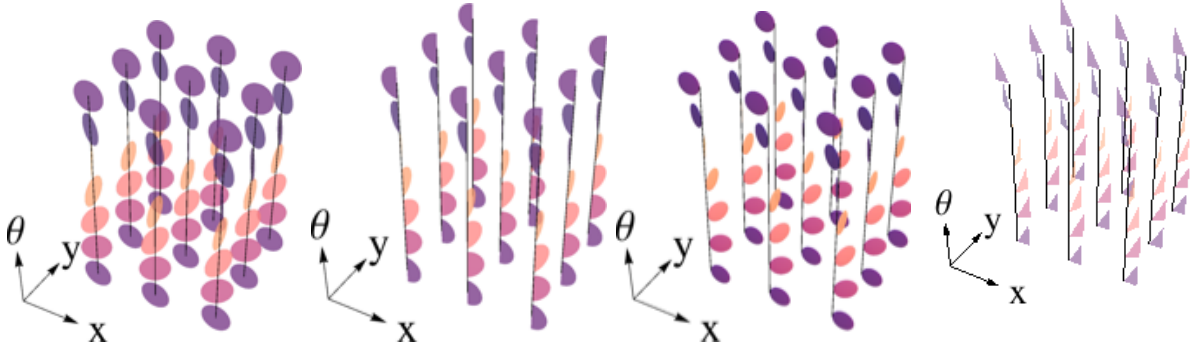


Figure 2: Control sets of The Reeds-Shepp reversible, Reeds-Shepp forward, Euler-Mumford and Dubins models. All have empty interior, reflecting the non-holonomy of the models.

where \mathcal{H} is differentiated w.r.t. the second variable $\hat{\mathbf{p}}$, see e.g. Appendix B of [DMMP16]. We end this introduction with the definition of an important geometrical object: the “unit balls” in each tangent space w.r.t. to the local metric, referred to as the *control sets*, see Figure 2. These sets, denoted $\mathcal{B}(\mathbf{p}) \subseteq \mathbb{E}$ where $\mathbf{p} \in \mathbb{M}$, provide geometric intuition as well as an elegant expression of the Hamiltonian (8)

$$\mathcal{B}(\mathbf{p}) := \{\hat{\mathbf{p}} \in \mathbb{E}; \mathcal{F}_{\mathbf{p}}(\hat{\mathbf{p}}) \leq 1\}, \quad \mathcal{H}_{\mathbf{p}}(\hat{\mathbf{p}}) = \frac{1}{2} \sup_{\hat{\mathbf{p}} \in \mathcal{B}(\mathbf{p})} \langle \hat{\mathbf{p}}, \hat{\mathbf{p}} \rangle_+^2. \quad (10)$$

Contributions and outline. In section §2 we introduce new discretizations of the generalized eikonal PDEs (7) associated to the hamiltonians of interest $\mathcal{H}^{\text{RS}\pm}$, $\mathcal{H}^{\text{RS}+}$, \mathcal{H}^{EM} and \mathcal{H}^{D} . For that purpose, we use an original reformulation of the Euler-Mumford hamiltonian. Our discretizations are monotone and causal, enabling the use of the single pass Fast-Marching algorithm, and rely on sparse and anisotropic stencils.

Section §3 is devoted to the convergence analysis, and our main results are stated in its introduction. We prove in §3.1 the discretized PDEs admit uniformly bounded solutions. We establish in §3.2 the convergence of the discrete solutions towards the value function u , defined by (6), at its points of continuity. We discuss in §3.3 the continuity properties of u , depending on the model and on the domain geometry.

Section §4 is devoted to the proof of Proposition 1.1, which is a key ingredient of our PDE discretization schemes. It is based on tools from lattice geometry such as Voronoi’s first reduction of quadratic forms, obtuse superbases of lattices, and Selling’s algorithm.

Numerical experiments presented in §5 illustrate the potential of our approach in motion planning and image segmentation tasks. We also compare, for validation, our minimal geodesics with those obtained with a shooting approach.

Remark 1.2 (Alternative approaches to curvature penalized shortest paths). *To the knowledge of the author, two alternative methods have been proposed to compute curvature penalized shortest paths via dynamic programming. Paths are approximated in [SUKG13] with collections of non-superposable short splines, each determined by three or four control points with integer coordinates, and the cost assigned to a path is the sum of the costs of the spline approximants. No convergence analysis is presented, and the numerical results do not address the models considered in this paper. The author remains doubtful that this method is appropriate for models which*

minimal paths feature singularities such as cusps (Reeds-Shepp reversible) or in place rotations (Reeds-Shepp forward), or are subject to a hard constraint on the radius of curvature (Dubins).

Another approach [LRr13] consists in using the original fast-marching scheme designed for euclidean distance computations [Tsi95], but with the following addition: each time a point is added to the propagated front, a local backtracing is performed to estimate the curvature of the geodesic reaching this point, and the front propagation cost is locally adjusted as a result. The method uses a two dimensional value map $u : \mathbb{R}^2 \rightarrow \mathbb{R}$, instead of the genuine three dimensional one $u : \mathbb{R}^2 \times \mathbb{S}^1 \rightarrow \mathbb{R}$, hence the physical projections of the paths extracted with this method never cross each other. This contradicts the observed behavior, see Figure 1, hence this approach cannot compute all curvature penalized minimal paths.

2 Discretization

In this section, we construct finite differences discretizations of the HJB PDEs (7) associated to the different models, which are *monotone* and *causal*, see Definition 2.1 below. For that purpose we derive the expression of the relevant hamiltonian, and construct an approximation of a specific form. The Reeds-Shepp, Euler-Mumford, and Dubins models are respectively addressed in §2.1, §2.2 and §2.3.

For that purpose, let us fix a grid scale $h > 0$ of the form $2\pi/k$ for some positive integer k , and introduce the grid $\mathbb{M}_h \subseteq \mathbb{M} := \mathbb{R}^2 \times \mathbb{S}^1$, discrete domain Ω_h , and formal discrete boundary $\partial\Omega_h$ defined by

$$\mathbb{M}_h := h\mathbb{Z}^2 \times (h\mathbb{Z}/2\pi\mathbb{Z}), \quad \Omega_h := \Omega \cap \mathbb{M}_h, \quad \partial\Omega_h := \mathbb{M}_h \setminus \Omega_h. \quad (11)$$

The properties of monotony and causality of a finite differences scheme are recalled in the next definition, in the sense of [Obe06] and [RT92] respectively. Monotony implies comparison principles, which are used in the convergence analysis §3. Causality allows to solve the discretized PDE in a single pass, which guarantees short computation times see §5.

Definition 2.1. A (finite differences) scheme on a finite set X is a continuous map $\mathfrak{F} : X \times \mathbb{R} \times \mathbb{R}^X \rightarrow \mathbb{R}$. The scheme is said:

- *Monotone*, iff \mathfrak{F} is non-decreasing w.r.t. the second and (each of the) third variables.
- *Causal*, iff \mathfrak{F} only depends on the positive part of the third variable.

To the scheme is associated a function $\mathbb{R}^X \rightarrow \mathbb{R}^X$ still (abusively) denoted by \mathfrak{F} , and defined by

$$(\mathfrak{F}U)(\mathbf{x}) := \mathfrak{F}(\mathbf{x}, U(\mathbf{x}), (U(\mathbf{x}) - U(\mathbf{y}))_{\mathbf{y} \in X}),$$

for all $\mathbf{x} \in X$, $U \in \mathbb{R}^X$.

2.1 The Reeds-Shepp car models

In the following, we describe the discretization of the Reeds-Shepp *forward* model, and postpone the discussion of the *reversible* model to Remark 2.6. The metric $\mathcal{F}^{\text{RS}+}$ of the Reeds-Shepp forward model is obtained by inserting the curvature cost expression $\mathcal{C}^{\text{RS}}(\kappa) := \sqrt{1 + \kappa^2}$ in the generic expression (3). Thus for all $\mathbf{p} = (\mathbf{x}, \theta) \in \mathbb{M}$ and all $\dot{\mathbf{p}} = (\dot{\mathbf{x}}, \dot{\theta}) \in \mathbb{E}$

$$\mathcal{F}_{\mathbf{p}}^{\text{RS}+}(\dot{\mathbf{p}}) = \sqrt{\|\dot{\mathbf{x}}\|^2 + |\xi\dot{\theta}|^2} \quad \text{if } \dot{\mathbf{x}} = \|\dot{\mathbf{x}}\|\mathbf{n}(\theta), \quad (12)$$

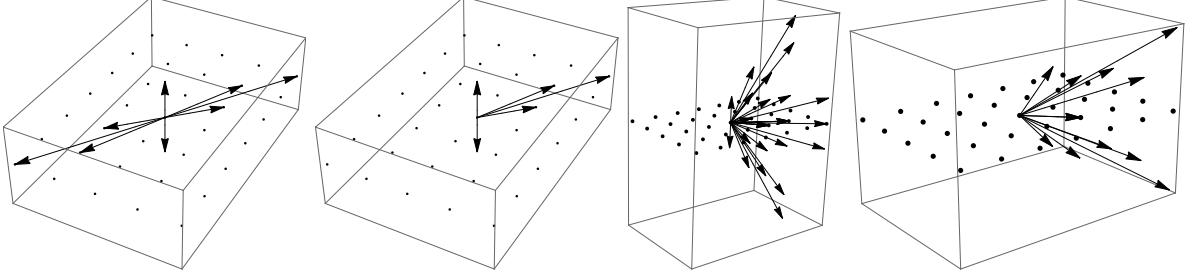


Figure 3: Discretization stencil of the Reeds-Shepp reversible, Reeds-Shepp forward, Euler-Mumford, and Dubins models. Note the sparseness and anisotropy of the stencils. Model parameters: $\theta = \pi/3$, $\xi = 0.2$. Discretization parameters: $\varepsilon = 0.1$, $K = 5$ for Euler-Mumford.

and $\mathcal{F}_{\mathbf{p}}^{\text{RS}+}(\mathbf{p}) = +\infty$ otherwise. The control set $\mathcal{B}^{\text{RS}+}(\mathbf{p})$ is defined as the unit ball of the metric $\mathcal{F}_{\mathbf{p}}^{\text{RS}+}$, for any $\mathbf{p} = (\mathbf{x}, \theta) \in \mathbb{M}$, see (10). Hence it is an half ellipse, or a half disk if $\xi = 1$, as illustrated on Figure 2.

$$\mathcal{B}^{\text{RS}+}(\mathbf{p}) = \{(\dot{\mathbf{x}}, \dot{\theta}) \in \mathbb{E}; \|\dot{\mathbf{x}}\|^2 + |\dot{\theta}|^2 \leq 1, \dot{\mathbf{x}} = \|\dot{\mathbf{x}}\|\mathbf{n}(\theta)\}.$$

The Lagrangian of the Reeds-Shepp model is defined as the half square of the metric (12). Hence denoting by $\mathbf{P}_{\mathbf{n}}(\dot{\mathbf{x}}) := \dot{\mathbf{x}} - \langle \mathbf{n}, \dot{\mathbf{x}} \rangle \mathbf{x}$ the component of a vector \mathbf{x} orthogonal to a direction \mathbf{n} , one has

$$2\mathcal{L}_{\mathbf{p}}^{\text{RS}+}(\dot{\mathbf{p}}) = (\langle \mathbf{n}(\theta), \dot{\mathbf{x}} \rangle_+^2 + \infty \langle \mathbf{n}(\theta), \dot{\mathbf{x}} \rangle_-^2) + \infty \|\mathbf{P}_{\mathbf{n}(\theta)}(\dot{\mathbf{x}})\|^2 + |\dot{\theta}|^2,$$

where, slightly abusively, we use infinite coefficients with the convention $0 \times \infty = 0$. The hamiltonian, also presented in [DMMP16], reads for all $\mathbf{p} = (\mathbf{x}, \theta) \in \overline{\Omega}$, and all $\hat{\mathbf{p}} = (\hat{\mathbf{x}}, \hat{\theta}) \in \mathbb{E}^*$

$$2\mathcal{H}_{\mathbf{p}}^{\text{RS}+}(\hat{\mathbf{p}}) = \langle \hat{\mathbf{x}}, \mathbf{n}(\theta) \rangle_+^2 + |\hat{\theta}/\xi|^2. \quad (13)$$

This expression follows from the piecewise quadratic and separable structure of the Lagrangian, and from two basic lemmas on the Legendre-Fenchel dual f^* of a function f , which are recalled below without proof.

Lemma 2.2 (Legendre-Fenchel dual of a separable sum). *Let $(\mathbf{e}_1, \dots, \mathbf{e}_d)$ be an orthogonal basis of \mathbb{R}^d , and let $f_1, \dots, f_d : \mathbb{R} \rightarrow \mathbb{R}$ be proper, convex and lower semi-continuous. Then*

$$\forall \mathbf{x} \in \mathbb{R}^d, f(\mathbf{x}) := \sum_{1 \leq i \leq d} f_i(\langle \mathbf{e}_i, \mathbf{x} \rangle) \quad \Rightarrow \quad \forall \mathbf{x} \in \mathbb{R}^d, f^*(\mathbf{x}) = \sum_{1 \leq i \leq d} f_i^*(\langle \mathbf{e}_i, \mathbf{x} \rangle).$$

Lemma 2.3 (Legendre-Fenchel dual of a quadratic function). *Let $a, b \in [0, \infty]$. Then*

$$\forall x \in \mathbb{R}, f(x) = \frac{1}{2}(a^2 x_-^2 + b^2 x_+^2) \quad \Rightarrow \quad \forall x \in \mathbb{R}, f^*(x) = \frac{1}{2}(a^{-2} x_-^2 + b^{-2} x_+^2).$$

We propose the following discretization scheme $H_{\varepsilon, h}^{\text{RS}+}$ for the Hamiltonian $\mathcal{H}^{\text{RS}+}$, which depends on a relaxation parameter $\varepsilon \in]0, 1]$ and on the grid scale h . Proposition 1.1 is instantiated in dimension two to provide the weights $\rho_{\hat{\mathbf{e}}}^\varepsilon(\mathbf{n}(\theta))$. The offsets appearing in this expression are illustrated on Figure 3. For any discrete map $U : \mathbb{M}_h \rightarrow \mathbb{R}$ and any $\mathbf{p} = (\mathbf{x}, \theta) \in \Omega_h$

$$2H_{\varepsilon, h}^{\text{RS}+}U(\mathbf{p}) := h^{-2} \sum_{\hat{\mathbf{e}} \in \mathbb{Z}^2} \rho_{\hat{\mathbf{e}}}^\varepsilon(\mathbf{n}(\theta)) (U(\mathbf{x}, \theta) - U(\mathbf{x} - h\hat{\mathbf{e}}, \theta))_+^2 \quad (14)$$

$$+ (\xi h)^{-2} \max\{0, U(\mathbf{x}, \theta) - U(\mathbf{x}, \theta - h), U(\mathbf{x}, \theta) - U(\mathbf{x}, \theta + h)\}^2.$$

Proposition 2.4. *The discretization scheme $H_{\varepsilon,h}^{RS+}$ is monotone and causal, for any $\varepsilon \in]0, 1]$ and $h > 0$. It is supported on 6 points at most, at distance at most $C_{\text{Wsh}}h/\varepsilon$ from \mathbf{p} . Furthermore if U coincides with a linear function on these points, then*

$$\mathcal{H}_{\mathbf{p}}^{RS+}(dU(\mathbf{p})) \leq H_{\varepsilon,h}^{RS+}U(\mathbf{p}) \leq \mathcal{H}_{\mathbf{p}}^{RS+}(dU(\mathbf{p})) + \frac{\varepsilon^2}{2}\|dU(\mathbf{p})\|^2.$$

Proof. The monotony and causality properties are clearly satisfied, see also Proposition 3.6 for a general class of schemes which obey these properties. The support cardinality and radius estimates follow from Proposition 1.1. If U is locally linear around $\mathbf{p} = (\mathbf{x}, \theta) \in \mathbb{M}_h$, then denoting $dU(\mathbf{p}) = (\hat{\mathbf{x}}, \hat{\theta})$ and observing that $U(\mathbf{x}, \theta) - U(\mathbf{x} - h\hat{\mathbf{e}}, \theta) = \langle \hat{\mathbf{x}}, \hat{\mathbf{e}} \rangle$ and $U(\mathbf{x}, \theta) - U(\mathbf{x}, \theta - h) = \hat{\theta}h$, one obtains

$$H_{\varepsilon,h}^{RS+}U(\mathbf{p}) = \sum_{\hat{\mathbf{e}} \in \mathbb{Z}^2} \rho_{\hat{\mathbf{e}}}^{\varepsilon}(\mathbf{n}(\theta)) \langle \hat{\mathbf{x}}, \hat{\mathbf{e}} \rangle_+^2 + \xi^{-2} \max\{0, \hat{\theta}, -\hat{\theta}\}^2,$$

and the announced estimate follows by (13) and Proposition 1.1. \square

Proposition 2.4 easily extends to three dimensional Reeds-Shepp forward model, posed on $\mathbb{R}^3 \times \mathbb{S}^2$. We refer to [DMMP16] for more discussion on this extension and numerical experiments², and focus our attention on two dimensional path models in this paper. Nevertheless we describe our discretization strategy in the following lines, since it is only briefly evoked in [DMMP16]. For that purpose, the two dimensional unit sphere is parametrized as $\mathbf{n}(\theta, \varphi) := (\cos \theta, \sin \theta \cos \varphi, \sin \theta \sin \varphi)$, where $(\theta, \varphi) \in \mathbb{A}_2 := [0, \pi] \times [0, 2\pi]$ are the similar to the Euler angles. The Reeds-Shepp forward metric reads in this context:

$$\tilde{\mathcal{F}}_{\mathbf{p}}^{\text{RS}+}(\hat{\mathbf{p}}) := \sqrt{\|\hat{\mathbf{x}}\|^2 + |\xi \hat{\theta}|^2 + |\hat{\varphi} \xi \sin \theta|^2} \quad \text{if } \hat{\mathbf{x}} = \|\hat{\mathbf{x}}\| \mathbf{n}(\theta, \varphi)$$

and $\tilde{\mathcal{F}}_{\mathbf{p}}^{\text{RS}+}(\hat{\mathbf{p}}) = +\infty$ otherwise, for all $\mathbf{p} = (\mathbf{x}, \theta, \varphi) \in \mathbb{R}^3 \times \mathbb{A}_2$ and $\hat{\mathbf{p}} = (\hat{\mathbf{x}}, \hat{\theta}, \hat{\varphi}) \in \mathbb{R}^3 \times \mathbb{R}^2$. Using, as above, the separable and piecewise quadratic structure of the Lagrangian, we obtain

$$2\tilde{\mathcal{H}}_{\mathbf{p}}^{\text{RS}+}(\hat{\mathbf{p}}) = \langle \hat{\mathbf{x}}, \mathbf{n}(\theta, \varphi) \rangle_+^2 + |\hat{\theta}/\xi|^2 + |\hat{\varphi}/(\xi \sin \theta)|^2$$

for all $\hat{\mathbf{p}} = (\hat{\mathbf{x}}, \hat{\theta}, \hat{\varphi}) \in (\mathbb{R}^3)^* \times (\mathbb{R}^2)^*$. The rectangle \mathbb{A}_2 is equipped with the adequate boundary conditions $(\theta, 0) \sim (\theta, 2\pi)$, $(0, \varphi) \sim (0, \psi)$, $(\pi, \varphi) \sim (\pi, \psi)$, for all $\theta \in [0, \pi]$, $\varphi, \psi \in [0, 2\pi]$, and discretized using a cartesian grid of scale $h = \pi/k$ for some positive integer k . Proposition 1.1 is instantiated in dimension three to provide the weights $\rho_{\hat{\mathbf{e}}}^{\varepsilon}(\mathbf{n}(\theta, \varphi))$.

$$\begin{aligned} 2\tilde{H}_{\varepsilon,h}^{\text{RS}+}U(\mathbf{p}) &:= h^{-2} \sum_{\hat{\mathbf{e}} \in \mathbb{Z}^3} \rho_{\hat{\mathbf{e}}}^{\varepsilon}(\mathbf{n}(\theta, \varphi)) (U(\mathbf{p}) - U(\mathbf{x} - h\hat{\mathbf{e}}, \theta, \varphi))_+^2 \\ &+ (\xi h)^{-2} \max\{0, U(\mathbf{p}) - U(\mathbf{x}, \theta - h, \varphi), U(\mathbf{p}) - U(\mathbf{x}, \theta + h, \varphi)\}^2 \\ &+ (\xi h \sin \theta)^{-2} \max\{0, U(\mathbf{p}) - U(\mathbf{x}, \theta, \varphi - h), U(\mathbf{p}) - U(\mathbf{x}, \theta, \varphi + h)\}^2. \end{aligned}$$

Proposition 2.5. *The discretization scheme $\tilde{H}_{\varepsilon,h}^{\text{RS}+}$ is monotone and causal. It is supported on 11 points at most, at distance at most $C_{\text{Wsh}}h/\varepsilon$ from \mathbf{p} . Furthermore if U coincides with a linear function on these points, then*

$$\tilde{\mathcal{H}}_{\mathbf{p}}^{\text{RS}+}(dU(\mathbf{p})) \leq \tilde{H}_{\varepsilon,h}^{\text{RS}+}U(\mathbf{p}) \leq \tilde{\mathcal{H}}_{\mathbf{p}}^{\text{RS}+}(dU(\mathbf{p})) + \frac{\varepsilon^2}{2}\|dU(\mathbf{p})\|^2.$$

²Using a semi-lagrangian discretization for three dimensional the Reeds-Shepp reversible model, and the present discretization for the forward model

We do not state the proofs Proposition 2.5 and of the following remark, since they are entirely similar to that of Proposition 2.4.

Remark 2.6 (The reversible Reeds-Shepp model). *The metric of the Reeds-Shepp reversible model has the same expression as (12), except for the modified constraint: $\dot{\mathbf{x}} = \langle \mathbf{n}(\theta), \dot{\mathbf{x}} \rangle \mathbf{n}(\theta)$. As a result, the Lagrangian and Hamiltonian read*

$$2\mathcal{L}_{\mathbf{p}}^{RS\pm}(\dot{\mathbf{p}}) = \langle \mathbf{n}(\theta), \dot{\mathbf{x}} \rangle^2 + \infty \|\mathbf{P}_{\mathbf{n}(\theta)}(\dot{\mathbf{x}})\|^2 + |\xi \dot{\theta}|^2, \quad 2\mathcal{H}_{\mathbf{p}}^{RS\pm}(\hat{\mathbf{p}}) = \langle \hat{\mathbf{x}}, \mathbf{n}(\theta) \rangle^2 + |\hat{\theta}/\xi|^2.$$

The discretization scheme (14) can be adapted by appropriately modifying its first line:

$$2H_{\varepsilon, h}^{RS\pm}U(\mathbf{p}) := h^{-2} \sum_{\dot{\mathbf{e}} \in \mathbb{Z}^2} \rho_{\dot{\mathbf{e}}}^{\varepsilon}(\mathbf{n}(\theta)) \max\{0, U(\mathbf{x}, \theta) - U(\mathbf{x} - h\dot{\mathbf{e}}, \theta), U(\mathbf{x}, \theta) - U(\mathbf{x} + h\dot{\mathbf{e}}, \theta)\}^2 + \dots$$

This scheme supported on 9 points, and for a linear U on these points one has the identity

$$H_{\varepsilon, h}^{RS\pm}U(\mathbf{p}) = \mathcal{H}_{\mathbf{p}}^{RS\pm}(dU(\mathbf{p})) + \frac{\varepsilon^2}{2} \|dU(\mathbf{p})\|^2.$$

A similar remark applies to the three dimensional Reeds-Shepp reversible model.

2.2 The Euler-Mumford elastica model

The metric \mathcal{F}^{EM} of the Euler-Mumford elastica model is obtained by inserting the curvature cost $\mathcal{C}^{\text{EM}}(\kappa) := 1 + \kappa^2$ in the generic expression (3). Thus for all $\mathbf{p} = (\mathbf{x}, \theta) \in \mathbb{M}$ and all $\dot{\mathbf{p}} = (\dot{\mathbf{x}}, \dot{\theta}) \in \mathbb{E}$

$$\mathcal{F}_{\mathbf{p}}^{\text{EM}}(\dot{\mathbf{p}}) = \|\dot{\mathbf{x}}\| + \frac{|\xi \dot{\theta}|^2}{\|\dot{\mathbf{x}}\|} \quad \text{if } \dot{\mathbf{x}} = \|\dot{\mathbf{x}}\| \mathbf{n}(\theta),$$

and $\mathcal{F}_{\mathbf{p}}^{\text{EM}}(\dot{\mathbf{p}}) = +\infty$ otherwise. Observing that

$$\|\dot{\mathbf{x}}\| + \frac{|\xi \dot{\theta}|^2}{\|\dot{\mathbf{x}}\|} \leq 1 \quad \Leftrightarrow \quad \|\dot{\mathbf{x}}\|^2 + |\xi \dot{\theta}|^2 \leq \|\dot{\mathbf{x}}\| \quad \Leftrightarrow \quad (\|\dot{\mathbf{x}}\| - 1/2)^2 + |\xi \dot{\theta}|^2 \leq 1/4$$

we obtain that the control sets \mathcal{B}^{EM} are ellipses, or disks if $\xi = 1$. Note, however, that the origin 0 of the tangent space \mathbb{E} is not in their center but on their boundary, see Figure 2.

$$\begin{aligned} \mathcal{B}^{\text{EM}}(\mathbf{p}) &= \{(\dot{\mathbf{x}}, \dot{\theta}) \in \mathbb{E}; (\|\dot{\mathbf{x}}\| - 1/2)^2 + |\xi \dot{\theta}|^2 \leq 1/4, \dot{\mathbf{x}} = \|\dot{\mathbf{x}}\| \mathbf{n}(\theta)\}, \\ &= \left\{ \frac{1}{2} ((a+1)\mathbf{n}(\theta), b/\xi); a, b \in \mathbb{R}, a^2 + b^2 \leq 1 \right\}. \end{aligned}$$

Lemma 2.7. *The Euler-Mumford elastica hamiltonian reads, for all $(\mathbf{p}, \hat{\mathbf{p}}) \in \Omega \times \mathbb{E}^*$*

$$2\mathcal{H}_{\mathbf{p}}^{\text{EM}}(\hat{\mathbf{p}}) := \frac{1}{4} \left(\langle \hat{\mathbf{x}}, \mathbf{n}(\theta) \rangle + \sqrt{\langle \hat{\mathbf{x}}, \mathbf{n}(\theta) \rangle^2 + |\hat{\theta}/\xi|^2} \right)^2. \quad (15)$$

Proof. The announced result follows from (10, right) and from the computation

$$2 \sup_{\dot{\mathbf{p}} \in \mathcal{B}^{\text{EM}}(\mathbf{p})} \langle \hat{\mathbf{p}}, \dot{\mathbf{p}} \rangle = \langle \hat{\mathbf{x}}, \mathbf{n}(\theta) \rangle + \sup_{a^2 + b^2 \leq 1} a \langle \hat{\mathbf{x}}, \mathbf{n}(\theta) \rangle + b \hat{\theta}/\xi = \langle \hat{\mathbf{x}}, \mathbf{n}(\theta) \rangle + \sqrt{\langle \hat{\mathbf{x}}, \mathbf{n}(\theta) \rangle^2 + |\hat{\theta}/\xi|^2}. \quad \square$$

The expression (15) suggests to regard the Euler/Mumford model as a degenerate case of Rander geometry [Ran41]. This approach is considered numerically in [CMC16]. Unfortunately, existing numerical schemes for eikonal equations involving Rander metrics are either limited to two dimensions [Mir13], or lack causality [Mir17] and thus cannot be solved using the Fast-Marching algorithm, which significantly impacts the numerical cost and the flexibility of their implementations. In this paper we advocate for a different approach, based on a second expression of the hamiltonian \mathcal{H}^{EM} , in integral form, which to our knowledge is original.

Proposition 2.8. *For all $(\mathbf{p}, \hat{\mathbf{p}}) \in \mathbb{M} \times \mathbb{E}^*$, one has*

$$2\mathcal{H}_{\mathbf{p}}^{\text{EM}}(\hat{\mathbf{p}}) = \frac{3}{4} \int_{-\pi/2}^{\pi/2} \langle \hat{\mathbf{p}}, (\mathbf{n}(\theta) \cos \varphi, \xi^{-1} \sin \varphi) \rangle_+^2 \cos(\varphi) d\varphi.$$

Proof. The first step of the proof, left as an exercise to the reader, is to show that

$$\int_{-\pi/2}^{\pi/2} (\cos(\varphi - \psi))_+^2 \cos \varphi d\varphi = \frac{1}{3}(1 + \cos \psi)^2, \quad (16)$$

for any $\psi \in \mathbb{R}$. The second step is the claim that for any $\dot{\mathbf{e}}_0, \dot{\mathbf{e}}_1 \in \mathbb{E}$ one has

$$\int_{-\pi/2}^{\pi/2} \langle \hat{\mathbf{p}}, \cos(\varphi)\dot{\mathbf{e}}_0 + \sin(\varphi)\dot{\mathbf{e}}_1 \rangle_+^2 \cos \varphi d\varphi = \frac{1}{3} \left(\sqrt{\langle \hat{\mathbf{p}}, \dot{\mathbf{e}}_0 \rangle^2 + \langle \hat{\mathbf{p}}, \dot{\mathbf{e}}_1 \rangle^2} + \langle \hat{\mathbf{p}}, \dot{\mathbf{e}}_0 \rangle \right)^2. \quad (17)$$

Indeed, if $\langle \hat{\mathbf{p}}, \dot{\mathbf{e}}_0 \rangle = \langle \hat{\mathbf{p}}, \dot{\mathbf{e}}_1 \rangle = 0$ then there is nothing to prove. Otherwise, up to rescaling $\hat{\mathbf{p}}$, we may assume that $\langle \hat{\mathbf{p}}, \dot{\mathbf{e}}_0 \rangle^2 + \langle \hat{\mathbf{p}}, \dot{\mathbf{e}}_1 \rangle^2 = 1$, thus $\langle \hat{\mathbf{p}}, \dot{\mathbf{e}}_0 \rangle = \cos \psi$ and $\langle \hat{\mathbf{p}}, \dot{\mathbf{e}}_1 \rangle = \sin \psi$ for some $\psi \in \mathbb{R}$. Therefore $\langle \hat{\mathbf{p}}, \cos(\varphi)\dot{\mathbf{e}}_0 + \sin(\varphi)\dot{\mathbf{e}}_1 \rangle = \cos \varphi \cos \psi + \sin \varphi \sin \psi = \cos(\varphi - \psi)$ for any $\varphi \in \mathbb{R}$, hence (17) follows from (16). Choosing $\mathbf{e}_0 := (\mathbf{n}(\theta), 0)$ and $\mathbf{e}_1 := (0_{\mathbb{R}^2}, \xi^{-1})$ we conclude the proof. \square

In order to discretize the Euler-Mumford hamiltonian, we consider a second order consistent quadrature rule on the interval $[-\pi/2, \pi/2]$ with cosine weight. Quadrature rules on the interval $[-1, 1]$ for the uniform cost, such as the Clenshaw-Curtis or Fejer rules [Féj33], are for instance easily adapted to our needs thanks to the identity

$$\int_{-1}^1 f(t) dt = \int_{-\pi/2}^{\pi/2} f(\sin \varphi) \cos \varphi d\varphi.$$

More precisely, let K be a positive integer, and let $(\alpha_k, \varphi_k) \in (\mathbb{R}_+ \times [-\pi/2, \pi/2])^K$ be such that for any twice continuously differentiable $f : [-\pi/2, \pi/2] \rightarrow \mathbb{R}$

$$\left| \sum_{1 \leq k \leq K} \alpha_k f(\varphi_k) - \int_{-\pi/2}^{\pi/2} f(\varphi) \cos(\varphi) d\varphi \right| \leq \frac{C}{K^2} \sup \{ |f''(t)|; t \in [-\pi/2, \pi/2] \}, \quad (18)$$

where C is independent of f and K . Note that choosing $f \equiv 1$ on $[-\pi/2, \pi/2]$, one obtains

$$\sum_{1 \leq k \leq K} \alpha_k = \int_{-\pi/2}^{\pi/2} \cos \varphi d\varphi = 2. \quad (19)$$

We propose the following discretization of the Euler-Mumford hamiltonian

$$2H_{\varepsilon, K, h}^{\text{EM}} U(\mathbf{p}) := \frac{3}{4} h^{-2} \sum_{0 \leq k \leq K} \alpha_k \sum_{\dot{\mathbf{e}} \in \mathbb{Z}^3} \rho_{\dot{\mathbf{e}}}^{\varepsilon}(\mathbf{n}(\theta) \cos \varphi_k, \xi^{-1} \sin \varphi_k) (U(\mathbf{p}) - U(\mathbf{p} - h\dot{\mathbf{e}}))_+^2.$$

It is based on the three dimensional instantiation of Proposition 1.1, applied to the vectors $(\mathbf{n}(\theta) \cos \varphi_k, \xi^{-1} \sin \varphi_k)$, $0 \leq k \leq K$ with the relaxation parameter $\varepsilon \in]0, 1]$.

Proposition 2.9. *The discretization scheme $H_{\varepsilon,K,h}^{EM}$ is monotone and causal, for any $\varepsilon \in]0, 1]$, $K \geq 1$, $h > 0$. It is supported on at most $6K + 1$ points, at distance at most $C_{\text{Wsh}}/\varepsilon$ from \mathbf{p} . Furthermore if U coincides with a linear function on these points, then with $C = C_0 \max\{1, \xi^{-2}\}$ for some absolute constant C_0*

$$\mathcal{H}_{\mathbf{p}}^{EM}(dU(\mathbf{p})) - CK^{-2}\|dU(\mathbf{p})\|^2 \leq H_{\varepsilon,K,h}^{EM}U(\mathbf{p}) \leq \mathcal{H}_{\mathbf{p}}^{EM}(dU(\mathbf{p})) + C(\varepsilon^2 + K^{-2})\|dU(\mathbf{p})\|^2.$$

Proof. Monotony, causality, and the stencil cardinality and radius estimates are proved as in Proposition 2.4. Let $\mathbf{p} = (\mathbf{x}, \theta) \in \Omega$ be fixed, and let $\hat{\mathbf{p}} = dU(\mathbf{p})$. Let $\dot{\mathbf{v}}(\varphi) := (\mathbf{n}(\theta) \cos \varphi, \xi^{-1} \sin \varphi)$ for all $\varphi \in [-\pi/2, \pi/2]$. Using Proposition 1.1 and observing that $\|\dot{\mathbf{v}}(\varphi)\| \leq \max\{1, \xi^{-1}\}$ one obtains

$$0 \leq \frac{8}{3}H_{\varepsilon,h}^{EM}U(\mathbf{p}) - \sum_{1 \leq k \leq K} \alpha_k \langle \hat{\mathbf{p}}, \dot{\mathbf{v}}(\varphi_k) \rangle_+^2 \leq \sum_{1 \leq k \leq K} \alpha_k \varepsilon^2 \max\{1, \xi^{-2}\} \|\hat{\mathbf{p}}\|^2,$$

where we used the non-negativity of the weights $(\alpha_k)_{k=0}^K$. Therefore using (19)

$$-C_1 \|\hat{\mathbf{p}}\|^2 K^{-2} \leq \frac{8}{3}H_{\varepsilon,h}^{EM}U(\mathbf{p}) - \int_{-\pi/2}^{\pi/2} \langle \hat{\mathbf{p}}, \dot{\mathbf{v}}(\varphi) \rangle_+^2 \sin \varphi \, d\varphi \leq C_1 \|\hat{\mathbf{p}}\|^2 K^{-2} + C_2 \varepsilon^2 \|\hat{\mathbf{p}}\|^2, \quad (20)$$

where $C_2 = 2 \max\{1, \xi^{-2}\}$, and where we applied (18) to the function $\varphi \mapsto \langle \hat{\mathbf{p}}, \dot{\mathbf{v}}(\varphi) \rangle_+^2$, which second derivative makes sense as an L^∞ function and is bounded by $C_1 \|\hat{\mathbf{p}}\|^2$. Here $C_1 = C_1(\xi)$ denotes an upper bound for the partial second derivative $\partial^2/\partial\varphi^2$ of the trigonometric polynomial

$$\langle \hat{\mathbf{q}}, \dot{\mathbf{v}}(\varphi) \rangle^2 = \langle \hat{\mathbf{q}}, (\mathbf{n}(\theta) \cos \varphi, \xi^{-1} \sin \varphi) \rangle^2 = a(\hat{\mathbf{q}}, \theta, \xi) \cos(2\varphi) + b(\hat{\mathbf{q}}, \theta, \xi) \sin(2\varphi), \quad (21)$$

uniformly w.r.t. $\theta \in \mathbb{S}^1$ and $\hat{\mathbf{q}} \in \mathbb{E}^*$ such that $\|\hat{\mathbf{q}}\| = 1$. Note that the coefficients a, b , hence also C_1 , are $\mathcal{O}(\xi^{-2})$. The positive part appearing in the expression $\langle \hat{\mathbf{p}}, \dot{\mathbf{v}}(\varphi) \rangle_+^2$ of (20) and not in (21) is not an issue, thanks to a minor technical argument presented in Lemma 2.10 below. The announced result follows from (20) and Proposition 2.8. \square

Lemma 2.10. *Let $f \in C^2(\mathbb{R}, \mathbb{R})$, and let $g(x) := f(x)_+^2$ for all $x \in \mathbb{R}$. Then $g'' \in L_{\text{loc}}^\infty(\mathbb{R})$ and for almost every $x \in \mathbb{R}$ one has $g''(x) = \frac{d}{dx}(f(x)^2)$ if $f(x) > 0$, otherwise $g''(x) = 0$.*

Proof. Clearly g is locally Lipschitz, with derivative $g'(x) = 2f'(x)f(x)_+$. This expression shows that g' is also locally Lipschitz, hence almost everywhere differentiable with a locally bounded derivative, which concludes the proof. \square

2.3 The Dubins car model

The metric of \mathcal{F}^D of the Dubins car model is obtained by inserting the cost function $\mathcal{C}^D(\kappa) := 1$ if $|\xi\kappa| \leq 1$, $\mathcal{C}^D(\kappa) = +\infty$ otherwise, in the generic expression (3). Hence for all $\mathbf{p} = (\mathbf{x}, \theta) \in \mathbb{M}$ and all $\dot{\mathbf{p}} = (\dot{\mathbf{x}}, \dot{\theta}) \in \mathbb{E}$

$$\mathcal{F}_{\mathbf{p}}(\dot{\mathbf{p}}) = \|\dot{\mathbf{x}}\| \quad \text{if } \dot{\mathbf{x}} = \|\dot{\mathbf{x}}\|\mathbf{n}(\theta) \text{ and } |\xi\dot{\theta}| \leq \|\dot{\mathbf{x}}\|, \quad (22)$$

and $\mathcal{F}_{\mathbf{p}}(\dot{\mathbf{p}}) = +\infty$ otherwise. The control set $\mathcal{B}^D(\mathbf{p})$ is an isosceles triangle, or a half square if $\xi = 1$, which apex is the origin of \mathbb{E} .

$$\mathcal{B}^D(\mathbf{p}) = \{(\dot{\mathbf{x}}, \dot{\theta}) \in \mathbb{E}; \xi|\dot{\theta}| \leq \|\dot{\mathbf{x}}\| \leq 1, \dot{\mathbf{x}} = \|\dot{\mathbf{x}}\|\mathbf{n}(\theta)\} = \{(a\mathbf{n}(\theta), b\xi^{-1}); 0 \leq |b| \leq a \leq 1\}.$$

The Dubins hamiltonian is the square of a piecewise linear function.

Lemma 2.11. For all $\mathbf{p} = (\mathbf{x}, \theta) \in \mathbb{M}$ and all $\hat{\mathbf{p}} = (\hat{\mathbf{x}}, \hat{\theta}) \in \mathbb{E}^*$, one has

$$2\mathcal{H}_{\mathbf{p}}^D(\hat{\mathbf{p}}) = \max\{0, \langle \hat{\mathbf{p}}, (\mathbf{n}(\theta), \xi^{-1}) \rangle, \langle \hat{\mathbf{p}}, (\mathbf{n}(\theta), -\xi^{-1}) \rangle\}^2 = (\langle \hat{\mathbf{x}}, \mathbf{n}(\theta) \rangle + \xi^{-1}|\hat{\theta}|)_+^2$$

Proof. The result therefore follows from the expression (10, right) of the hamiltonian, and from the observation that the linear function $\langle \hat{\mathbf{p}}, \cdot \rangle$ always attains its maximum at an extreme point of the convex set $\mathcal{B}^D(\mathbf{p})$, hence at one the three vertices 0 , $(\mathbf{n}(\theta), \xi^{-1})$ and $(\mathbf{n}(\theta), -\xi^{-1})$ of this triangle. \square

We propose the following discretization scheme $H_{\varepsilon, h}^D$, with gridscale $h > 0$ and relaxation parameter $\varepsilon \in]0, 1]$. It relies on the three dimensional instantiation of Proposition 1.1 applied to the two vectors $(\mathbf{n}(\theta), \pm\xi^{-1})$. For any $U : \mathbb{M}_h \rightarrow \mathbb{R}$ and any $\mathbf{p} = (\mathbf{x}, \theta) \in \Omega_h$, define $H_{\varepsilon, h}^D U(\mathbf{p}) :=$

$$h^{-2} \max \left\{ \sum_{\dot{\mathbf{e}} \in \mathbb{Z}^3} \rho_{\dot{\mathbf{e}}}^\varepsilon(\mathbf{n}(\theta), \xi^{-1})(U(\mathbf{p}) - U(\mathbf{p} - h\dot{\mathbf{e}}))_+^2, \sum_{\dot{\mathbf{e}} \in \mathbb{Z}^3} \rho_{\dot{\mathbf{e}}}^\varepsilon(\mathbf{n}(\theta), -\xi^{-1})(U(\mathbf{p}) - U(\mathbf{p} - h\dot{\mathbf{e}}))_+^2 \right\}.$$

Proposition 2.12. The discretization scheme $H_{\varepsilon, h}^D U(\mathbf{p})$ is monotone and causal. It is supported on 13 points at most, within distance $C_{\text{WSh}}h/\varepsilon$ from \mathbf{p} . Furthermore if U coincides with a linear function on these points then

$$\mathcal{H}_{\mathbf{p}}^D(dU(\mathbf{p})) \leq H_{\varepsilon, h}^D(\mathbf{p}) \leq \mathcal{H}_{\mathbf{p}}^D(dU(\mathbf{p})) + \frac{\varepsilon^2}{2} \|dU(\mathbf{p})\|^2.$$

The proof, entirely similar to Proposition 2.4, is left to the reader.

3 Convergence analysis

This section is devoted to the convergence analysis of the discretization schemes introduced in §2, and applied to the optimal control problem (6). We prove in Theorems 3.1 and 3.2 that the resulting discrete systems of equations are solvable using the fast-marching algorithm, and that the obtained discrete solutions converge to the continuous ones at the points where they are continuous, as the grid scale h and relaxation parameter ε tend to 0 suitably. We also establish in Proposition 3.3 some continuity properties of the value function to our optimal control problem (6).

For that purpose, following the notations of [BCD97], we introduce a close relative $\hat{u} : \bar{\Omega} \rightarrow \mathbb{R}$ to the value function u defined by (6). For any $\mathbf{q} \in \bar{\Omega}$, denoting by \mathcal{F} the metric of the model

$$\hat{u}(\mathbf{q}) := \inf_{\mathbf{p} \in \mathbb{R}^2 \setminus \bar{\Omega}} d_{\mathcal{F}}(\mathbf{p}, \mathbf{q}).$$

Theorem 3.1. Let $\Omega \subseteq \mathbb{M}$ be an open and bounded domain, and let $\alpha : \mathbb{M} \rightarrow]0, \infty[$ have Lipschitz regularity. Then for any $h > 0$ and $\varepsilon \in]0, 1]$ the system

$$H_{\varepsilon, h}^{RS+} U(\mathbf{p}) = \frac{1}{2} \alpha(\mathbf{p})^2 \text{ for all } \mathbf{p} \in \Omega_h, \quad U(\mathbf{p}) = 0 \text{ for all } \mathbf{p} \in \partial\Omega_h, \quad (23)$$

admits a unique solution denoted $U_{\varepsilon, h} : \mathbb{M}_h \rightarrow \mathbb{R}$. This solution can be computed using the fast marching algorithm with complexity $\mathcal{O}(N_h \ln N_h)$, where $N_h := \#(\Omega_h)$.

Let $U_n := U_{\varepsilon_n, h_n}$, where $\varepsilon_n \rightarrow 0$ and $h_n/\varepsilon_n \rightarrow \infty$ as $n \rightarrow \infty$. Define for all $\mathbf{p} \in \bar{\Omega}$

$$\underline{u}(\mathbf{p}) := \lim_{r \rightarrow 0} \liminf_{n \rightarrow \infty} \inf_{\mathbb{M}_h \cap B(\mathbf{p}, r)} U_n, \quad \bar{u}(\mathbf{p}) := \lim_{r \rightarrow 0} \limsup_{n \rightarrow \infty} \sup_{\mathbb{M}_h \cap B(\mathbf{p}, r)} U_n.$$

Then $u \leq \underline{u} \leq \bar{u} \leq \hat{u}$ on $\bar{\Omega}$.

The first part of this result, on the discretized systems, is established in §3.1. The second part, on the comparison with the exact solutions u and \hat{u} , is addressed in §3.2. These results are of course not limited to the forward Reeds-Shepp model.

Theorem 3.2. *Theorem 3.1 applies to the Reeds-Shepp reversible, Euler-Mumford elastica, and Dubins models as well. Obviously, the discretization schemes are $H_{\varepsilon,h}^{RS\pm}$, $H_{\varepsilon,K,h}^{EM}$ and $H_{\varepsilon,h}^D$, and the metrics are $\mathcal{F}^{RS\pm}$, \mathcal{F}^{EM} and \mathcal{F}^D in problem (6). In the Euler-Mumford case, the additional discretization parameter K must be taken into account as follows: the fast-marching complexity is $\mathcal{O}(KN_h \ln N_h)$, and convergence holds for $U_n = U_{\varepsilon_n, K_n, h_n}$ provided $\varepsilon_n \rightarrow 0$, $h_n/\varepsilon_n \rightarrow 0$ and $K_n \rightarrow \infty$ as $n \rightarrow \infty$.*

The convergence result presented in Theorem 3.1 is incomplete until one proves that $u = \hat{u}$ on a large subset of the domain $\bar{\Omega}$. Our knowledge on this topic is gathered in the following proposition, proved in §3.3. As a side product, this result establishes some continuity properties of the value function to the optimal control problem (6), which are interesting from a qualitative point of view. The interior of a set A is denoted by $\text{int}(A)$.

Proposition 3.3. *Under the assumptions of Theorem 3.1, and in addition $\text{int}(\bar{\Omega}) = \Omega$. The value functions $u, \hat{u} : \bar{\Omega} \rightarrow \mathbb{R}$ are equal in the following cases:*

- (Reeds-Shepp reversible model) $u = \hat{u}$ on $\bar{\Omega}$.
- (Reeds-Shepp forward model) $u = \hat{u}$ on Ω , if this domain has the form $\Omega = \Omega_0 \times \mathbb{S}^1$.
- (Euler-Mumford model) $u = \hat{u}$ on Ω .
- (Dubins model) $u = \hat{u}$ on a dense subset of Ω .

Furthermore, in each case, u and \hat{u} are continuous at each point $\mathbf{p} \in \bar{\Omega}$ where $u(\mathbf{p}) = \hat{u}(\mathbf{p})$.

The most interesting aspect of Proposition 3.3 is what it does *not* prove. In particular, u^{RS+} and u^{EM} need not be continuous at the boundary of $\bar{\Omega}$, and u^D may be discontinuous in the interior of Ω , as well as u^{RS+} if Ω has not the shape specified in Proposition 3.3. The assumption $\text{int}(\bar{\Omega}) = \Omega$ is formulated as $\overline{\text{int} \mathcal{T}} = \mathcal{T}$ in [BCD97], where $\mathcal{T} := \mathbb{M} \setminus \Omega$ is the target set. It forbids the presence of isolated points in the target, which are inconvenient from a theoretical perspective, although they are common in applications.

In order to simplify the proofs, we introduce the dual \mathcal{F}^* of any metric \mathcal{F} , defined for any point $\mathbf{p} \in \mathbb{M}$ and co-vector $\hat{\mathbf{p}} \in \mathbb{E}^*$ by

$$\mathcal{F}_{\mathbf{p}}^*(\hat{\mathbf{p}}) := \sup_{\dot{\mathbf{p}} \neq 0} \frac{\langle \hat{\mathbf{p}}, \dot{\mathbf{p}} \rangle}{\mathcal{F}_{\mathbf{p}}(\dot{\mathbf{p}})} = \sup_{\dot{\mathbf{p}} \in \mathcal{B}(\mathbf{p})} \langle \hat{\mathbf{p}}, \dot{\mathbf{p}} \rangle = \sqrt{2\mathcal{H}_{\mathbf{p}}(\hat{\mathbf{p}})}. \quad (24)$$

where the control set \mathcal{B} and hamiltonian \mathcal{H} are defined by (10). The dual norm $\mathcal{F}_{\mathbf{p}}^*$ is positively 1-homogeneous and obeys the triangular inequality:

$$\mathcal{F}_{\mathbf{p}}^*(\lambda \hat{\mathbf{p}}) = \lambda \mathcal{F}_{\mathbf{p}}^*(\hat{\mathbf{p}}) \quad \mathcal{F}_{\mathbf{p}}^*(\hat{\mathbf{p}}_1 + \hat{\mathbf{p}}_2) \leq \mathcal{F}_{\mathbf{p}}^*(\hat{\mathbf{p}}_1) + \mathcal{F}_{\mathbf{p}}^*(\hat{\mathbf{p}}_2) \quad (25)$$

for any $\lambda \geq 0$, $\mathbf{p} \in \mathbb{M}$, $\hat{\mathbf{p}}, \hat{\mathbf{p}}_1, \hat{\mathbf{p}}_2 \in \mathbb{E}$.

3.1 Existence, uniqueness and boundedness of a discrete solution

We establish the existence and uniqueness of a solution to the discretized problem (23) for the models of interest. We also prove upper bounds on this solution which are independent of the gridscale h , assuming that the relaxation parameter satisfies $\varepsilon \leq h$. (The property remains valid if $\varepsilon \leq Ch$, where C is an absolute constant.)

Definition 3.4. *Let \mathfrak{F} be a PDE discretization scheme on a finite set X , in the sense of Definition 2.1. A discrete map $U \in \mathbb{R}^X$ is called a sub- (resp. strict sub-, resp. super-, resp. strict super-) solution of the scheme \mathfrak{F} iff $\mathfrak{F}U \leq 0$ (resp. $\mathfrak{F}U < 0$, resp. $\mathfrak{F}U \geq 0$, resp. $\mathfrak{F}U > 0$) pointwise on X . If $\mathfrak{F}U = 0$, then U is a solution to the scheme.*

When the scheme \mathfrak{F} is obvious from context, we simply speak of sub- and super-solution. The existence, uniqueness, and computability of the solutions to PDE schemes are discussed in the next result, using the notions of *monotony* and *causality* introduced in Definition 2.1. Theorem 3.5 is not an original contribution, but gathers classical results from [Tsi95, RT92, Obe06], see also [Mir17] for a proof.

Theorem 3.5 (Solving monotone schemes). *Let \mathfrak{F} be a monotone scheme on a finite set X s.t.*

- (i) *There exists a sub-solution U^- and a super-solution U^+ to the scheme \mathfrak{F} .*
- (ii) *Any super-solution to \mathfrak{F} is the pointwise limit of a sequence of strict super-solutions.*

Then there exists a unique solution $U \in \mathbb{R}^X$ to $\mathfrak{F}U = 0$, and it satisfies $U^- \leq U \leq U^+$. If in addition the scheme is causal, then this solution can be obtained via the Dynamic-Programming algorithm, also called Dijkstra or Fast-Marching, with complexity $\mathcal{O}(M \ln N)$ where

$$N = \#(X), \quad M = \#(\{(x, y) \in X \times X; \mathfrak{F}U(x) \text{ depends on } U(y)\}). \quad (26)$$

The logarithmic factor $\ln N$ in the complexity comes from the cost of maintaining a priority queue. We counted as elementary, complexity-wise, a scheme dependent local update which in the case of our schemes amounts to solving a univariate quadratic equation. We refer to [RT92] for more details on the Fast-Marching algorithm.

General properties of our PDE schemes. In this paragraph, we prove that the PDE discretization schemes introduced in §2 are monotone, causal, admit a sub-solution, and satisfy Property (ii) of Theorem 3.5. For that purpose we express them as specializations of a generic design, described in the next proposition.

Proposition 3.6. *Let X be a finite set, and let $F : \mathbb{R}^X \rightarrow \mathbb{R}^X$ be defined by*

$$(FU(\mathbf{x}))^2 := \max_{i \in I} \sum_{y \in X \cup \partial X} b(i, \mathbf{x}, \mathbf{y})(U(\mathbf{x}) - U(\mathbf{y}))_+^2, \quad (27)$$

for all $U : X \rightarrow \mathbb{R}$ and all $\mathbf{x} \in X$. We denoted by I and ∂X some arbitrary finite sets, and by $b : I \times X \times (X \cup \partial X) \rightarrow [0, \infty[$ some non-negative weights. By convention, U is extended by 0 on ∂X .

Then $F(\lambda U) = \lambda F(U)$ and $F(U + V) \leq F(U) + F(V)$, pointwise on X , for any $\lambda \geq 0$ and any $U, V : \mathbb{R}^X \rightarrow \mathbb{R}$. Let also

$$HU(\mathbf{x}) := \frac{1}{2}(FU(\mathbf{x}))^2 \quad \mathfrak{F}U(\mathbf{x}) := -a(\mathbf{x}) + HU(\mathbf{x}), \quad (28)$$

where $a : X \rightarrow]0, \infty[$. Then \mathfrak{F} is a monotone and causal scheme, admits $U \equiv 0$ as sub-solution, and $(1 + \varepsilon)U$ is a strict super-solution for any super-solution U and any $\varepsilon > 0$.

Proof. The 1-Homogeneity of F is obvious. The triangular inequality follows from the expression

$$FU(\mathbf{x}) = \max_{i \in I} \left\| \left(\sqrt{b(i, \mathbf{x}, \mathbf{y})} (U(\mathbf{x}) - U(\mathbf{y}))_+ \right)_{y \in X \cup \partial X} \right\|,$$

and from the basic inequality $(a + b)_+ \leq a_+ + b_+$ applied to $a = U(\mathbf{x}) - U(\mathbf{y})$, $b = V(\mathbf{x}) - V(\mathbf{y})$.

The scheme \mathfrak{F} is monotone since F is non-decreasing w.r.t. the differences $(U(\mathbf{x}) - U(\mathbf{y}))_{y \in X}$, and it is causal since \mathfrak{F} only depends on their positive part. The null map $U \equiv 0$ satisfies $\mathfrak{F}U(\mathbf{x}) = -a(\mathbf{x}) < 0$ hence is a (strict) sub-solution. Finally, if U is a super-solution and $\varepsilon > 0$, then $\mathfrak{F}((1 + \varepsilon)U) = (1 + \varepsilon)^2 \mathfrak{F}U + ((1 + \varepsilon)^2 - 1)a \geq 2\varepsilon a > 0$ pointwise, by homogeneity of F , hence $(1 + \varepsilon)U$ is a strict super-solution. \square

Each of the schemes introduced in §2 can be written in the form H of Proposition 3.6. A slight reformulation is nevertheless required for the Reeds-Shepp models $H_{\varepsilon, h}^{\text{RS}+}U(\mathbf{p})$, $H_{\varepsilon, h}^{\text{RS}\pm}U(\mathbf{p})$, which involve symmetric finite differences, hence expressions of the form

$$\sum_{1 \leq i \leq N} \max \{0, U(\mathbf{p}) - U(\mathbf{q}_i), U(\mathbf{x}) - U(\mathbf{r}_i)\}^2 = \sum_{1 \leq i \leq N} \max \{(U(\mathbf{p}) - U(\mathbf{q}_i))_+^2, (U(\mathbf{p}) - U(\mathbf{r}_i))_+^2\}.$$

This expression can be put in the form (27) using the distributivity of the “+” operator over the “max” operator, namely $a + \max\{b, c\} = \max\{a + b, a + c\}$. For consistency of (28, right) with (23), one must choose $a(\mathbf{x}) = \frac{1}{2}\alpha(\mathbf{x})^2$.

Construction of a continuous super-solution. In this paragraph, we construct a super-solution to the generalized eikonal PDE (7), which is discretized in the next paragraph so as to yield a gridscale independent discrete super-solution. See §3.2 for more discussion on super-solutions to the PDE (7). In the rest of this subsection, we let for all $\mathbf{p} = (\mathbf{x}, \theta) \in \mathbb{M}$

$$u(\mathbf{p}) := \alpha_0 + \langle \mathbf{n}(\theta_0), \mathbf{x} \rangle + \frac{\xi}{2} d_{\mathbb{S}^1}(\theta, \theta_0)^2, \quad (29)$$

where $\alpha_0 = C_{\text{WS}} + \max\{\|\mathbf{p}\|; \mathbf{p} \in \Omega\}$. (In other sections of this paper, the symbol u still stands for the value function defined by (6).) The angle $\theta_0 \in \mathbb{S}^1$ in (29) is arbitrary but fixed, and $d_{\mathbb{S}^1}$ denotes the distance function on $\mathbb{S}^1 := \mathbb{R}/(2\pi\mathbb{Z})$. For all $\mathbf{p} = (\mathbf{x}, \theta) \in \mathbb{M}$ such that $d_{\mathbb{S}^1}(\theta, \theta_0) \neq \pi$, one has

$$du(\mathbf{p}) = (\mathbf{n}(\theta_0), \xi\varphi) \in \mathbb{E}^*, \quad (30)$$

where $\varphi \in]-\pi, \pi[$ is the unique element congruent with $\theta - \theta_0$ modulo 2π . The function u is *not* differentiable where $d_{\mathbb{S}^1}(\theta, \theta_0) = \pi$, but by convention we still define $du(\mathbf{p})$ as (30) with $\varphi := \pi$. As shown in the following lemma, this expression defines a super-gradient of u .

Lemma 3.7. *Let $u : \mathbb{M} \rightarrow \mathbb{R}$ be defined by (29). Then for all $\mathbf{p} = (\mathbf{x}, \theta) \in \mathbb{M}$ and $\dot{\mathbf{p}} = (\dot{\mathbf{x}}, \dot{\theta}) \in \mathbb{E}$ one has*

$$u(\mathbf{p} + \dot{\mathbf{p}}) \leq u(\mathbf{p}) + \langle du(\mathbf{p}), \dot{\mathbf{p}} \rangle + \frac{\xi}{2} \dot{\theta}^2.$$

Proof. Let $\varphi \in]-\pi, \pi[$ be congruent with $\theta - \theta_0$ modulo 2π . Then $d_{\mathbb{S}^1}(\theta + \dot{\theta}, \theta_0)^2 \leq |\varphi + \dot{\theta}|^2 = \varphi^2 + 2\varphi\dot{\theta} + \dot{\theta}^2 = d_{\mathbb{S}^1}(\theta, \theta_0)^2 + 2\langle \varphi, \dot{\theta} \rangle + \dot{\theta}^2$, which implies the announced result. \square

The next proposition lower bounds the dual metric applied to the differential of (29).

Proposition 3.8. *Let \mathcal{F} be $\mathcal{F}^{\text{RS}+}$, $\mathcal{F}^{\text{RS}\pm}$, \mathcal{F}^{EM} , or \mathcal{F}^{D} . Then the dual metric (24) obeys $\mathcal{F}_{\mathbf{p}}^*(du(\mathbf{p})) \geq c_0$ for any $\mathbf{p} \in \mathbb{M}$, where $c_0 > 0$ is an absolute constant.*

Proof. Let $\mathbf{p} = (\mathbf{x}, \theta) \in \Omega$ and let $\varphi \in]-\pi, \pi]$ be congruent with $\theta - \theta_0$ modulo 2π . Then

$$\begin{aligned}\mathcal{F}_{\mathbf{p}}^{\text{RS}+*}(du(\mathbf{p}))^2 &= \langle \mathbf{n}(\theta), \mathbf{n}(\theta_0) \rangle_+^2 + |\theta - \theta_0|^2 = (\cos \varphi)_+^2 + \varphi^2, \\ \mathcal{F}_{\mathbf{p}}^{\text{RS}\pm*}(du(\mathbf{p}))^2 &= \langle \mathbf{n}(\theta), \mathbf{n}(\theta_0) \rangle^2 + |\theta - \theta_0|^2 = (\cos \varphi)^2 + \varphi^2, \\ 2\mathcal{F}_{\mathbf{p}}^{\text{EM}*}(du(\mathbf{p})) &= \langle \mathbf{n}(\theta), \mathbf{n}(\theta_0) \rangle + \sqrt{\langle \mathbf{n}(\theta), \mathbf{n}(\theta_0) \rangle^2 + |\theta - \theta_0|^2} = \cos \varphi + \sqrt{\cos^2 \varphi + \varphi^2}, \\ \mathcal{F}_{\mathbf{p}}^{\text{D}*}(du(\mathbf{p})) &= (\langle \mathbf{n}(\theta), \mathbf{n}(\theta_0) \rangle + |\theta - \theta_0|)_+ = (\cos \varphi + |\varphi|)_+.\end{aligned}$$

The right-hand sides are continuous and non-vanishing functions of $\varphi \in [-\pi, \pi]$. More precisely, one easily finds the following lower bounds: for the two Reeds-Shepp models and the Dubins model $c_0 = 1$, attained for $\varphi = 0$; for the Euler-Mumford elastica model $c_0 = \pi/4$, attained for $\varphi = \pi/2$. \square

Proposition 3.8 implies that λu is a super-solution of the HJB PDE (7), in the sense of Definition 3.14 below, where $\lambda = \|\alpha\|_\infty/c_0$. Indeed, this follows from the positive 1-homogeneity of \mathcal{F}^* , and the non-negativity of u on $\partial\Omega$. We do *not* directly use this fact in this subsection, since we aim at constructing a *discrete* super-solution, but it explains the particular role played by u .

Discretization of the super-solution. We construct a discrete super-solution to the problem (23) by sampling the continuous one constructed in Proposition 3.8. This implies the existence of a bounded solution to our PDE discretization, see Corollary 3.11. For that purpose, a preliminary estimate on the discrete hamiltonian regularity is required.

Lemma 3.9. *Let $F := \sqrt{2H}$ where H is $H_{\varepsilon,h}^{\text{RS}+}$, $H_{\varepsilon,h}^{\text{RS}\pm}$, $H_{\varepsilon,K,h}^{\text{EM}}$ or $H_{\varepsilon,h}^{\text{D}}$, and where $\varepsilon \leq 1$. Let $\mathbf{p}_0 \in \Omega_h$, and let $V, W : \mathbb{M}_h \rightarrow \mathbb{R}$ obey for all $\dot{\mathbf{p}} \in \mathbb{M}_h$*

$$V(\mathbf{p}_0 + \dot{\mathbf{p}}) \geq V(\mathbf{p}_0) - \|\dot{\mathbf{p}}\|^2, \quad W(\mathbf{p}_0 + \dot{\mathbf{p}}) \geq W(\mathbf{p}_0) - \|\dot{\mathbf{p}}\|.$$

Then for some $C = C_0(1 + \xi^{-1})$, where C_0 is an absolute constant, one has

$$FV(\mathbf{p}_0) \leq Ch/\varepsilon, \quad FW(\mathbf{p}_0) \leq C.$$

Proof. For any $\dot{\mathbf{n}} \in \mathbb{R}^d$ one obtains using Proposition 1.1

$$h^{-2} \sum_{\dot{\mathbf{e}} \in \mathbb{Z}^d} \rho_{\dot{\mathbf{e}}}^\varepsilon(\dot{\mathbf{n}}) (W(\mathbf{p}_0) - W(\mathbf{p}_0 - h\dot{\mathbf{e}}))_+^2 \leq h^{-2} \sum_{\dot{\mathbf{e}} \in \mathbb{Z}^d} \rho_{\dot{\mathbf{e}}}^\varepsilon(\dot{\mathbf{n}}) \|h\dot{\mathbf{e}}\|^2 = \|\dot{\mathbf{n}}\|^2 (1 + (d-1)\varepsilon^2) \quad (31)$$

In the case of V , observing that $V(\mathbf{p}_0) - V(\mathbf{p}_0 - h\dot{\mathbf{e}}) \leq \|h\dot{\mathbf{e}}\|^2 \leq (C_{\text{WS}}h/\varepsilon)\|h\dot{\mathbf{e}}\|$ and reasoning similarly, we obtain the upper bound (31, right) multiplied by $(C_{\text{WS}}h/\varepsilon)^2$.

The announced result is equivalent to $HV(\mathbf{p}_0) \leq \frac{1}{2}(Ch/\varepsilon)^2$ (resp. $HW(\mathbf{p}_0) \leq \frac{1}{2}C^2$). It follows from the previous estimates since the discretized hamiltonians of interest are sums of expressions like (31, left), with $\|\dot{\mathbf{n}}\| = \mathcal{O}(1 + \xi^{-1})$. In the case of $H_{\varepsilon,K,h}^{\text{EM}}$ one must additionally observe that $\sum_{k=1}^K \alpha_k = 2$ is bounded independently of K , see (19). \square

In the following two results, the notation $C \lesssim 1 + \xi^\alpha$, where $\alpha \in \mathbb{R}$, means that C depends only on the parameter ξ and satisfies $C \leq C'(1 + \xi^\alpha)$ for all $\xi \in]0, \infty[$, where C' is an absolute constant.

Proposition 3.10. *Let $F := \sqrt{2H}$ where H is $H_{\varepsilon,h}^{RS+}$, $H_{\varepsilon,h}^{RS\pm}$ or $H_{\varepsilon,h}^D$, and where $0 < h \leq \varepsilon \leq 1$. Define $U : \mathbb{Z}^h \rightarrow \mathbb{R}$ by $U(\mathbf{p}) = u(\mathbf{p})$ for all $\mathbf{p} \in \Omega_h$, and $U(\mathbf{p}) = 0$ for all $\mathbf{p} \in \partial\Omega_h$, where u is defined in (29). Then*

$$FU(\mathbf{p}) \geq c_0 - C_0 h / \varepsilon \quad (32)$$

for all $\mathbf{p} \in \Omega_h$, where $C_0 \lesssim 1 + \xi$ and c_0 is from Proposition 3.8. In the Euler-Mumford case, the constant c_0 in (32) must be replaced with $\sqrt{c_0^2 - 2C_1 K^{-2}}$, where $C_1 \lesssim 1 + \xi^{-2}$ is the constant from Proposition 2.9.

Proof. In this proof we let $\mathbf{p}_0 = (\mathbf{x}_0, \theta_0) \in \Omega_h$ be fixed, $\mathbf{p} = (\mathbf{x}, \theta) \in \Omega_h$ be an arbitrary point, and denote by $\dot{\theta} \in] - \pi, \pi]$ the unique angle congruent to $\theta - \theta_0$. Let $\bar{U} : \mathbb{M}_h \rightarrow \mathbb{R}$ be defined by $\bar{U}(\mathbf{p}) := u(\mathbf{p}_0) + \langle du(\mathbf{p}_0), (\mathbf{x} - \mathbf{x}_0, \dot{\theta}) \rangle$. By consistency of the discretization, see Propositions 2.4, 2.9, 2.12, and by Proposition 3.8 we obtain, denoting by \mathcal{H} the hamiltonian of the model

$$H\bar{U}(\mathbf{p}_0) \geq \mathcal{H}_{\mathbf{p}_0}(du(\mathbf{p}_0)) \geq \frac{1}{2}c_0^2, \quad (33)$$

except in the Euler-Mumford case, where $H\bar{U}(\mathbf{p}_0) \geq \frac{1}{2}c_0^2 - C_1 K^{-2}$, with $C_1 \lesssim 1 + \xi^{-2}$. Thus $F\bar{U}(\mathbf{p}_0) \geq c_0$, or $F\bar{U}(\mathbf{p}_0) \geq \sqrt{c_0^2 - 2C_1 K^{-2}}$ in the Euler-Mumford case.

For any $\mathbf{p} \in \Omega_h$ one has $\bar{U}(\mathbf{p}) + \frac{\xi}{2}\dot{\theta}^2 \geq U(\mathbf{p})$, by Lemma 3.7, with the above notation for $\dot{\theta} \in] - \pi, \pi]$. On the other hand, if $\mathbf{p} \in \partial\Omega_h$ is within distance C_{WS} of Ω_h , then $\bar{U}(\mathbf{p}) \geq 0 = U(\mathbf{p})$, by choice of α_0 in the definition of u , see (29). Hence denoting $V := \bar{U} - U$ we obtain $V(\mathbf{p}_0 + \dot{\mathbf{p}}) = \bar{U}(\mathbf{p}_0 + \dot{\mathbf{p}}) - U(\mathbf{p}_0 + \dot{\mathbf{p}}) \geq -\frac{\xi}{2}\|\dot{\mathbf{p}}\|^2$ for any $\dot{\mathbf{p}} \in h\mathbb{Z}^3$ such that $\|\dot{\mathbf{p}}\| \leq C_{\text{WS}}$. Therefore $FV(\mathbf{p}_0) \leq \xi C_2(1 + \xi^{-1})h/\varepsilon = C_2(1 + \xi)h/\varepsilon$, by Lemma 3.9 and the 1-homogeneity of F , where C_2 is independent of ξ . We used the fact that the expression of $FV(\mathbf{p}_0)$ only involves points within distance $C_{\text{WS}}h/\varepsilon \leq C_{\text{WS}}$ of \mathbf{p}_0 , see Propositions 2.4, 2.9, 2.12. Using the triangular inequality $F\bar{U} = F(U + V) \leq FU + FV$, pointwise on Ω_h , see Proposition 3.6, we thus obtain

$$FU(\mathbf{p}_0) \geq F\bar{U}(\mathbf{p}_0) - FV(\mathbf{p}_0) \geq c_0 - C_2(1 + \xi)h/\varepsilon.$$

In the Euler-Mumford case the constant c_0 in the above expression must be replaced with $\sqrt{c_0^2 - 2C_1 K^{-2}}$, see (33). The result follows. \square

Corollary 3.11. *Assume that $0 < h \leq \varepsilon \leq 1$ and $\varepsilon \leq K_0 h$, where $K_0 \lesssim 1 + \xi$. Let H be the discretized Hamiltonian $H_{\varepsilon,h}^{RS+}$, $H_{\varepsilon,h}^{RS\pm}$ or $H_{\varepsilon,h}^D$. Then the system of equations $HU(\mathbf{p}) = \alpha(\mathbf{p})^2/2$ for all $\mathbf{p} \in \Omega_h$, and $U(\mathbf{p}) = 0$ for all $\mathbf{p} \in \mathbb{M}_h$, admits a unique solution $U : \mathbb{M}_h \rightarrow \mathbb{R}$, which is bounded independently of h and ε .*

The same holds for the Hamiltonian $H_{\varepsilon,K,h}^{EM}$, provided $K \geq K_1 \gtrsim 1 + \xi^{-1}$.

Proof. Assume that the parameters ε , h and K obey the above constraints, with the constants $K_0 = 2C_0$ and $K_1 = 4\sqrt{C_1}$, where C_0 and C_1 are from Proposition 3.10. Then the considered system of equations admits the super-solution λU , where U is defined in Proposition 3.10 and $\lambda = 2\|\alpha\|_{L^\infty}/c_0$. Applying Theorem 3.5, which assumptions were established in Proposition 3.6 for the models of interest, except for the existence of a super-solution which we just proved, we conclude the proof. \square

3.2 Discontinuous viscosity solutions of eikonal PDEs

In this subsection, we establish Theorem 3.1 using the theory of discontinuous solutions to static first order Hamilton-Jacobi-Bellman PDEs. We rely on the framework of section V of [BCD97],

intended for optimal control problems without controllability, either local or global. Let \mathcal{F} be $\mathcal{F}^{\text{RS}+}$, $\mathcal{F}^{\text{RS}\pm}$, \mathcal{F}^{EM} or \mathcal{F}^{D} , and consider the PDE.

$$\forall \mathbf{p} \in \Omega, \mathcal{F}^*(\mathbf{p}, du(\mathbf{p})) = \alpha(\mathbf{p}), \quad \forall \mathbf{p} \in \partial\Omega, u(\mathbf{p}) = 0 \text{ or } \mathcal{F}^*(\mathbf{p}, du(\mathbf{p})) = \alpha(\mathbf{p}), \quad (34)$$

where \mathcal{F}^* refers to the dual metric, defined on the co-tangent space $\mathbb{M} \times \mathbb{E}^*$, see (24). In comparison with our initial formulation (7), two remarks are in order: (I) we used the relation $\mathcal{H} = \frac{1}{2}(\mathcal{F}^*)^2$ relating the hamiltonian \mathcal{H} with the dual metric \mathcal{F}^* (24) to reformulate the HJB PDE in Ω , and (II) we emphasized that boundary conditions must be interpreted in a relaxed sense, following the notations of [BCD97], due to the possible discontinuity of the solution. The study of solutions to this system relies on one sided notions of continuity.

Definition 3.12. *Let (X, d) be metric space, and let $u : X \rightarrow \mathbb{R}$. The function u is said Lower-Semi-Continuous (resp. Upper-Semi-Continuous) iff for any converging sequence $\mathbf{p}_n \rightarrow \mathbf{p} \in X$*

$$\liminf_{n \rightarrow \infty} u(\mathbf{p}_n) \geq u(\mathbf{p}) \quad (\text{resp. } \limsup_{n \rightarrow \infty} u(\mathbf{p}_n) \leq u(\mathbf{p}).)$$

The acronyms USC and LSC refer to these properties, and B stands for Bounded in BUSC and BLSC. Recall that the cartesian grid of scale h is denoted $\mathbb{M}_h \subseteq \mathbb{M}$, see (35).

Lemma 3.13. *For each $n \geq 0$ let $h_n > 0$ and $U_n : \mathbb{M}_{h_n} \rightarrow \mathbb{R}$. Assume that $h_n \rightarrow 0$ as $n \rightarrow \infty$, and that U_n is uniformly bounded independently of n . Then $\bar{u}, \underline{u} : \mathbb{M} \rightarrow \mathbb{R}$ defined as follows are respectively BUSC and BLSC*

$$\underline{u}(\mathbf{p}) := \lim_{r \rightarrow 0} \liminf_{n \rightarrow \infty} \inf_{\substack{\mathbf{q} \in \mathbb{M}_{h_n} \\ \|\mathbf{q} - \mathbf{p}\| < r}} U_n(\mathbf{q}), \quad \bar{u}(\mathbf{p}) := \lim_{r \rightarrow 0} \limsup_{n \rightarrow \infty} \sup_{\substack{\mathbf{q} \in \mathbb{M}_{h_n} \\ \|\mathbf{q} - \mathbf{p}\| < r}} U_n(\mathbf{q}). \quad (35)$$

Proof. We focus on the case of \underline{u} , since the case of \bar{u} is similar. First note that $\underline{u}(\mathbf{p})$ is well defined and uniformly bounded w.r.t. $\mathbf{p} \in \mathbb{M}$. Indeed (i) for any fixed $r > 0$, and for sufficiently large n , the set $\mathbb{M}_{h_n} \cap B(\mathbf{p}, r)$ is non-empty since $h_n \rightarrow 0$ as $n \rightarrow \infty$, (ii) U_n is uniformly bounded, and (iii) the leftmost limit as $r \rightarrow 0$ is monotone, namely increasing as r decreases to 0, hence well defined.

In order to establish the Lower Semi-Continuity of \underline{u} , let us consider an arbitrary sequence $(\mathbf{p}_n)_{n \geq 0}$ converging to $\mathbf{p} \in \mathbb{M}$. Let also $r_n \rightarrow 0$ and $\varepsilon_n \rightarrow 0$ be vanishing sequences of positive reals. By construction, for any $n \geq 0$ there exists $\varphi(n) \geq n$ and $\mathbf{q}_n \in B(\mathbf{p}_n, r_n)$ such that $U_{\varphi(n)}(\mathbf{q}_n) \leq \underline{u}(\mathbf{p}_n) + \varepsilon_n$. Then, as announced, since $\mathbf{q}_n \rightarrow \mathbf{p}$ and $\varphi(n) \rightarrow \infty$ as $n \rightarrow \infty$,

$$\liminf_{n \rightarrow \infty} \underline{u}(\mathbf{p}_n) \geq \liminf_{n \rightarrow \infty} U_{\varphi(n)}(\mathbf{q}_n) \geq \underline{u}(\mathbf{p}). \quad \square$$

Following [BE84], we introduce the concept of sub- and super-solutions to the system (34).

Definition 3.14. *• A sub-solution of (34) is a BUSC $\bar{u} : \bar{\Omega} \rightarrow \mathbb{R}$ such that for any $\mathbf{p} \in \bar{\Omega}$ and any $\varphi \in C^1(\bar{\Omega}, \mathbb{R})$ for which $\bar{u} - \varphi$ attains a local maximum at \mathbf{p} , one has:*

$$\mathbf{p} \in \Omega \Rightarrow \mathcal{F}^*(\mathbf{p}, d\varphi(\mathbf{p})) \leq \alpha(\mathbf{p}), \quad \mathbf{p} \in \partial\Omega \Rightarrow \min\{\bar{u}(\mathbf{p}), \mathcal{F}^*(\mathbf{p}, d\varphi(\mathbf{p})) - \alpha(\mathbf{p})\} \leq 0.$$

• A super-solution is a BLSC $\underline{u} : \bar{\Omega} \rightarrow \mathbb{R}$ such that for any $\mathbf{p} \in \bar{\Omega}$ and any $\varphi \in C^1(\bar{\Omega}, \mathbb{R})$ for which $\underline{u} - \varphi$ attains a local minimum at \mathbf{p} , one has:

$$\mathbf{p} \in \Omega \Rightarrow \mathcal{F}^*(\mathbf{p}, d\varphi(\mathbf{p})) \geq \alpha(\mathbf{p}), \quad \mathbf{p} \in \partial\Omega \Rightarrow \max\{\underline{u}(\mathbf{p}), \mathcal{F}^*(\mathbf{p}, d\varphi(\mathbf{p})) - \alpha(\mathbf{p})\} \geq 0.$$

It known that replacing “local maximum” with “strict global maximum” (resp. “local minimum” with “strict global minimum”) in Definition 3.14 yields an equivalent definition, see [BE84].

Following a classical strategy [BR06], we estimate in the next lemma the discretization error of our numerical scheme when applied to continuously differentiable functions, and conclude in the next proposition that suitable limits of solutions to our discrete numerical schemes are sub- and super-solutions to the HJB PDE (34).

Lemma 3.15. *Let $F_{\varepsilon,h} := \sqrt{2H_{\varepsilon,h}}$ where $H_{\varepsilon,h}$ is $H_{\varepsilon,h}^{RS+}$, $H_{\varepsilon,h}^{RS\pm}$ or $H_{\varepsilon,h}^D$ and $0 < h \leq \varepsilon \leq 1$. Let $\varphi \in C^1(\mathbb{M}, \mathbb{R})$, and let ω be the modulus of continuity of $d\varphi$. Then*

$$|F_{\varepsilon,h}\varphi(\mathbf{p}) - \mathcal{F}^*(\mathbf{p}, d\varphi(\mathbf{p}))| \leq C(\omega(C_{\text{WS}}h/\varepsilon) + \varepsilon\|d\varphi(\mathbf{p})\|). \quad (36)$$

In the Euler-Mumford case, $|F_{\varepsilon,K,h}\varphi(\mathbf{p}) - \mathcal{F}^(\mathbf{p}, d\varphi(\mathbf{p}))| \leq C(\omega(C_{\text{WS}}h/\varepsilon) + (\varepsilon + K_n^{-1})\|d\varphi(\mathbf{p})\|)$.*

Proof. In this proof, if $\mathbf{p} = (\mathbf{x}, \theta)$, $\mathbf{q} = (\mathbf{x}', \theta') \in \mathbb{M} = \mathbb{R}^2 \times \mathbb{S}^1$, then $\mathbf{q} - \mathbf{p}$ (abusively) stands for $(\mathbf{x}' - \mathbf{x}, \varphi) \in \mathbb{E} := \mathbb{R}^2 \times \mathbb{R}$ where $\varphi \in]-\pi, \pi]$ is congruent with $\theta' - \theta$. Fix the point $\mathbf{p} \in \mathbb{M}$, and define the tangent map $\Phi : \mathbf{q} \in \mathbb{M} \mapsto \varphi(\mathbf{p}) + \langle d\varphi(\mathbf{p}), \mathbf{q} - \mathbf{p} \rangle$. Then $|\varphi(\mathbf{q}) - \Phi(\mathbf{q})| \leq \|\mathbf{p} - \mathbf{q}\|\omega(\|\mathbf{p} - \mathbf{q}\|)$ for any $\mathbf{q} \in \mathbb{M}$. This implies $F(\varphi - \Phi)(\mathbf{p}) \leq C\omega(C_{\text{WS}}h/\varepsilon)$ where $F := F_{\varepsilon,h}$ and $C \lesssim 1 + \xi^{-1}$, by Lemma 3.9, the 1-homogeneity of F , and since any point \mathbf{q} appearing in the expression of $FU(\mathbf{p})$ satisfies $\|\mathbf{p} - \mathbf{q}\| \leq C_{\text{WS}}h/\varepsilon$. Proceeding likewise for $F(\Phi - \varphi)(\mathbf{p})$ and using the triangular inequality, proved for F in Proposition 3.6, we obtain

$$|F\varphi(\mathbf{p}) - F\Phi(\mathbf{p})| \leq \max\{F(\Phi - \varphi)(\mathbf{p}), F(\varphi - \Phi)(\mathbf{p})\} \leq C\omega(C_{\text{WS}}h/\varepsilon).$$

The second contribution to (36) comes from the estimate

$$|F\Phi(\mathbf{p}) - \mathcal{F}^*(\mathbf{p}, d\varphi(\mathbf{p}))| = \sqrt{2}|\sqrt{H\Phi(\mathbf{p})} - \sqrt{\mathcal{H}(\mathbf{p}, d\varphi(\mathbf{p}))}| \leq \sqrt{2}\sqrt{|H\Phi(\mathbf{p}) - \mathcal{H}(\mathbf{p}, d\varphi(\mathbf{p}))|},$$

where we used the classical inequality $|\sqrt{a} - \sqrt{b}| \leq \sqrt{|a - b|}$ for any $a, b \geq 0$. Inserting the discretization error of the Hamiltonian, see Propositions 2.4, 2.9 and 2.12, we conclude the proof. \square

Proposition 3.16. *Let $\underline{u}, \bar{u} : \mathbb{M} \rightarrow \mathbb{R}$ be defined as in Theorem 3.1 (resp. Theorem 3.2). Then \underline{u} is a super-solution, and \bar{u} is a sub-solution, in the sense of Definition 3.14.*

Proof. We focus on the case of \bar{u} , since the case of \underline{u} is similar. By lemma 3.13, \bar{u} is BUSC as required. Let $\mathbf{p} \in \bar{\Omega}$ and $\varphi \in C^1(\bar{\Omega}, \mathbb{R})$ be such that \bar{u} attains a *strict global* maximum at \mathbf{p} .

For each $n \geq 0$, define $X_n := \{\mathbf{q} \in \mathbb{M}_{h_n}; d(\mathbf{q}, \Omega) \leq C_{\text{WS}}h_n\}$, and let $\mathbf{p}_n \in X_n$ be a point where $U_n - \varphi$ attains its global maximum. Then $U_n(\mathbf{p}_n) - \varphi(\mathbf{p}_n) \rightarrow \bar{u}(\mathbf{p}) - \varphi(\mathbf{p})$ as $n \rightarrow \infty$, up to extracting a sub-sequence (because of the \liminf operator in (35)). This implies $\mathbf{p}_n \rightarrow \mathbf{p}$ as $n \rightarrow \infty$, by strictness of the maximum of $\bar{u} - \varphi$ at \mathbf{p} . In addition $U_n(\mathbf{p}_n) = (U_n(\mathbf{p}_n) - \varphi(\mathbf{p}_n)) + \varphi(\mathbf{p}_n) \rightarrow (\bar{u}(\mathbf{p}) - \varphi(\mathbf{p})) + \varphi(\mathbf{p}) = \bar{u}(\mathbf{p})$ as $n \rightarrow \infty$, by choice of the sequence $(\mathbf{p}_n)_{n \geq 0}$ and by continuity of φ . In order to conclude the proof, we distinguish whether the test point $\mathbf{p} \in \bar{\Omega}$ lies in the interior or on the boundary of the domain.

Case where $\mathbf{p} \in \Omega$. By construction of \mathbf{p}_n , one has $U_n(\mathbf{p}_n) - U_n(\mathbf{q}) \geq \varphi(\mathbf{p}_n) - \varphi(\mathbf{q})$ for all $\mathbf{q} \in X_n$. Hence

$$\alpha(\mathbf{p}_n) = FU(\mathbf{p}_n) \geq F\varphi(\mathbf{q}_n) \geq \mathcal{F}^*(\mathbf{p}_n, d\varphi(\mathbf{p}_n)) - C(\omega(C_{\text{WS}}h_n/\varepsilon_n) + \varepsilon_n\|d\varphi(\mathbf{p}_n)\|),$$

where the first inequality is by monotony of the discretized operator $F := F_{\varepsilon,h}$, and the second one is by Lemma 3.15. Thus $\alpha(\mathbf{p}) = \lim \alpha(\mathbf{p}_n) \geq \lim \mathcal{F}^*(\mathbf{p}_n, d\varphi(\mathbf{p}_n)) = \mathcal{F}^*(\mathbf{p}, d\varphi(\mathbf{p}))$ as $n \rightarrow \infty$.

Case where $\mathbf{p} \in \partial\Omega$. We distinguish two sub-cases: if $\mathbf{p}_n \in \Omega$ for infinitely many integers $n \geq 0$, then $\mathcal{F}^*(\mathbf{p}, d\varphi(\mathbf{p})) \leq \alpha(\mathbf{p})$ as before, thus the (relaxed) boundary condition is satisfied as desired. Otherwise, up to extracting a subsequence, one has $0 = U_n(\mathbf{p}_n) \rightarrow \bar{u}(\mathbf{p})$ as $n \rightarrow \infty$, thus $\bar{u}(\mathbf{p}) = 0$ and the boundary condition is satisfied. \square

The following result concludes the proof of Theorems 3.1 and 3.2.

Proposition 3.17 (Adapted from [BCD97]). *The value function u is the smallest super-solution to the HJB PDE (34), and \hat{u} is the largest sub-solution.*

The fact that u is the smallest super-solution follows from Theorem 3.7 in chapter V [BCD97], and the fact that \hat{u} is the largest super-solution from Theorem 4.29 in the same chapter. To be complete, we describe below the slight reformulation of the optimal control problem (6) required to match the notations of [BCD97], and check that the assumptions used in [BCD97] are satisfied. For that purpose, we introduce a compact and convex set $\mathbb{A} \subseteq \mathbb{R} \times \mathbb{R}$ and regard its elements $a = (\dot{x}, \dot{\theta}) \in \mathbb{A}$ as a (scalar) physical velocity, and an angular velocity. The following instantiations of \mathbb{A} are considered

$$\begin{aligned} \mathbb{A}^{\text{RS}^+} &:= \{(\dot{x}, \dot{\theta}) \in \mathbb{R}^2; \dot{x}^2 + \dot{\theta}^2 \leq 1, \dot{x} \geq 0\}, & \mathbb{A}^{\text{RS}^\pm} &:= \{(\dot{x}, \dot{\theta}) \in \mathbb{R}^2; \dot{x}^2 + \dot{\theta}^2 \leq 1\}, \\ \mathbb{A}^{\text{EM}} &:= \{(\dot{x}, \dot{\theta}) \in \mathbb{R}^2; (\dot{x} - 1/2)^2 + \dot{\theta}^2 \leq (1/2)^2\}, & \mathbb{A}^{\text{D}} &:= \{(\dot{x}, \dot{\theta}) \in \mathbb{R}^2; 0 \leq |\dot{\theta}| \leq \dot{x}\}. \end{aligned} \quad (37)$$

Define $f : \mathbb{M} \times \mathbb{A} \rightarrow \mathbb{E}$ and $l : \mathbb{M} \times \mathbb{A} \rightarrow \mathbb{R}$ as

$$f((\mathbf{x}, \theta), (\dot{x}, \dot{\theta})) := -(\dot{x}\mathbf{n}(\theta), \dot{\theta})/\alpha(\mathbf{x}, \theta), \quad l((\mathbf{x}, \theta), a) := 1, \quad (38)$$

where $\alpha : \mathbb{M} \rightarrow]0, \infty[$ is the local cost function. Let also $\mathcal{T} := \mathbb{M} \setminus \Omega$ be the target region. Consider, following [BCD97], the optimal control problem

$$v(\mathbf{p}) := \inf_{(a, T) \in \mathcal{A}} \int_0^T l(\mathbf{q}_{\mathbf{p}, a}(t), a(t)) e^{-t} dt, \quad \text{subject to } \begin{cases} \mathbf{q}'_{\mathbf{p}, a}(t) = f(\mathbf{q}_{\mathbf{p}, a}(t), a(t)), \forall t \in [0, T], \\ \mathbf{q}_{\mathbf{p}, a}(0) = \mathbf{p} \text{ and } \mathbf{q}_{\mathbf{p}, a}(T) \in \mathcal{T}, \end{cases} \quad (39)$$

where elements of \mathcal{A} are pairs of all (free) control times $T \geq 0$ and measurable function $a : [0, T]$ to \mathbb{A} . We claim that, with the choices (37), one has

$$v(\mathbf{p}) = \int_0^{u(\mathbf{p})} e^{-t} dt = 1 - \exp(-u(\mathbf{p})), \quad (40)$$

for any $\mathbf{p} \in \bar{\Omega}$. Indeed, consider a Lipschitz path $\gamma : [0, 1] \rightarrow \bar{\Omega}$ from $\partial\Omega$ to $\mathbf{p} \in \Omega$ and such that $u(\mathbf{p}) = \text{length}_{\mathcal{F}}(\gamma) < \infty$. Introduce a time reparametrization $\eta : [0, T] \rightarrow \bar{\Omega}$ of γ , from $\partial\Omega$ to \mathbf{p} , at unit speed w.r.t. the reversed metric in the sense that $\mathcal{F}_{\eta(t)}(-\dot{\eta}(t)) = 1$ for all $t \in [0, T]$. Then clearly $T = \text{length}_{\mathcal{F}}(\gamma) = u(\mathbf{p})$, and one can uniquely define controls $a : [0, T] \rightarrow \mathbb{A}$ by $f(\eta(t), a(t)) = -\dot{\eta}(t)$ for all $t \in [0, T]$. Introducing an additional time-reversal reparametrization, $t \in [0, T] \mapsto T - t$, required since (39) considers contrary to us paths from \mathbf{p} to $\partial\Omega$, we obtain $v(\mathbf{p}) \leq \int_0^T e^{-t} dt = 1 - \exp(-u(\mathbf{p}))$. Conversely, admissible paths for (39) can be reparametrized into admissible paths for (6), and the identity (40) follows. Similarly, one can define \hat{v} by replacing \mathcal{T} with its interior in (39), and obtain that $\hat{v} = 1 - \exp(-\hat{u})$ in $\bar{\Omega}$.

The following PDEs are thus equivalent, the rightmost being the one considered in [BCD97]

$$\mathcal{H}_{\mathbf{p}}(du(\mathbf{p})) = \frac{1}{2}\alpha(\mathbf{p})^2, \quad \mathcal{F}_{\mathbf{p}}^*(du(\mathbf{p})) = \alpha(\mathbf{p}), \quad v(\mathbf{p}) + \mathcal{F}_{\mathbf{p}}(dv(\mathbf{p})) - \alpha(\mathbf{p}) = 0,$$

where $\mathbf{p} \in \Omega$ is arbitrary. The main reason why [BCD97] considers $v = 1 - \exp(-u)$ instead of u is that v remains bounded whereas even for problems lacking global controllability, whereas u may take infinite values. This technicality is however irrelevant for the problems considered in this paper, since global controllability does hold as shown in §3.1.

Finally, we need to check the specific assumptions of Theorem 3.7 and 4.29 in chapter V of [BCD97]. These are (I) the compactness of the set \mathbb{A} of controls (37), (II) the Lipschitz continuity of f and l , see (38), which follows from the Lipschitz continuity of the cost α , and its boundedness below on the compact domain $\bar{\Omega}$, and (III) the closedness of \mathcal{T} , following from the openness of Ω .

3.3 Continuity properties of the value function

This subsection is devoted to the proof of Proposition 3.3. Two points of this result follow from general arguments. Point (I) indeed follows from the locally controllability of the Reeds-Shepp reversible model, which is due to its sub-riemannian structure and Chow's theorem, see [Mon06] and the discussion in [DMMP16]. In fact, the value function u is $1/2$ -Holder continuous in this case. Point (IV) on the Dubins model follows from another general argument of [BCD97], involving Baire's theorem, see Lemma 3.25. In contrast the proof of points (II) and (III) on the Reeds-Shepp forward and Euler-Mumford models requires a geometrical perturbation argument, which involves lifting diffeomorphisms from \mathbb{R}^2 to $\mathbb{M} := \mathbb{R}^2 \times \mathbb{S}^1$, as presented below.

The argument $\arg(\dot{\mathbf{x}})$ of a non-zero vector $\dot{\mathbf{x}} \in \mathbb{R}^2$ is defined as the unique angle $\theta \in \mathbb{S}^1$ such that $\dot{\mathbf{x}} = \|\dot{\mathbf{x}}\|\mathbf{n}(\theta)$. Matrix vector product is denoted by “ \cdot ”.

Lemma 3.18. *Let ψ be a C^n diffeomorphism of \mathbb{R}^2 , where $n \geq 2$. Define $\Psi(\mathbf{x}, \theta) = (\mathbf{y}, \varphi)$ by*

$$\mathbf{y} := \psi(\mathbf{x}), \quad \varphi := \arg(d\psi(\mathbf{x}) \cdot \mathbf{n}(\theta)), \quad (41)$$

for all $(\mathbf{x}, \theta) \in \mathbb{R}^2 \times \mathbb{S}^1$. Then Ψ is a C^{n-1} diffeomorphism of $\mathbb{R}^2 \times \mathbb{S}^1$. Furthermore, let $(\dot{\mathbf{x}}, \dot{\theta}) \in \mathbb{R}^2 \times \mathbb{R}$ and let $(\dot{\mathbf{y}}, \dot{\varphi}) := d\Psi(\mathbf{x}, \theta) \cdot (\dot{\mathbf{x}}, \dot{\theta})$. Then

$$\underline{K}\|\dot{\mathbf{x}}\| \leq \|\dot{\mathbf{y}}\| \leq \bar{K}\|\dot{\mathbf{x}}\|, \quad |\dot{\varphi}| \leq (\bar{K}|\dot{\theta}| + K_2\|\dot{\mathbf{x}}\|)/\underline{K}, \quad (42)$$

where $\underline{K} = \|(d\psi(\mathbf{x}))^{-1}\|^{-1}$, $\bar{K} := \|d\psi(\mathbf{x})\|$, and $K_2 := \|d^2\psi(\mathbf{x})\|$.

Proof. The bijectivity of $\theta \in \mathbb{S}^1 \mapsto \varphi := \arg(d\psi(\mathbf{x}) \cdot \mathbf{n}(\theta))$, for any fixed \mathbf{x} , follows from the invertibility of $d\psi(\mathbf{x})$. The estimate (42, left) follows from the definition of the operator norm $\|A\| := \sup_{\dot{\mathbf{x}} \neq 0} \|A\dot{\mathbf{x}}\|/\|\dot{\mathbf{x}}\|$ of a matrix A . The upper bound on $|\dot{\varphi}|$ is obtained by composing the following two Taylor expansions: the first one

$$\arg(\mathbf{x} + \dot{\mathbf{x}}) = \arg(\mathbf{x}) + \|\mathbf{x}\|^{-2}\langle \mathbf{x}^\perp, \dot{\mathbf{x}} \rangle + o(\|\dot{\mathbf{x}}\|),$$

is obtained by basic geometric reasoning, and the second one

$$d\psi(\mathbf{x} + \dot{\mathbf{x}}) \cdot \mathbf{n}(\theta + \dot{\theta}) = d\psi(\mathbf{x}) \cdot \mathbf{n}(\theta) + (d^2\psi(\mathbf{x}) \cdot \dot{\mathbf{x}}) \cdot \mathbf{n}(\theta) + \dot{\theta}d\psi(\mathbf{x}) \cdot \mathbf{n}(\theta)^\perp + o(\|\dot{\mathbf{x}}\| + |\dot{\theta}|),$$

by bi-linearity of the matrix-vector product. \square

The next lemma upper bounds the composition of the metric, of the models RS+, RS± and EM, with the tangent map to a diffeomorphism of the form (41). No similar estimate can be established for the Dubins metric, due to the hard constraint $|\xi\theta| \leq \|\dot{\mathbf{x}}\|$ appearing in (22).

Lemma 3.19. *Under the assumptions of Lemma 3.18, denoting $\mathbf{p} := (\mathbf{x}, \theta)$, $\dot{\mathbf{p}} := (\dot{\mathbf{x}}, \dot{\theta})$, $\mathbf{q} := (\mathbf{y}, \varphi)$ and $\dot{\mathbf{q}} := (\dot{\mathbf{y}}, \dot{\varphi})$, one has*

$$\mathcal{F}_{\mathbf{q}}^{RS+}(\dot{\mathbf{q}}) \leq K_{RS}\mathcal{F}_{\mathbf{p}}^{RS+}(\dot{\mathbf{p}}), \quad \mathcal{F}_{\mathbf{q}}^{RS\pm}(\dot{\mathbf{q}}) \leq K_{RS}\mathcal{F}_{\mathbf{p}}^{RS\pm}(\dot{\mathbf{p}}), \quad \mathcal{F}_{\mathbf{q}}^{EM}(\dot{\mathbf{q}}) \leq K_{EM}\mathcal{F}_{\mathbf{p}}^{EM}(\dot{\mathbf{p}}),$$

with $K_{RS}^2 := \max\{\overline{K}^2 + \xi^2\varepsilon(1+\varepsilon), (1+\varepsilon)\overline{K}\}$ and $K_{EM} := \max\{\overline{K} + \xi^2\varepsilon(1+\varepsilon)/\underline{K}, (1+\varepsilon)\overline{K}^2/\underline{K}\}$, where $\varepsilon := K_2/\underline{K}$ and $\overline{K} := \overline{K}/\underline{K}$.

Proof. By construction of the diffeomorphism Ψ , the colinearity constraint involved in the definition (3) of the metrics is preserved: $\dot{\mathbf{x}} = \|\dot{\mathbf{x}}\|\mathbf{n}(\theta) \Rightarrow \dot{\mathbf{y}} = \|\dot{\mathbf{y}}\|\mathbf{n}(\varphi)$, and likewise for the unsigned colinearity constraint $\dot{\mathbf{x}} = \langle \dot{\mathbf{x}}, \mathbf{n}(\theta) \rangle \mathbf{n}(\theta) \Rightarrow \dot{\mathbf{y}} = \langle \dot{\mathbf{y}}, \mathbf{n}(\varphi) \rangle \mathbf{n}(\varphi)$. Using the inequality $(a + \varepsilon b)^2 \leq (1 + \varepsilon)(a^2 + \varepsilon b^2)$, valid for any $a, b \in \mathbb{R}$, $\varepsilon > 0$, we obtain as announced

$$\begin{aligned} \|\dot{\mathbf{y}}\|^2 + \xi^2\dot{\varphi}^2 &\leq (\overline{K}\|\dot{\mathbf{x}}\|)^2 + \xi^2(\overline{K}\dot{\theta} + \varepsilon\|\dot{\mathbf{x}}\|)^2 \leq \left(\overline{K}^2 + \xi^2\varepsilon(1+\varepsilon)\right)\|\dot{\mathbf{x}}\|^2 + (1+\varepsilon)\overline{K}^2\xi^2\dot{\theta}^2 \\ \|\dot{\mathbf{y}}\| + \xi^2\frac{\dot{\varphi}^2}{\|\dot{\mathbf{y}}\|} &\leq \overline{K}\|\dot{\mathbf{x}}\| + \xi^2\frac{(\overline{K}\dot{\theta}^2 + \varepsilon\|\dot{\mathbf{x}}\|)^2}{\underline{K}\|\dot{\mathbf{x}}\|} \leq (\overline{K} + \xi^2\varepsilon(1+\varepsilon)/\underline{K})\|\dot{\mathbf{x}}\| + (1+\varepsilon)\frac{\overline{K}^2}{\underline{K}}\xi^2\frac{\dot{\theta}^2}{\|\dot{\mathbf{x}}\|}. \square \end{aligned}$$

The previous lemma is next specialized to diffeomorphisms defined by the flow of a vector field.

Corollary 3.20. *Let $\nu : \mathbb{R}^2 \rightarrow \mathbb{R}^2$ be a vector field with continuous and uniformly bounded first and second derivatives. Let $(\psi_t)_{t \geq 0}$ be the family of C^2 diffeomorphisms of \mathbb{R}^2 defined by*

$$\psi_0(\mathbf{x}) = \mathbf{x}, \quad \frac{d}{dt}\psi_t(\mathbf{x}) = \nu(\psi_t(\mathbf{x})). \quad (43)$$

Then for any path $\gamma \in \text{Lip}([0, 1], \mathbb{R}^2 \times \mathbb{S}^1)$ one has $\text{length}_{\mathcal{F}}(\psi_t \circ \gamma) \leq (1 + Ct)\text{length}_{\mathcal{F}}(\gamma)$ where $C = C(\nu, \xi)$, and where the metric \mathcal{F} is \mathcal{F}^{RS+} , $\mathcal{F}^{RS\pm}$ or \mathcal{F}^{EM} .

Proof. Define for any $t \geq 0$ the constants

$$\underline{K}(t) := \inf_{\mathbf{x} \in \mathbb{R}^2} \|(\text{d}\psi_t(\mathbf{x}))^{-1}\|^{-1}, \quad \overline{K}(t) := \sup_{\mathbf{x} \in \mathbb{R}^2} \|\text{d}\psi_t(\mathbf{x})\|, \quad K_2(t) := \sup_{\mathbf{x} \in \mathbb{R}^2} \|\text{d}^2\psi_t(\mathbf{x})\|.$$

The Taylor expansion $\psi_t(\mathbf{x}) = \mathbf{x} + t\nu(\mathbf{x}) + o(t)$ can be differentiated twice w.r.t. $\mathbf{x} \in \mathbb{R}^2$ since the two sides are C^2 smooth. This yields $\text{d}\psi_t(\mathbf{x}) = \text{Id} + t\text{d}\nu(\mathbf{x}) + o(t)$ and $\text{d}^2\psi_t(\mathbf{x}) = t\text{d}^2\nu(\mathbf{x}) + o(t)$. Hence $\underline{K}(t) = 1 + \mathcal{O}(t)$, $\overline{K}(t) = 1 + \mathcal{O}(t)$ and $K_2(t) = \mathcal{O}(t)$. Therefore the corresponding constants of Lemma 3.19 obey $K_{RS}(t) = 1 + \mathcal{O}(t)$ and $K_{EM}(t) = 1 + \mathcal{O}(t)$. Inserting these estimates into the path length expression (4), and using the Lipschitz regularity of the cost function α , we obtain the announced result. \square

The following lemma further specializes the diffeomorphisms considered, which are designed so as to offset one endpoint of a given path, and leave the other endpoint unaffected.

Lemma 3.21. *Let $\gamma : [0, 1] \rightarrow \mathbb{R}^2 \times \mathbb{S}^1$ be a Lipschitz path. Denote $\gamma(0) = (\mathbf{x}_0, \theta_0)$, $\gamma(1) := (\mathbf{x}_1, \theta_1)$, and assume that $\mathbf{x}_0 \neq \mathbf{x}_1$. Let \mathcal{F} be \mathcal{F}^{RS+} , $\mathcal{F}^{RS\pm}$ or \mathcal{F}^{EM} and let us assume that $\text{length}_{\mathcal{F}}(\gamma) < \infty$. Then there exists a family of diffeomorphisms $\psi_{\dot{\mathbf{p}}}$, $\dot{\mathbf{p}} \in \mathbb{R}^2 \times \mathbb{R}$ such that: for any sufficiently small $\dot{\mathbf{p}}$*

$$\text{length}_{\mathcal{F}}(\psi_{\dot{\mathbf{p}}} \circ \gamma) \leq (1 + \mathcal{O}(\|\dot{\mathbf{p}}\|))\text{length}_{\mathcal{F}}(\gamma), \quad \psi_{\dot{\mathbf{p}}}(\gamma(0)) = \gamma(0) + \dot{\mathbf{p}}, \quad \psi_{\dot{\mathbf{p}}}(\gamma(1)) = \gamma(1).$$

Proof. Denote $r := \|\mathbf{x}_0 - \mathbf{x}_1\| > 0$. Let $\nu_1, \nu_2, \nu_3 : \mathbb{R}^2 \rightarrow \mathbb{R}^2$ be smooth vector fields supported on $B(\mathbf{x}_0, r/2)$, and defined by $\nu_1(\mathbf{x}) = (1, 0)$, $\nu_2(\mathbf{x}) = (0, 1)$, and $\nu_3(\mathbf{x}) = \mathbf{x}_0 + (\mathbf{x} - \mathbf{x}_0)^\perp$ respectively for all $\mathbf{x} \in B(\mathbf{x}_0, r/4)$. Let ψ_t^ν denote the diffeomorphism generated by the flow at time t of a vector field ν , as defined in (43).

By construction, one has $\psi_{t_1}^{\nu_1}(\mathbf{x}, \theta) = (\mathbf{x} + (t_1, 0), \theta)$, $\psi_{t_2}^{\nu_2}(\mathbf{x}, \theta) = (\mathbf{x} + (0, t_2), \theta)$, and $\psi_{t_3}^{\nu_3}(\mathbf{x}, \theta) = (\mathbf{x}_0 + R_{t_3}(\mathbf{x} - \mathbf{x}_0), \theta + t_3)$ for any sufficiently small $t_1, t_2, t_3 \in \mathbb{R}$, for any $\mathbf{x} \in \mathbb{R}^2$ sufficiently close to \mathbf{x}_0 , and for any $\theta \in \mathbb{R}$. Also $\psi_{t_1}^{\nu_1} = \psi_{t_2}^{\nu_2} = \psi_{t_3}^{\nu_3} = \text{Id}$ on a neighborhood of \mathbf{x}_1 , for any sufficiently small t_1, t_2, t_3 . Defining $\psi_{\mathbf{p}} := \psi_{t_1}^{\nu_1} \circ \psi_{t_2}^{\nu_2} \circ \psi_{t_3}^{\nu_3}$, where $\mathbf{p} = (t_1, t_2, t_3) \in \mathbb{R}^2 \times \mathbb{R}$, and using Corollary 3.20 one obtains the announced result. \square

Points (II) and (III) of Proposition 3.3 are established in the next proposition and corollary. For that purpose, we need to distinguish a particular class of degenerate paths: we say that $\gamma : [0, 1] \rightarrow \mathbb{R}^2 \times \mathbb{S}^1$ is a *purely angular motion* iff it has the form $\gamma(t) = (\mathbf{x}, \theta(t))$, for all $t \in [0, 1]$, where $\mathbf{x} \in \mathbb{R}^2$ is a constant and $\theta : [0, 1] \rightarrow \mathbb{S}^1$ is an arbitrary function.

Proposition 3.22. *Let $\mathbf{p} \in \Omega$ and let be such that the minimal path $\gamma : [0, 1] \rightarrow \overline{\Omega}$ for $u(\mathbf{p})$ is not a purely angular motion. Assume also that $\text{int}(\overline{\Omega}) = \Omega$. Then $u(\mathbf{p}) = \hat{u}(\mathbf{p})$.*

Proof. As noted in the introduction, a minimal path γ exists by Appendix A of [CMC16] (it may be non-unique). Since γ is not a purely angular motion, there exists $t_* \in]0, 1]$ such that denoting $\mathbf{p}_0 = (\mathbf{x}_0, \theta_0) = \gamma(0)$ and $\mathbf{p}_1 = (\mathbf{x}_1, \theta_1) = \gamma(t_*)$ one has $\mathbf{x}_0 \neq \mathbf{x}_1$. Denote $\gamma_0 := \gamma|_{[0, t_*]}$ and $\gamma_1 := \gamma|_{[t_*, 1]}$. For any sufficiently small $\mathbf{p} \in \mathbb{R}^2 \times \mathbb{R}$ we may construct an admissible path from $\mathbf{p}_0 + \mathbf{p}$ to \mathbf{p}_1 , by concatenation of $\psi_{\mathbf{p}} \circ \gamma_0$ with γ_1 , where $\psi_{\mathbf{p}}$ is as defined in Lemma 3.21. If $\mathbf{p}_0 + \mathbf{p} \in \mathbb{M} \setminus \overline{\Omega}$ this implies

$$\hat{u}(\mathbf{p}) \leq \text{length}_{\mathcal{F}}(\psi_{\mathbf{p}} \circ \gamma_0) + \text{length}_{\mathcal{F}}(\gamma_1) \leq (1 + \mathcal{O}(\|\mathbf{p}\|)) \text{length}_{\mathcal{F}}(\gamma) = (1 + \mathcal{O}(\|\mathbf{p}\|))u(\mathbf{p}).$$

The assumption $\text{int}(\overline{\Omega}) = \Omega$ implies that one can find arbitrarily small $\mathbf{p} \in \mathbb{E}$ such that $\mathbf{p}_0 + \mathbf{p} \in \mathbb{M} \setminus \overline{\Omega}$, hence $\hat{u}(\mathbf{p}) \leq u(\mathbf{p})$. Finally $\hat{u}(\mathbf{p}) = u(\mathbf{p})$ since by construction $\hat{u}(\mathbf{p}) \geq u(\mathbf{p})$. \square

Corollary 3.23. *Under the assumptions of Proposition 3.3. The Reeds-Shepp forward model satisfies $u = \hat{u}$ on Ω if this domain has the shape $\Omega = U \times \mathbb{S}^1$. The Euler-Mumford model satisfies $u = \hat{u}$ on Ω .*

Proof. We only need to show that purely angular motions cannot be minimizing for the optimal control problem (6) under these assumptions, and apply Lemma 3.21. In the case where $\Omega = U \times \mathbb{S}^1$, the domain shape forbids that a purely angular motion has one endpoint in $\partial\Omega$ and the other in Ω , hence it is not even an admissible candidate path. In the Euler-Mumford case, any non-constant purely angular motion has infinite length, hence it cannot be minimizing. \square

The continuity of the value function(s) u and \hat{u} at the points where $u = \hat{u}$, announced in Proposition 3.3, follows from a simple and general argument, presented in the next lemma. Recall that u and \hat{u} are respectively BLSC and BUSC, since they are sub and super-solutions of (34), see Proposition 3.17.

Lemma 3.24. *Let (X, d) be a metric space, and let $u, \hat{u} : X \rightarrow \mathbb{R}$ be respectively LSC and USC, and obey $u \leq \hat{u}$ on X . If $\mathbf{p} \in X$ is such that $u(\mathbf{p}) = \hat{u}(\mathbf{p})$, then u and \hat{u} are continuous at \mathbf{p} .*

Proof. Let $(\mathbf{p}_n)_{n \geq 0}$ be an arbitrary sequence converging to $\mathbf{p} \in X$. Using that u is LSC, $u \leq \hat{u}$, and \hat{u} is USC, one obtains

$$u(\mathbf{p}) \leq \liminf_{n \rightarrow \infty} u(\mathbf{p}_n) \leq \limsup_{n \rightarrow \infty} \hat{u}(\mathbf{p}_n) \leq \hat{u}(\mathbf{p}).$$

If $u(\mathbf{p}) = \hat{u}(\mathbf{p})$ then the sequences $u(\mathbf{p}_n)$ and $\hat{u}(\mathbf{p}_n)$ must be converging to this common limit, which implies the announced continuity of u and \hat{u} at \mathbf{p} . \square

Finally, we discuss the case of the Dubins model. By Corollary 4.30 section V in [BCD97], one has $\hat{u}_* = u \leq \hat{u}$, hence $u = \hat{u}$ at each point of continuity of \hat{u} . The next elementary lemma, based on Baire's theorem, shows that these points are dense, which concludes the proof of Proposition 3.3. Recall that a residual set is an intersection of open dense sets, i.e. the complement of a meager set. By Baire's theorem any residual subset of a complete metric space is dense.

Lemma 3.25. *Let (X, d) be a metric space, and let $u : X \rightarrow \mathbb{R}$ be BLSC or BUSC. Then u is continuous on a residual set.*

Proof. We focus on the BLSC case, and note that the BUSC case follows by considering $-u$. Let u^* be the upper semi-continuous envelope of u , and for each $n \geq 1$ let $C_n := \{\mathbf{x} \in X; u^*(\mathbf{x}) - u(\mathbf{x}) < 1/n\}$. For any $\mathbf{x} \in X$, one has the equivalences:

$$u \text{ is continuous at } \mathbf{x} \iff u^*(\mathbf{x}) = u(\mathbf{x}) \iff \mathbf{x} \in \bigcap_{n \geq 1} C_n.$$

In the following, we fix $n \geq 1$ and establish that C_n is open and dense, hence $\bigcap_{n \geq 1} C_n$ is a residual set which concludes the proof. The openness of C_n follows from the upper semi-continuity of $u^* - u$. Assume for contradiction that C_n is not dense, hence that there exists an open ball $B(\mathbf{x}_0, r)$ on which $u^* - u \geq 1/n$ identically. Let also $M := \sup\{u(\mathbf{x}) - u(\mathbf{y}); \mathbf{x}, \mathbf{y} \in X\}$, which is finite by assumption.

Let $K > 2nM$ be an integer. We construct inductively a sequence $(\mathbf{x}_k)_{0 \leq k \leq K}$ by choosing \mathbf{x}_{k+1} such that $d(\mathbf{x}_k, \mathbf{x}_{k+1}) < r/K$ and $u(\mathbf{x}_{k+1}) > u(\mathbf{x}_k) + 1/(2n)$. This is possible since $d(\mathbf{x}_k, \mathbf{x}_0) < kr/K \leq r$, hence $\mathbf{x}_k \notin C_n$, thus $u(\mathbf{x}_k) + 1/(2n) < u^*(\mathbf{x}_k) = \limsup_{\mathbf{y} \rightarrow \mathbf{x}_k} u(\mathbf{y})$. Eventually we obtain $u(\mathbf{x}_K) - u(\mathbf{x}_0) = \sum_{i=0}^{K-1} u(\mathbf{x}_{i+1}) - u(\mathbf{x}_i) > K/(2n) \geq M$, which contradicts the definition of M . Hence C_n must be dense, and the proof is complete. \square

4 Basis reduction techniques

This section is devoted to the proof of Proposition 1.1, using techniques from lattice geometry. For that purpose, we study an optimization problem referred to as Voronoi's first reduction of quadratic forms [Sch09], using special coordinate systems known as obtuse superbases of lattices [CS92]. Similar techniques are used for the discretization on cartesian grids of anisotropic diffusion in [BOZ04, FM13], of Monge-Ampere equations in [BCM15], and of anisotropic eikonal equations in [Mir17].

For that purpose, we need to introduce some notation. Let $d \geq 1$ be the ambient dimension, $d \in \{2, 3\}$ for the applications intended in this paper. The canonical d -dimensional euclidean space, and d -dimensional integer lattice are denoted

$$\mathbb{E}_d := \mathbb{R}^d, \quad \mathbb{L}_d := \mathbb{Z}^d.$$

The dual space and dual lattice are denoted \mathbb{E}_d^* and \mathbb{L}_d^* . Thanks to the euclidean structure, there is a canonical identification $\mathbb{E}_d \cong \mathbb{E}_d^*$ and $\mathbb{L}_d \cong \mathbb{L}_d^*$, but the distinction is kept for clarity. Let $S(\mathbb{E}_d) \subseteq L(\mathbb{E}_d, \mathbb{E}_d^*)$ denote the set of symmetric linear maps, and let $S^{++}(\mathbb{E}_d) \subseteq S^+(\mathbb{E}_d) \subseteq S(\mathbb{E}_d)$ be the subsets of positive definite and semi-definite ones. To each $M \in S^{++}(\mathbb{E}_d)$ is associated a scalar product $\langle \cdot, \cdot \rangle_M$ and a norm $\|\cdot\|_M$, defined for all $\dot{\mathbf{e}}, \dot{\mathbf{f}} \in \mathbb{E}_d$ by

$$\langle \dot{\mathbf{e}}, \dot{\mathbf{f}} \rangle_M := \langle M\dot{\mathbf{e}}, \dot{\mathbf{f}} \rangle, \quad \|\dot{\mathbf{e}}\|_M := \sqrt{\langle \dot{\mathbf{e}}, \dot{\mathbf{e}} \rangle_M}.$$

Let us point out that it is equivalent, up to a linear change of coordinates, to study the geometry of an arbitrary lattice of \mathbb{E}_d w.r.t. the canonical euclidean norm, or to study the geometry of the canonical lattice \mathbb{L}_d w.r.t. the norm $\|\cdot\|_M$ induced by an arbitrary $M \in S^{++}(\mathbb{E}_d)$.

Voronoi's first reduction [Sch09] consists of a convex set $\mathcal{P} \subseteq S^{++}(\mathbb{E}_d^*)$, and for each $M \in S^{++}(\mathbb{E}_d)$ of a linear programming problem $\mathcal{L}(M)$:

$$\mathcal{P} := \{D \in S^{++}(\mathbb{E}_d^*); \forall \hat{\mathbf{v}} \in \mathbb{L}_d^* \setminus \{0\}, \|\hat{\mathbf{v}}\|_D \geq 1\}, \quad \mathcal{L}(M) := \inf_{D \in \mathcal{P}} \text{Tr}(MD). \quad (44)$$

Denote by $\langle\langle M, D \rangle\rangle := \text{Tr}(MD)$ the duality bracket between $S(\mathbb{E})$ and $S(\mathbb{E}^*)$, and observe that $\|\hat{\mathbf{v}}\|_D^2 = \langle\langle D, \hat{\mathbf{v}} \otimes \hat{\mathbf{v}} \rangle\rangle$, where $\hat{\mathbf{v}} \otimes \hat{\mathbf{v}} \in S^+(\mathbb{E}_d)$ denotes the outer product of a co-vector $\hat{\mathbf{v}} \in \mathbb{E}_d^*$ with itself. One can therefore rephrase Voronoi's optimization problem $\mathcal{L}(M)$ to make its linear structure more apparent:

$$\text{minimize } \langle\langle M, D \rangle\rangle \quad \text{subject to } \langle\langle D, \hat{\mathbf{v}} \otimes \hat{\mathbf{v}} \rangle\rangle \geq 1 \text{ for all } \hat{\mathbf{v}} \in \mathbb{L}_d^* \setminus \{0\}. \quad (45)$$

The linear program (45) was shown by Voronoi to be feasible in arbitrary dimension $d \geq 1$, in the sense that $\mathcal{L}(M)$ has a non-empty and compact set of minimizers for any $M \in S^{++}(\mathbb{E}_d)$. The Karush-Kuhn-Tucker optimality conditions for this problem read as follows: there exists non-negative weights and integral co-vectors $(\lambda_k, \hat{\mathbf{v}}_k)_{k=1}^K$, where $K = \dim S(\mathbb{E}_d) = d(d+1)/2$, such that

$$M = \sum_{k=1}^K \lambda_k \hat{\mathbf{v}}_k \otimes \hat{\mathbf{v}}_k. \quad (46)$$

This formula is reminiscent of the eigenvector-eigenvalue decomposition, but the number of terms is larger: $d(d+1)/2$ instead of d . It is used, presented perhaps slightly differently, to design monotone finite differences PDE schemes [BOZ04, FM13, Mir17]. We describe Selling's algorithm in §4.1, a constructive, simple and efficient method for solving (45). We estimate in §4.2 the largest norm of the co-vectors appearing in (46). We finally conclude in §4.3 the proof of Proposition 1.1.

4.1 Obtuse superbases and Selling's algorithm

We introduce in this section the concept of obtuse superbase of lattice, a preferred coordinate system which provides, in particular, a complete solution to Voronoi's first reduction (44), see Proposition 4.6. An obtuse superbase exists for all lattices of dimension two and three, and can be constructed using Selling's algorithm, see Proposition 4.7. The results of this subsection are mostly reformulations of [CS92, BK10], but they are prerequisites for the original results of the next subsections. Proofs are provided for completeness.

Definition 4.1. *A superbase of \mathbb{L}_d is a $(d+1)$ -plet $(\hat{\mathbf{e}}_0, \dots, \hat{\mathbf{e}}_d) \in \mathbb{L}_d^{d+1}$ such that $\hat{\mathbf{e}}_0 + \dots + \hat{\mathbf{e}}_d = 0$ and $|\det(\hat{\mathbf{e}}_0, \dots, \hat{\mathbf{e}}_d)| = 1$. A superbase is said M -obtuse, where $M \in S^{++}(\mathbb{E}_d)$, iff $\langle \hat{\mathbf{e}}_i, \hat{\mathbf{e}}_j \rangle_M \leq 0$ for all $0 \leq i < j \leq d$.*

We attach to each superbase a family of $d(d+1)$ co-vectors.

Definition 4.2. *Let $(\hat{\mathbf{e}}_0, \dots, \hat{\mathbf{e}}_d)$ be a superbase of \mathbb{L}_d . For all distinct $i, j \in \llbracket 0, d \rrbracket$, we define a co-vector $\hat{\mathbf{v}}_{ij} \in \mathbb{L}_d^*$ by the linear equalities*

$$\langle \hat{\mathbf{v}}_{ij}, \hat{\mathbf{e}}_k \rangle = \delta_{ik} - \delta_{jk}, \quad \text{for all } 0 \leq k \leq d, \quad (47)$$

Note that $\hat{\mathbf{v}}_{ij} = -\hat{\mathbf{v}}_{ji}$, and that the definition (47) of the d -dimensional co-vector $\hat{\mathbf{v}}_{ij}$ using $d + 1$ linear constraints makes sense thanks to the compatibility relation

$$\langle \hat{\mathbf{v}}_{ij}, \dot{\mathbf{e}}_0 + \cdots + \dot{\mathbf{e}}_d \rangle = \langle \hat{\mathbf{v}}_{ij}, 0 \rangle = 0, \quad \text{and } (\delta_{i0} - \delta_{j0}) + \cdots + (\delta_{id} - \delta_{jd}) = \delta_{ii} - \delta_{jj} = 0.$$

In dimension $d \in \{2, 3\}$ the construction of Definition 4.2 has a simple geometrical interpretation

$$\text{Case } d = 2 : \hat{\mathbf{v}}_{ij} = \pm \dot{\mathbf{e}}_k^\perp, \quad \text{Case } d = 3 : \hat{\mathbf{v}}_{ij} = \pm \dot{\mathbf{e}}_k \times \dot{\mathbf{e}}_l, \quad (48)$$

where (i, j, k) is a permutation of $\{0, 1, 2\}$, (resp. (i, j, k, l) of $\{0, 1, 2, 3\}$), and the \pm sign refers to its signature.

Proposition 4.3. *With the notations of Definition 4.2, $(\hat{\mathbf{v}}_{01}, \hat{\mathbf{v}}_{12}, \dots, \hat{\mathbf{v}}_{d0})$ is a superbase of \mathbb{L}_d^* .*

Proof. By construction $\langle \hat{\mathbf{v}}_{01} + \cdots + \hat{\mathbf{v}}_{d0}, \dot{\mathbf{e}}_k \rangle = 0$ for any $0 \leq k \leq d$, hence $\hat{\mathbf{v}}_{01} + \cdots + \hat{\mathbf{v}}_{d0} = 0$ as required. Furthermore using the change of basis formula for determinants one obtains

$$\det(\hat{\mathbf{v}}_{12}, \dots, \hat{\mathbf{v}}_{d0}) \det(\dot{\mathbf{e}}_1, \dots, \dot{\mathbf{e}}_d) = \det[\hat{\mathbf{v}}_{i,i+1}(\dot{\mathbf{e}}_j)]_{i,j=1}^d = \det[\delta_{i,j} - \delta_{i+1,j}]_{i,j=1}^d = 1. \quad \square$$

The next lemma describes the decomposition of a symmetric matrix M using the directions $\hat{\mathbf{v}}_{ij} \in \mathbb{L}_d^*$ attached to a superbase. As one can suspect, it is related to the KKT relations (46), see Proposition 4.6 below.

Lemma 4.4. *Let $M \in \mathbb{S}(\mathbb{E}_d)$, and let $(\dot{\mathbf{e}}_0, \dots, \dot{\mathbf{e}}_d)$ be a superbase of \mathbb{Z}^d . Then*

$$M = \sum_{i < j} \lambda_{ij} \hat{\mathbf{v}}_{ij} \otimes \hat{\mathbf{v}}_{ij}, \quad \text{where } \lambda_{ij} := -\langle \dot{\mathbf{e}}_i, M \dot{\mathbf{e}}_j \rangle \quad (49)$$

Proof. For any $i, j, k, l \in \llbracket 0, d \rrbracket$ such that $i \neq j$ and $k \neq l$, one has $\langle \hat{\mathbf{v}}_{ij}, \dot{\mathbf{e}}_k \rangle \langle \hat{\mathbf{v}}_{ij}, \dot{\mathbf{e}}_l \rangle = -1$ if $\{i, j\} = \{k, l\}$, and 0 otherwise. Hence denoting by M' the r.h.s. of (49) one has $\langle \dot{\mathbf{e}}_k, M' \dot{\mathbf{e}}_l \rangle = -\lambda_{kl} = \langle \dot{\mathbf{e}}_k, M \dot{\mathbf{e}}_l \rangle$ for all $k \neq l$. Equality also holds if $k = l$, using the identity $\dot{\mathbf{e}}_k = -\sum_{i \neq k} \dot{\mathbf{e}}_i$. Since $(\dot{\mathbf{e}}_1, \dots, \dot{\mathbf{e}}_d)$ is a basis of \mathbb{E}_d , this implies $M = M'$ as announced. \square

The following lemma attaches to any superbase b of \mathbb{L}_d a *vertex* D_b of the polytope \mathcal{P} , defined in (44). Vertices of \mathcal{P} are referred to as *perfect forms*, and play a central role in lattice geometry [Sch09]. Voronoi proved that the polytope \mathcal{P} has only finitely many distinct equivalence classes of vertices under the action of linear changes of coordinates preserving the lattice \mathbb{L}_d , see [Sch09]. The perfect forms $\{D_b; b \text{ superbase of } \mathbb{L}_d\}$ are such a class, and in fact are the only one³ in dimension $d \leq 3$.

Lemma 4.5. *Let $b = (\dot{\mathbf{e}}_0, \dots, \dot{\mathbf{e}}_d)$ be a superbase of \mathbb{L}_d , and let*

$$D_b := \frac{1}{2^d} \sum_{I \subseteq \llbracket 0, d \rrbracket} \dot{\mathbf{e}}_I \otimes \dot{\mathbf{e}}_I, \quad \text{where } \dot{\mathbf{e}}_I := \sum_{i \in I} \dot{\mathbf{e}}_i.$$

Then $\|\hat{\mathbf{v}}_{ij}\|_{D_b} = 1$ for all $0 \leq i < j \leq d$ and $\|\hat{\mathbf{v}}\|_{D_b} \geq 1$ for any $\hat{\mathbf{v}} \in \mathbb{L}_d^ \setminus \{0\}$. In particular D_b is a vertex of the polytope $\mathcal{P} \subseteq \mathbb{S}(\mathbb{E}_d)$, at the intersection of the facets defined by $\{D \in \mathcal{P}; \langle D, \hat{\mathbf{v}}_{ij} \otimes \hat{\mathbf{v}}_{ij} \rangle = 1\}$, $i, j \in \llbracket 0, d \rrbracket$.*

³Indeed, as shown below, the minimum (44) of the linear program $\mathcal{L}(M)$ on K is always attained at a matrix D_b attached to a superbase b .

Proof. Let $\delta_i^I = 1$ if $i \in I$ and $\delta_i^I = 0$ otherwise, for any $i \in \llbracket 0, d \rrbracket$ and $I \subseteq \llbracket 0, d \rrbracket$. Clearly $(\delta_i^I)^2 = \delta_i^I$, and for any pairwise distinct $i_0, \dots, i_k \in \llbracket 0, d \rrbracket$ one has

$$\sum_{I \subseteq \llbracket 0, d \rrbracket} \delta_{i_0}^I \cdots \delta_{i_k}^I = \#\{I \subseteq \llbracket 0, d \rrbracket; \{i_0, \dots, i_k\} \subseteq I\} = 2^{d-k}.$$

Hence for any pairwise distinct $i, j, k, l \in \llbracket 0, d \rrbracket$, noting that $\langle \hat{\mathbf{v}}_{ij}, \dot{\mathbf{e}}_I \rangle = \delta_i^I - \delta_j^I$ for any $I \subseteq \llbracket 0, d \rrbracket$,

$$2^d \langle \hat{\mathbf{v}}_{ij}, \hat{\mathbf{v}}_{ik} \rangle_{D_b} = \sum_{I \subseteq \llbracket 0, d \rrbracket} (\delta_i^I - \delta_j^I)(\delta_i^I - \delta_k^I) = \sum_{I \subseteq \llbracket 0, d \rrbracket} (\delta_i^I - \delta_j^I \delta_j^I - \delta_i^I \delta_k^I + \delta_j^I \delta_k^I) = 2^d - 2^{d-1} - 2^{d-1} + 2^{d-1}.$$

This establishes $\langle \hat{\mathbf{v}}_{ij}, \hat{\mathbf{v}}_{ik} \rangle_{D_b} = 1/2$. Likewise $\langle \hat{\mathbf{v}}_{ij}, \hat{\mathbf{v}}_{kl} \rangle_{D_b} = 0$, and $\|\hat{\mathbf{v}}_{ij}\|_{D_b}^2 = \langle \hat{\mathbf{v}}_{ij}, \hat{\mathbf{v}}_{ij} \rangle_{D_b} = 1$ as announced. Since $(\hat{\mathbf{v}}_{12}, \dots, \hat{\mathbf{v}}_{d0})$ is a basis of \mathbb{L}_d^* , see Proposition 4.3, we obtain by bilinearity that $\|\hat{\mathbf{v}}\|_{D_b}^2 \in \mathbb{Z}$ for all $\hat{\mathbf{v}} \in \mathbb{L}_d^*$. Since D_b is positive definite, one has $\|\hat{\mathbf{v}}\|_{D_b} > 0$ for all $\hat{\mathbf{v}} \in \mathbb{E}_d^* \setminus \{0\}$, hence $\|\hat{\mathbf{v}}\|_{D_b} \geq 1$ for all $\hat{\mathbf{v}} \in \mathbb{L}_d^* \setminus \{0\}$ as announced.

By definition $D_b \in \mathcal{P}$, and D_b obeys the $d(d+1)/2 = \dim \mathbb{S}(\mathbb{E}_d)$ linear equalities $\langle\langle D_b, \hat{\mathbf{v}}_{ij} \otimes \hat{\mathbf{v}}_{ij} \rangle\rangle = 1$, for all $0 \leq i < j \leq d$, which are linearly independent by Lemma 4.4. Thus D_b is a vertex of \mathcal{P} . \square

The two previous lemmas, combined, yield a complete solution to the optimization problem (44), when an M -obtuse superbase is known.

Proposition 4.6. *Let $M \in \mathbb{S}^{++}(\mathbb{E}_d)$, and let us assume that there exists an M -obtuse superbase b of \mathbb{L}_d . Then D_b is a minimizer of $\mathcal{L}(M)$, and applying Lemma 4.4 to the basis b yields the explicit value $\mathcal{L}(M) = \sum_{i < j} \lambda_{ij}$, as well as an optimality certificate: the Karush-Kuhn-Tucker conditions are (49, left).*

Proof. Clearly $D_b \in \mathcal{P}$, and for any $D \in \mathcal{P}$ one has $\langle M, D - D_b \rangle = \sum_{i < j} \lambda_{ij} (\langle\langle D, \hat{\mathbf{v}}_{ij} \otimes \hat{\mathbf{v}}_{ij} \rangle\rangle - \langle\langle D_b, \hat{\mathbf{v}}_{ij} \otimes \hat{\mathbf{v}}_{ij} \rangle\rangle) = \sum_{i < j} \lambda_{ij} (\|\hat{\mathbf{v}}_{ij}\|_D^2 - 1) \geq 0$. The result follows. \square

The previous proposition leaves open the question of existence of an M -obtuse superbase b , given $M \in \mathbb{S}^{++}(\mathbb{E}_d)$. In dimension $d \in \{2, 3\}$, such a b always exists, and can be constructed via Selling's algorithm [Sel74] which is implemented "as is" in our numerical experiments §5. Note that this algorithm could in principle be accelerated by a preliminary basis reduction step [Ngu04], but the advantage is only visible for extremely large condition numbers, which are irrelevant for applications to anisotropic PDEs.

Proposition 4.7 (Selling's algorithm). *Let $M \in \mathbb{S}^{++}(\mathbb{E}_d)$, where $d \in \{2, 3\}$, and let $b = (\dot{\mathbf{e}}_0, \dots, \dot{\mathbf{e}}_d)$ be a superbase of \mathbb{L}^d . Define a second superbase b' of \mathbb{L}_d by*

$$\text{Case } d = 2 : b' := (-\dot{\mathbf{e}}_0, \dot{\mathbf{e}}_1, \dot{\mathbf{e}}_0 - \dot{\mathbf{e}}_1), \quad \text{Case } d = 3 : b' := (-\dot{\mathbf{e}}_0, \dot{\mathbf{e}}_1, \dot{\mathbf{e}}_0 + \dot{\mathbf{e}}_2, \dot{\mathbf{e}}_0 + \dot{\mathbf{e}}_3).$$

Then $\text{Tr}(MD_b) - \text{Tr}(MD_{b'}) = 2^{2-d} \langle \dot{\mathbf{e}}_0, \dot{\mathbf{e}}_1 \rangle_M$. Selling's algorithm consists in iteratively, and until b is an M -obtuse superbase: (a) reordering the superbase b so that $\langle \dot{\mathbf{e}}_0, \dot{\mathbf{e}}_1 \rangle_M > 0$, and (b) applying the transformation $b \leftarrow b'$.

This algorithm terminates, and in particular there exists an M -obtuse superbase of \mathbb{L}_d .

Proof. Applying Definition 4.1 we find that b' is indeed a superbase of \mathbb{L}_d . The expression of $\text{Tr}(MD_b) - \text{Tr}(MD_{b'})$ follows from a direct computation. Denoting by b_n be the superbase

obtained at the n -th step of Selling's algorithm, one observes that $\text{Tr}(MD_{b_n})$ strictly decreases as n increases by construction. In view of

$$2^d \text{Tr}(MD_b) = \sum_{I \subseteq \{0, \dots, d\}} \|\dot{\mathbf{e}}_I\|_M^2 \geq \sum_{0 \leq i \leq d} \|\dot{\mathbf{e}}_i\|_M^2$$

we observe that there are only finitely many superbases $b = (\dot{\mathbf{e}}_0, \dots, \dot{\mathbf{e}}_d) \in \mathbb{L}_d^d$ such that $\text{Tr}(MD_b)$ is below any given bound, hence Selling's algorithm must terminate, and the result follows. \square

A closer inspection shows that Selling's algorithm is equivalent to the Simplex algorithm applied to the linear program (45). Selling's algorithm is also described in Appendix B of [BK10]. In dimension $d = 2$, Selling's algorithm is equivalent to exploring the an arithmetic structure named the Stern-Brocot tree, see [BOZ04] for details on this approach and an application to HJB PDEs.

4.2 Radius of the decomposition

We bound in this section the norm of the integral co-vectors involved in the matrix decomposition (46). Our estimate is sharper than the one presented in [Mir17], which has significant consequences on the convergence analysis §3, see the discussion after Theorem 4.11. The results of this subsection and of the next are new to the author's knowledge.

Our first step is to upper bound the norm of the elements of an M -obtuse superbase.

Proposition 4.8. *Let $M \in \mathbb{S}_d^{++}$ and let $b = (\dot{\mathbf{e}}_0, \dots, \dot{\mathbf{e}}_d)$ be an M -obtuse superbase (if one exists). Then $\|\dot{\mathbf{e}}_i\| \leq C \text{Cond}(M)$, for each $0 \leq i \leq d$, where $C_d := \sqrt{2^{d-1}d}$ and $\text{Cond}(M) := \sqrt{\|M\| \|M^{-1}\|}$.*

Proof. Denote by λ_{\min}^2 and λ_{\max}^2 the smallest and largest eigenvalues of M . Observe that $2^d D_b \succeq \dot{\mathbf{e}}_i \otimes \dot{\mathbf{e}}_i + (-\dot{\mathbf{e}}_i) \otimes (-\dot{\mathbf{e}}_i) = 2\mathbf{e}_i \otimes \dot{\mathbf{e}}_i$, where $A \succeq B$ means that $A - B \in \mathbb{S}^+(\mathbb{E}_d)$. Observe also that $\text{Id}, D_b \in \mathcal{P}$, and that D_b is optimal for (45). Thus, as announced

$$\lambda_{\min}^2 \|\dot{\mathbf{e}}_i\|^2 \leq \|\dot{\mathbf{e}}_i\|_M^2 \leq 2^{d-1} \text{Tr}(MD_b) \leq 2^{d-1} \text{Tr}(M \text{Id}) \leq 2^{d-1} d \lambda_{\max}^2. \quad \square$$

In order to proceed, we recall some identities relating the scalar products associated to M and $D := M^{-1}$, where $M \in \mathbb{S}^{++}(\mathbb{E}_d)$. For any $\dot{\mathbf{e}}_0, \dot{\mathbf{e}}_1, \dot{\mathbf{e}}_2 \in \mathbb{E}_d$

$$\text{If } d = 2 \quad (\det M) \langle \dot{\mathbf{e}}_0^\perp, \dot{\mathbf{e}}_1^\perp \rangle_D = \langle \dot{\mathbf{e}}_0, \dot{\mathbf{e}}_1 \rangle_M, \quad (50)$$

$$\text{If } d = 3 \quad (\det M) \langle \dot{\mathbf{e}}_0 \times \dot{\mathbf{e}}_1, \dot{\mathbf{e}}_0 \times \dot{\mathbf{e}}_2 \rangle_D = \|\dot{\mathbf{e}}_0\|_M^2 \langle \dot{\mathbf{e}}_1, \dot{\mathbf{e}}_2 \rangle_M - \langle \dot{\mathbf{e}}_0, \dot{\mathbf{e}}_1 \rangle_M \langle \dot{\mathbf{e}}_0, \dot{\mathbf{e}}_2 \rangle_M, \quad (51)$$

where \times denotes the cross product of three dimensional vectors. These identities are easily checked when $M = \text{Id}$, and otherwise follow from a change of variables by $M^{\frac{1}{2}}$.

In the next two propositions, we investigate the geometrical properties relating a superbase $(\dot{\mathbf{e}}_0, \dots, \dot{\mathbf{e}}_d)$ of \mathbb{L}_d with the dual superbase $(\hat{\mathbf{v}}_{01}, \hat{\mathbf{v}}_{12}, \dots, \hat{\mathbf{v}}_{d0})$ introduced in Proposition 4.3. Proposition 4.10 is in particular a new and original technical argument.

Proposition 4.9. *Let $(\dot{\mathbf{e}}_0, \dot{\mathbf{e}}_1, \dot{\mathbf{e}}_2)$ be an M -obtuse superbase of \mathbb{L}_2 , where $M \in \mathbb{S}^{++}(\mathbb{E}_2)$. Then $(\hat{\mathbf{v}}_{01}, \hat{\mathbf{v}}_{12}, \hat{\mathbf{v}}_{20})$ is a D -obtuse superbase of \mathbb{L}_2^* , where $D := M^{-1}$.*

Proof. By (48) the dual superbase is $(\dot{\mathbf{e}}_2^\perp, \dot{\mathbf{e}}_0^\perp, \dot{\mathbf{e}}_1^\perp)$, and the result follows from (50). \square

Proposition 4.10. *Let $b = (\dot{\mathbf{e}}_0, \dot{\mathbf{e}}_1, \dot{\mathbf{e}}_2, \dot{\mathbf{e}}_3)$ be an M -obtuse superbase of \mathbb{L}_3 , where $M \in \mathbb{S}^{++}(\mathbb{E}_3)$. Then at least one of $\hat{b}_0 := (\hat{\mathbf{v}}_{01}, \hat{\mathbf{v}}_{12}, \hat{\mathbf{v}}_{23}, \hat{\mathbf{v}}_{30})$, $\hat{b}_1 := (\hat{\mathbf{v}}_{01}, \hat{\mathbf{v}}_{13}, \hat{\mathbf{v}}_{32}, \hat{\mathbf{v}}_{20})$, and $\hat{b}_2 := (\hat{\mathbf{v}}_{02}, \hat{\mathbf{v}}_{21}, \hat{\mathbf{v}}_{13}, \hat{\mathbf{v}}_{30})$ is a D -obtuse superbase of \mathbb{L}_3^* , where $D := M^{-1}$.*

Proof. All three of \hat{b}_0, \hat{b}_1 and \hat{b}_2 are superbases of \mathbb{L}_3^* , by applying Proposition 4.3 to permutations of b . One has $\langle \hat{\mathbf{v}}_{ij}, \hat{\mathbf{v}}_{jk} \rangle_D = \langle \hat{\mathbf{e}}_k \times \hat{\mathbf{e}}_l, \hat{\mathbf{e}}_i \times \hat{\mathbf{e}}_l \rangle_D \leq 0$ by (48) and (51), and by the M -obtuseness of b , whenever $\{i, j, k, l\} = \{0, 1, 2, 3\}$. The remaining scalar products of interest are

$$\alpha_0 := \langle \hat{\mathbf{v}}_{13}, \hat{\mathbf{v}}_{20} \rangle_D, \quad \alpha_1 := \langle \hat{\mathbf{v}}_{12}, \hat{\mathbf{v}}_{03} \rangle_D, \quad \alpha_2 := \langle \hat{\mathbf{v}}_{01}, \hat{\mathbf{v}}_{23} \rangle_D.$$

Recalling that $\hat{\mathbf{v}}_{ij} = -\hat{\mathbf{v}}_{ji}$ for any $i \neq j$ one observes the following: if $\alpha_1 \geq 0 \geq \alpha_2$ then \hat{b}_0 is D -obtuse, if $\alpha_2 \geq 0 \geq \alpha_0$ then \hat{b}_1 is D -obtuse, and if $\alpha_0 \geq 0 \geq \alpha_1$ then \hat{b}_2 is D -obtuse. On the other hand, expressing $(\alpha_i)_{i=0}^2$ in terms of cross products yields

$$\alpha_0 := \langle \hat{\mathbf{e}}_2 \times \hat{\mathbf{e}}_0, \hat{\mathbf{e}}_1 \times \hat{\mathbf{e}}_3 \rangle, \quad \alpha_1 := \langle \hat{\mathbf{e}}_0 \times \hat{\mathbf{e}}_3, \hat{\mathbf{e}}_1 \times \hat{\mathbf{e}}_2 \rangle, \quad \alpha_2 := \langle \hat{\mathbf{e}}_2 \times \hat{\mathbf{e}}_3, \hat{\mathbf{e}}_0 \times \hat{\mathbf{e}}_1 \rangle,$$

and inserting the identity $\hat{\mathbf{e}}_0 := -(\hat{\mathbf{e}}_1 + \hat{\mathbf{e}}_2 + \hat{\mathbf{e}}_3)$ in the above expressions one obtains that $\alpha_0 + \alpha_1 + \alpha_2 = 0$. Therefore these three scalars cannot have the same sign strictly. Thus in the sequence $\alpha_0, \alpha_1, \alpha_2, \alpha_0$ there is at least one non-negative scalar α_i followed with a non-positive scalar α_{i+1} , where indices are understood modulo 3. By the previous argument, \hat{b}_{i-1} is D -obtuse, and the announced result follows. \square

In the rest of this section, we denote by C_d the constant of Proposition 4.8.

Theorem 4.11. *Let $(\hat{\mathbf{e}}_0, \dots, \hat{\mathbf{e}}_d)$ be an M -obtuse superbase of \mathbb{Z}^d , where $M \in S^{++}(\mathbb{E}_d)$ and $d \in \{2, 3\}$. Then $\|\hat{\mathbf{v}}_{ij}\| \leq 2C_d \text{Cond}(M)$ for all $i \neq j$.*

Proof. Case $d = 2$. By Propositions 4.8 and 4.9, one has $\|\hat{\mathbf{v}}_{ij}\| \leq C_d \text{Cond}(D) = C_d \text{Cond}(M)$ as announced (the factor 2 is here useless). Case $d = 3$. By Propositions 4.8 and 4.10, assuming w.l.o.g. that \hat{b}_0 is D -obtuse, the co-vectors $\hat{\mathbf{v}}_{01}, \hat{\mathbf{v}}_{12}, \hat{\mathbf{v}}_{23}, \hat{\mathbf{v}}_{30}$ have their norm bounded by $C_d \text{Cond}(D) = C_d \text{Cond}(M)$. The remaining two co-vectors $\hat{\mathbf{v}}_{02}$ and $\hat{\mathbf{v}}_{13}$ can be expressed as:

$$\hat{\mathbf{v}}_{13} = \hat{\mathbf{e}}_2 \times \hat{\mathbf{e}}_0 = \hat{\mathbf{e}}_2 \times (-\hat{\mathbf{e}}_1 - \hat{\mathbf{e}}_2 - \hat{\mathbf{e}}_3) = -\hat{\mathbf{e}}_2 \times \hat{\mathbf{e}}_1 - \hat{\mathbf{e}}_2 \times \hat{\mathbf{e}}_3 = \hat{\mathbf{v}}_{30} + \hat{\mathbf{v}}_{01},$$

and likewise $\hat{\mathbf{v}}_{02} = \hat{\mathbf{v}}_{01} + \hat{\mathbf{v}}_{12}$. Thus $\|\hat{\mathbf{v}}_{13}\| \leq \|\hat{\mathbf{v}}_{30}\| + \|\hat{\mathbf{v}}_{01}\| \leq 2C_d \text{Cond}(M)$, and likewise $\|\hat{\mathbf{v}}_{02}\| \leq 2C_d \text{Cond}(M)$. The announced result follows. \square

Our next result describes a non-negative, lattice-adapted decomposition of symmetric tensors. It coincides with the one considered in Proposition 1.1 of [Mir17], up to the stencils radius estimate which is sharper: linear on the condition number of M , instead of quadratic $\|\hat{\mathbf{v}}\| \leq C \text{Cond}(M)^2$ in dimension 3. This improvement has theoretical consequences, since the assumption $h_n/\varepsilon_n \rightarrow 0$ in Theorem 3.1 would otherwise need to be replaced with the stronger (and unrealistic in applications) assumption $h_n/\varepsilon_n^2 \rightarrow 0$. PDE schemes of small stencil size are appreciated in numerical implementations, for reasons of robustness, accuracy, implementation of boundary conditions, or parallelization potential.

Corollary 4.12. *Let $M \in S^{++}(\mathbb{E}_d)$, where $d \in \{2, 3\}$. Then there exists non-negative weights $\rho_{\hat{\mathbf{v}}}(M)$, supported on at most $d(d+1)/2$ elements $\hat{\mathbf{v}} \in \mathbb{L}_d^*$, such that*

$$\sum_{\hat{\mathbf{v}} \in \mathbb{L}_d^*} \rho_{\hat{\mathbf{v}}}(M) \hat{\mathbf{v}} \otimes \hat{\mathbf{v}} = M. \quad (52)$$

Furthermore, $\|\hat{\mathbf{v}}\| \leq 2C_d \text{Cond}(M)$ whenever $\rho_{\hat{\mathbf{v}}}(M) > 0$, and $\sum_{\hat{\mathbf{v}} \in \mathbb{L}_d^} \rho_{\hat{\mathbf{v}}}^\varepsilon(\hat{\mathbf{n}}) \|\hat{\mathbf{v}}\|^2 = \text{Tr}(M)$.*

Proof. By Proposition 4.7 there exists an M -obtuse superbase, by Lemma 4.4 it yields a decomposition of the announced form (53), and by Theorem 4.11 the norms of the support co-vectors are bounded as announced. The last identity follows by taking the trace of (52). \square

Corollary 4.13. *Let $d \in \{2, 3\}$, let $0 < \varepsilon \leq 1$, and let $\hat{\mathbf{n}} \in \mathbb{E}_d^*$ such that $\|\hat{\mathbf{n}}\| = 1$. Then there exists non-negative weights $\rho_{\hat{\mathbf{v}}}^\varepsilon(\hat{\mathbf{n}})$, supported on at most $d(d+1)/2$ elements $\hat{\mathbf{v}} \in \mathbb{L}_d^*$, such that*

$$\forall \dot{\mathbf{p}} \in \mathbb{E}_d, \quad \sum_{\hat{\mathbf{v}} \in \mathbb{L}_d^*} \rho_{\hat{\mathbf{v}}}^\varepsilon(\hat{\mathbf{n}}) \langle \hat{\mathbf{v}}, \dot{\mathbf{p}} \rangle^2 = \langle \hat{\mathbf{n}}, \dot{\mathbf{p}} \rangle^2 + \varepsilon^2 (\|\dot{\mathbf{p}}\|^2 - \langle \hat{\mathbf{n}}, \dot{\mathbf{p}} \rangle^2). \quad (53)$$

Furthermore $\|\hat{\mathbf{v}}\| \leq 2C_d \varepsilon^{-1}$ whenever $\rho_{\hat{\mathbf{v}}}^\varepsilon(\hat{\mathbf{n}}) > 0$, and $\sum \rho_{\hat{\mathbf{v}}}^\varepsilon(\hat{\mathbf{n}}) \|\hat{\mathbf{v}}\|^2 = 1 + \varepsilon^2(d-1)$.

Proof. Apply Corollary 4.12 to $M = \hat{\mathbf{n}} \otimes \hat{\mathbf{n}} + \varepsilon^2(\text{Id} - \hat{\mathbf{n}} \otimes \hat{\mathbf{n}}) \in \text{S}^{++}(\mathbb{E}_d)$, which eigenvalues are 1 with eigenvector $\hat{\mathbf{n}}$, and ε^2 with multiplicity $d-1$, thus $\text{Cond}(M) = \varepsilon^{-1}$. \square

4.3 Taking positive parts of linear forms

We conclude in this section the proof of Proposition 1.1. Our main technical result, presented below, shows how to use decompositions of anisotropic symmetric positive definite tensors, as in Corollary 4.13, to build approximations of positive parts of linear forms.

Proposition 4.14. *Let $\hat{\mathbf{n}} \in \mathbb{E}_d^*$ with $\|\hat{\mathbf{n}}\| = 1$, and let $\varepsilon > 0$. Let $\hat{\mathbf{v}}_1, \dots, \hat{\mathbf{v}}_K \in \mathbb{E}_d^*$ and $\rho_1, \dots, \rho_K \geq 0$ be such that for all $\dot{\mathbf{p}} \in \mathbb{E}^d$*

$$\sum_{1 \leq k \leq K} \rho_k \langle \hat{\mathbf{v}}_k, \dot{\mathbf{p}} \rangle^2 = \langle \hat{\mathbf{n}}, \dot{\mathbf{p}} \rangle^2 + \varepsilon^2 (\|\dot{\mathbf{p}}\|^2 - \langle \hat{\mathbf{n}}, \dot{\mathbf{p}} \rangle^2). \quad (54)$$

Assume that⁴ $\langle \hat{\mathbf{v}}_k, \hat{\mathbf{n}} \rangle \geq 0$ for each $1 \leq k \leq K$. Then for all $\dot{\mathbf{p}} \in \mathbb{E}_d$ one has

$$\langle \hat{\mathbf{n}}, \dot{\mathbf{p}} \rangle_+^2 \leq \sum_{1 \leq k \leq K} \rho_k \langle \hat{\mathbf{v}}_k, \dot{\mathbf{p}} \rangle_+^2 \leq \langle \hat{\mathbf{n}}, \dot{\mathbf{p}} \rangle_+^2 + \varepsilon^2 (\|\dot{\mathbf{p}}\|^2 - \langle \hat{\mathbf{n}}, \dot{\mathbf{p}} \rangle^2). \quad (55)$$

Proof. In this proof, we identify \mathbb{E}_d with its dual \mathbb{E}_d^* thanks to the euclidean structure, and thus drop the “dot” and “hat” superscripts on vectors and co-vectors for clarity. We assume that $\rho_k = 1$, for all $1 \leq k \leq K$, up to replacing \mathbf{v}_k with $\sqrt{\rho_k} \mathbf{v}_k$.

Denote by $\mathbf{v}_k^* := \mathbf{v}_k - \langle \mathbf{v}_k, \mathbf{n} \rangle \mathbf{n}$ the orthogonal projection of \mathbf{v}_k on the hyperplane orthogonal to \mathbf{n} , where $1 \leq k \leq K$. Then by (54)

$$\sum_{1 \leq k \leq K} \langle \mathbf{n}, \mathbf{v}_k \rangle^2 = 1, \quad \sum_{1 \leq k \leq K} \mathbf{v}_k^* \otimes \mathbf{v}_k^* = \varepsilon^2 (\text{Id} - \mathbf{n} \otimes \mathbf{n}).$$

The proof of (55) is split into two parts, depending on the sign of $\langle \mathbf{n}, \mathbf{p} \rangle$. If $\langle \mathbf{n}, \mathbf{p} \rangle \leq 0$, then $\langle \mathbf{v}_k, \mathbf{p} \rangle = \langle \mathbf{v}_k, \mathbf{n} \rangle \langle \mathbf{n}, \mathbf{p} \rangle + \langle \mathbf{v}_k^*, \mathbf{p} \rangle \leq \langle \mathbf{v}_k^*, \mathbf{p} \rangle$ for all $1 \leq k \leq K$, thus as announced

$$\sum_{1 \leq k \leq K} \langle \mathbf{v}_k, \mathbf{p} \rangle_+^2 \leq \sum_{1 \leq k \leq K} \langle \mathbf{v}_k^*, \mathbf{p} \rangle_+^2 \leq \sum_{1 \leq k \leq K} \langle \mathbf{v}_k^*, \mathbf{p} \rangle^2 = \varepsilon^2 (\|\mathbf{p}\|^2 - \langle \mathbf{n}, \mathbf{p} \rangle^2).$$

In contrary if $\langle \mathbf{n}, \mathbf{p} \rangle \geq 0$, then the second inequality of (55) is immediate. In addition $\langle \mathbf{v}_k, \mathbf{p} \rangle_+^2 \geq \langle \mathbf{v}_k, \mathbf{p} \rangle^2 - \langle \mathbf{v}_k^*, \mathbf{p} \rangle^2$ for any $1 \leq k \leq K$. (Indeed, if $\langle \mathbf{v}_k, \mathbf{p} \rangle \geq 0$ then $\langle \mathbf{v}_k, \mathbf{p} \rangle_+^2 = \langle \mathbf{v}_k, \mathbf{p} \rangle^2 \geq \langle \mathbf{v}_k, \mathbf{p} \rangle^2 - \langle \mathbf{v}_k^*, \mathbf{p} \rangle^2$, and in contrary if $\langle \mathbf{v}_k, \mathbf{p} \rangle \leq 0$ then $0 \geq \langle \mathbf{v}_k, \mathbf{p} \rangle = \langle \mathbf{v}_k, \mathbf{n} \rangle \langle \mathbf{n}, \mathbf{p} \rangle + \langle \mathbf{v}_k^*, \mathbf{p} \rangle \geq \langle \mathbf{v}_k^*, \mathbf{p} \rangle$, thus $\langle \mathbf{v}_k, \mathbf{p} \rangle_+^2 = 0 \geq \langle \mathbf{v}_k, \mathbf{p} \rangle^2 - \langle \mathbf{v}_k^*, \mathbf{p} \rangle^2$.) Hence, we conclude

$$\sum_{1 \leq k \leq K} \langle \mathbf{v}_k, \mathbf{p} \rangle_+^2 \geq \sum_{1 \leq k \leq K} (\langle \mathbf{v}_k, \mathbf{p} \rangle^2 - \langle \mathbf{v}_k^*, \mathbf{p} \rangle^2) = (\langle \hat{\mathbf{n}}, \dot{\mathbf{p}} \rangle^2 + \varepsilon^2 \|\mathbf{p}^*\|^2) - \varepsilon^2 \|\mathbf{p}^*\|^2 = \langle \mathbf{n}, \mathbf{p} \rangle^2,$$

where we denoted $\mathbf{p}^* := \mathbf{p} - \langle \mathbf{p}, \mathbf{n} \rangle \mathbf{n}$, so that $\|\mathbf{p}^*\|^2 = \|\dot{\mathbf{p}}\|^2 - \langle \hat{\mathbf{n}}, \dot{\mathbf{p}} \rangle^2$. \square

⁴The scalar product $\langle \hat{\mathbf{v}}_k, \hat{\mathbf{n}} \rangle$ makes sense thanks to the euclidean structure on \mathbb{E}_d and \mathbb{E}_d^* .

Combining Corollary 4.13 with Proposition 4.14 we conclude the proof of Proposition 1.1, thanks to the following two remarks. (I) The assumption $\langle \hat{\mathbf{v}}_k, \hat{\mathbf{n}} \rangle \geq 0$ for all $0 \leq k \leq K$ in Proposition 4.14 is not restrictive, since one can always replace $\hat{\mathbf{v}}_k$ with its opposite $-\hat{\mathbf{v}}_k$ without incidence on (54). (II) The roles of \mathbb{E}_d and \mathbb{E}_d^* are exchanged in Proposition 1.1.

5 Numerical experiments

This section is devoted to a numerical validation of the proposed PDE schemes, and to an illustration of their potential applications. For validation, compare in §5.1 the geodesics obtained via direct resolution of the the Hamilton equations against the results of our PDE discretization. A second validation, discussed in §A, is based on numerical counterparts of the control sets of Figure 2. We investigate applications to motion planning in §5.2, and to vessel tracking in medical data in §5.3. The test cases presented in this paper are based on synthetic data. Experiments closer to applications and involving real data will be the subject of future work.

Free and open source numerical codes for reproducing (most of) the numerical experiments, as well as additional examples, are available on the author’s webpage⁵.

5.1 Comparison with geodesic shooting

Consider a model with a smooth Hamiltonian \mathcal{H} , such as the reversible Reeds-Shepp model or the Euler-Mumford model. Minimal paths are known to obey⁶ the Hamilton equations of geodesics, which read

$$\frac{d\mathbf{p}}{dt} = -\frac{\partial \mathcal{H}}{\partial \hat{\mathbf{p}}}, \quad \frac{d\hat{\mathbf{p}}}{dt} = \frac{\partial \mathcal{H}}{\partial \mathbf{p}}, \quad (56)$$

where $\mathbf{p}(t)$ and $\hat{\mathbf{p}}(t)$ are respectively the state and the co-state of the geodesic at time $t \in [0, 1]$. Given an initial point \mathbf{p}_0 , and a target point \mathbf{p}_1 , one can try to adjust the initial co-state $\hat{\mathbf{p}}_0$ so that the solution to (56) starting from $(\mathbf{p}(0), \hat{\mathbf{p}}(0)) = (\mathbf{p}_0, \hat{\mathbf{p}}_0)$ satisfies $\mathbf{p}(1) = \mathbf{p}_1$. We tried this procedure, referred to as geodesic shooting, using a fourth order Runge-Kutta method for solving (56) in our experiments, and a Newton method for adjusting $\hat{\mathbf{p}}_0$.

Another approach to the computation of geodesics is to numerically solve the PDE (7), and then extract the minimal geodesics as streamlines of the geodesic flow (9). We use a second order Euler scheme for that latter ODE, together with the following upwind estimate of the flow direction $d\mathcal{H}_{\mathbf{p}}(du(\mathbf{p}))$, where $\mathbf{p} \in \mathbb{M}$. Assume that the local hamiltonian $\mathcal{H}_{\mathbf{p}}$ is approximated in the following form

$$H(\hat{\mathbf{p}}) = \frac{1}{2} \sum_{1 \leq k \leq K} \rho_k \langle \hat{\mathbf{p}}, \dot{\mathbf{e}}_k \rangle_+^2. \quad (57)$$

Differentiating we obtain the first order approximation

$$dH(\hat{\mathbf{p}}) = \sum_{1 \leq k \leq K} \rho_k \langle \hat{\mathbf{p}}, \dot{\mathbf{e}}_k \rangle_+ \dot{\mathbf{e}}_k, \quad \text{thus} \quad d\mathcal{H}_{\mathbf{p}}(du(\mathbf{p})) \approx \sum_{1 \leq k \leq K} \rho_k \left(\frac{u(\mathbf{p}) - u(\mathbf{p} - h\dot{\mathbf{e}}_k)}{h} \right)_+ \dot{\mathbf{e}}_k.$$

Let us mention that our numerical codes also implement a second backtracing method, inspired by the diffuse numerical geodesics described in [BCPS10], and which yields similar results. However we observed that many alternative backtracing methods did (often) fail, in particular with the Dubins model, due to the discontinuity of value function u .

⁵github.com/Mirebeau/HamiltonFastMarching

⁶Except perhaps *abnormal* geodesics, which we do not discuss here, see [Mon06].

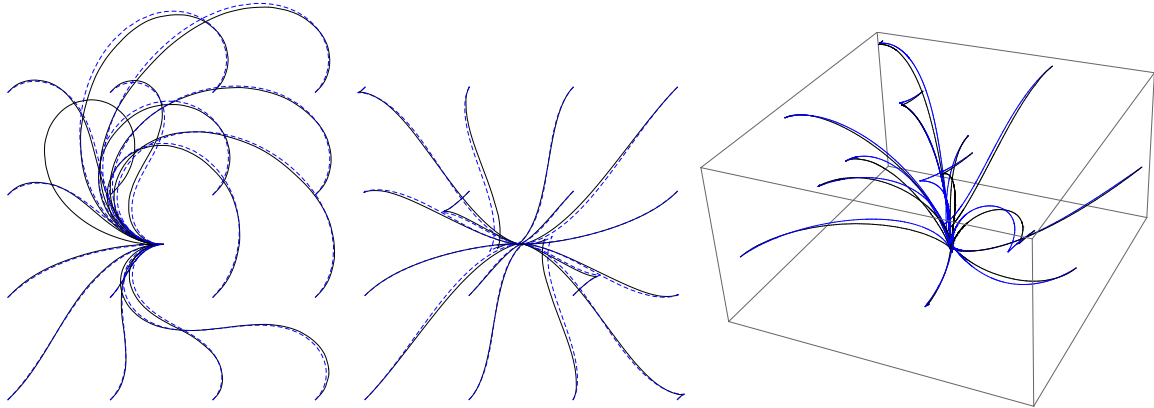


Figure 4: Comparison of Minimal geodesics obtained by PDE resolution and backtracing (black), or geodesic shooting (blue), for Euler-Mumford (left) and Reeds-Shepp reversible models in 2D (center) or 3D (right).

In favorable cases, geodesic shooting is more precise than the PDE and backtracing approach. However it is also much less general and robust, for the following reasons. (I) Geodesic shooting cannot address the Reeds-Shepp forward and Dubins models, due to their non twice differentiable hamiltonians. (II) It is incompatible with the presence of obstacles, and with non-smooth cost functions α . (III) It lacks guarantees regarding the global optimality of the extracted geodesics, despite their local optimality.

A comparison of geodesic shooting with the proposed approach is presented on Figure 4. A similar experiment was presented in [Mir17] for the Reeds-Shepp reversible model, but not for the Euler-Mumford model.

5.2 Motion planning

Motion planning is a natural field of application for minimal path methods, see for instance [KBKh94], and the different models considered in this paper may account for the maneuverability constraints of a number of vehicles. For instance, the reversible Reeds-Shepp model describes wheelchairs or wheelchair-like robots. The forward only variant is appropriate for vehicles of the same type, but which cannot see behind themselves. Minimal paths w.r.t. the Euler-Mumford elastica model have the advantage of being smooth, and their curvature penalization is physically meaningful. The hard upper bound constraint of the Dubins model on the curvature is relevant for the numerous vehicles subject to a minimum turning radius. See [MD17] for more applications to motion planning of the numerical methods presented in this paper, including two player games where an opponent choses the obstacles.

Our experiments, presented on Figures 7, 8, 9 and 10, show that the numerical schemes introduced in this paper can be used to solve complex motion planning problems, on domains involving numerous walls, in CPU time below 1s on a standard laptop⁷. Within that time, the PDE (7) is numerically solved on the full domain, here discretized on a $90^2 \times 60$ grid, which yields a complete strategy to reach the given target. Larger grid scales yield more accurate paths, at the price of longer computation times (but still quasi-linear in the number of pixels). Memory usage is dominated by the storage of the value function, namely one floating point number per grid point. Once the PDE is solved, extracting a minimal path from an arbitrary point in the

⁷Laptop processor: 2.7GHz Intel®Core i7 using a single core

domain has an almost negligible cost.

The chosen domain for this experiment is $[0, 1]^2 \times \mathbb{S}^1$, the relaxation parameter is $\varepsilon = 0.1$, and various values are considered for ξ , which we recall is homogeneous to a radius of curvature. The different qualitative properties of the four models appear clearly, in particular the cusps of the Reeds-Shepp reversible model minimal paths, the in-place rotations of the Reeds-Shepp forward paths, the smoothness of the Euler-Mumford paths, and the lower-bounded radius of curvature of the Dubins paths.

On the rightmost sub-figures of Figure 10, illustrating the Dubins model, the author acknowledges that two paths fail, in some places, to obey the prescribed lower-bound on the radius of curvature. This is due to the approximate nature of the PDE discretization, and to fact that no path obeying this lower bound exists between these endpoints. These artifacts can easily be eliminated by post-processing.

5.3 Tubular structure segmentation

Minimal path methods are a major tool in image processing [PPKC], in particular for the segmentation of tubular structures in two or three dimensional medical data [BC10, CCM14]. In the case of two dimensional images, the projections of different e.g. blood vessels cross each other, which causes to *shortcuts* or *leakages* in the segmentation. Curvature penalization is a natural tool to address these issues [SBD⁺15].

We present on Figure 2 a synthetic test case for this application. The domain $\bar{\Omega} = [0, 1]^2 \times \mathbb{S}^1$, is discretized on a $73^2 \times 60$ grid. Let us emphasize that the $\mathcal{O}(N \ln N)$ time complexity and $\mathcal{O}(N)$ space complexity of the proposed method makes it suitable for larger problems as well. The cost function $\alpha = \alpha(\mathbf{x}, \theta)$ is set to $\alpha = 1/4$ where \mathbf{x} belongs to the S shaped tubular structure, $\alpha = 1/3$ on the straight one, and $\alpha = 1$ elsewhere. We would like to emphasize that such vessel segmentation results can be considerably improved by choosing cost functions $\alpha = \alpha(\mathbf{x}, \theta)$ depending on both the physical position \mathbf{x} and the orientation θ , see [BC10, SBD⁺15], instead of \mathbf{x} alone as here. Our “inefficient” choice of cost function α is intended to exacerbate the differences between the different models, by making the problem harder.

The PDE (7) is numerically solved, with $u = 0$ at two seed points, shown in blue on Figure 11, and with outflow boundary conditions on $\partial\Omega$. Note that by point we mean an element of $\mathbb{M} = \mathbb{R}^2 \times \mathbb{S}^1$, represented by an arrow on the figures. Minimal paths from two points, shown in red, are backtraced. Ideally, we would like these paths to follow the S tubular structure and end in the leftmost blue point.

The Reeds-Shepp reversible model fails this test, because the minimal paths shift into reverse gear, and thus end at the incorrect blue point. The Reeds-Shepp forward model performs slightly better, ending at the correct endpoint, and correctly extracting the bottom part of the S structure for the larger value of ξ . However the top part of the S structure is not correctly extracted, because the minimal path intended to do so takes a shortcut through the second straight structure, because of its ability to perform in-place rotations. (Again, let us emphasize that the Reeds-Shepp models can be perfectly suitable for tubular structure segmentation, when contrary to this experiment an orientation dependent cost function $\alpha = \alpha(\mathbf{x}, \theta)$ is provided, see [DMMP16].)

The Euler-Mumford model is able to extract the S shaped tubular structure for a large range of parameters ξ , from 0.55 to 1.25. Excessively small values of ξ allow tight turns and therefore shortcuts through the intersecting structure (recall that ξ should be interpreted as a radius of curvature). Excessively large values of ξ make it too costly to follow the S structure, hence the path takes wider turns in the background of the image. We regard the Euler-Mumford model

as the best choice among those considered here for image segmentation tasks, in view of our numerical experiments and of the literature [Mum94].

The Dubins model is also able to extract the S shaped tubular structure, but for a narrower range of parameters ξ than in the Euler-Mumford case, from 0.25 to 0.38. Excessively small or excessively large choices of ξ lead to symptoms, respectively shortcuts and excursions in the image background, similar to those observed in the Euler-Mumford case. We expect the Dubins model to be less efficient than the Euler-Mumford model in practical image segmentation tasks, since it requires a finer tuning of the parameter ξ , matching the curvature of the extracted structures.

Conclusion

In this paper, we introduced numerical PDE methods for solving a family of non-holonomic optimal control problems, associated to the Reeds-Shepp (reversible or forward only), Euler-Mumford and Dubins models. The design and analysis of these methods uses tools from different branches of mathematics, including (i) an original reformulation of the Euler-Mumford hamiltonian, (ii) a convergence analysis in the setting of discontinuous viscosity solutions to HJB PDEs, and (iii) a finite differences scheme based on lattice geometry. The discretized PDEs are solved in a single pass via the dynamic programming principle, which guarantees fast computation times. Synthetic test cases illustrate the potential of these methods in motion planning and image segmentation, and can be reproduced using free and open source codes.

Future works include (i) computing three dimensional⁸ Euler-Mumford and Dubins minimal paths, by solving PDEs on $\mathbb{R}^3 \times \mathbb{S}^2$, and addressing other instances of non-holonomic optimal control problems, (ii) implementing GPU accelerations of the solver, in the spirit of [WDB⁺08], (iii) designing mesh-based, instead of cartesian grid based, discretizations of the HJB PDEs considered in this paper, and (iv) developing practical applications of our globally optimal, curvature penalized minimal paths.

Acknowledgement. The author thanks Da-Chen⁹, Jorg Portegies¹⁰ and Erik Bekkers¹¹, for careful testing, bug-fixing, and feed-back on the numerical codes.

A Local validation of the numerical scheme, via the control sets

We present a local validation of our PDE discretization procedure, by comparing the model control sets (10), see also Figure 2, with some numerical counterparts.

Consider a compact and convex set $\mathcal{B} \subseteq \mathbb{E} = \mathbb{R}^3$, containing the origin, and the corresponding hamiltonian \mathcal{H} . Contrary to the rest of this paper, the potential dependency of \mathcal{B} and \mathcal{H} on some underlying base point $\mathbf{p} \in \mathbb{M}$ is not considered, since the discussion is purely local. Let also H be an approximation of \mathcal{H} , for instance of the form (57). Consider the set

$$B := \{\dot{\mathbf{p}} \in \mathbb{E}; \forall \hat{\mathbf{p}} \in \mathbb{E}^*, H(\hat{\mathbf{p}}) \leq 1/2 \Rightarrow \langle \hat{\mathbf{p}}, \dot{\mathbf{p}} \rangle \leq 1\}, \quad (58)$$

and note that $B = \mathcal{B}$ if $H = \mathcal{H}$. We regard the closeness of B and \mathcal{B} , inspected visually, as a good witness of the closeness of H and \mathcal{H} .

⁸The three dimensional Reeds-Shepp model is already addressed here and in [DMMP16].

⁹Post-Doctoral researcher at University Paris-Dauphine.

¹⁰PhD student under the direction of R. Duits at TU/e University, Eindhoven.

¹¹Post-Doctoral researcher at TU/e University, Eindhoven.

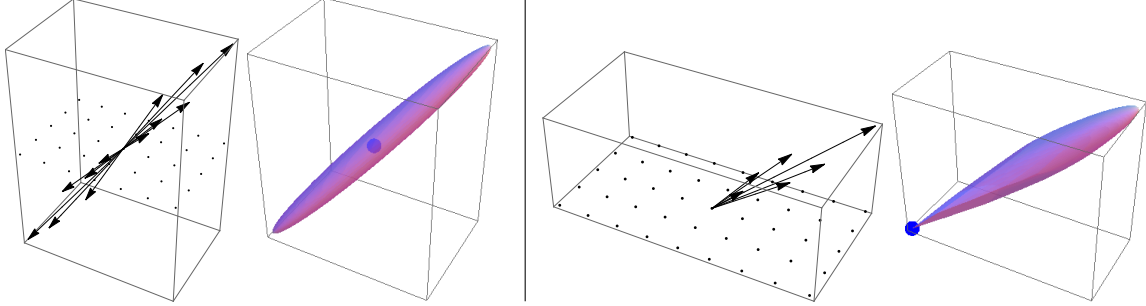


Figure 5: Illustration of §A. Left: Discretization stencil for an quadratic anisotropic hamiltonian. The hamiltonian and control set representation are exact. Right: Discretization stencil of Proposition 1.1, for a hamiltonian $\mathcal{H}(\hat{\mathbf{p}}) = \frac{1}{2}\langle \hat{\mathbf{p}}, \hat{\mathbf{n}} \rangle_+^2$. The approximate control set (58) is close to the segment $[0, \hat{\mathbf{n}}]$, but slightly fatter.

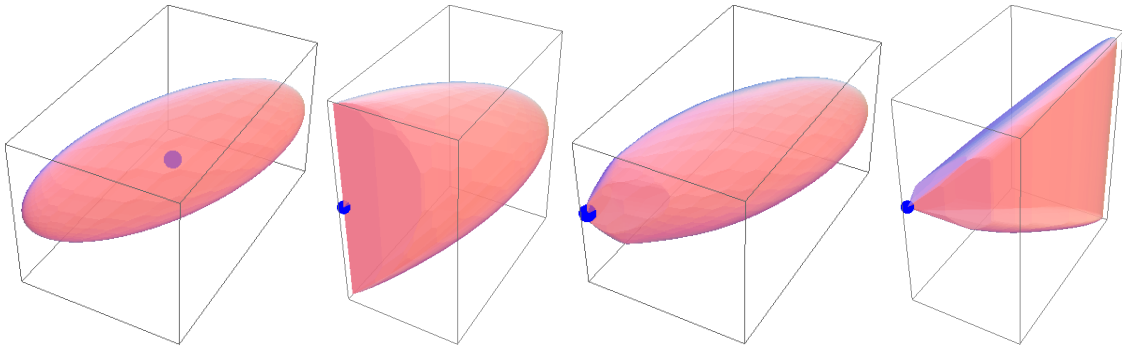


Figure 6: Approximate control set (58) for the Reeds-Shepp reversible, Reeds-Shepp forward, Euler-Mumford and Dubins models. The shapes of the original control sets, see Figure 2 are recognizable, elongated due to the model parameter choice $\xi = 0.2$, and slightly fatter due to the effect of discretization, with relaxation parameter $\varepsilon = 0.1$. Orientation $\theta = \pi/3$. See Figure 3 for the corresponding stencils.

On Figure 5, left, is illustrated the case where \mathcal{B} is an ellipsoid, with principal axes of length $(1, 0.1, 0.1)$. In that case \mathcal{H} is a quadratic function, and the discrete representation using Corollary 4.13 is exact. One therefore has $H = \mathcal{H}$, thus $B = \mathcal{B}$ as can be observed. This particular case is at the foundation of [Mir17].

On figure 5, right, is illustrated the case where $\mathcal{B} = [0, \hat{\mathbf{n}}]$ is a segment, where $\hat{\mathbf{n}} \in \mathbb{E}$ is a unit vector, and therefore $\mathcal{H}(\hat{\mathbf{p}}) = \frac{1}{2}\langle \hat{\mathbf{p}}, \hat{\mathbf{n}} \rangle_+^2$. The discretization is performed using Proposition 1.1 with $\varepsilon = 0.1$, via the basis reduction techniques presented in §4. As can be observed, the vectors $\hat{\mathbf{e}}_k$, $1 \leq k \leq K$, are almost aligned with $\hat{\mathbf{n}}$, and the set B is close to the segment \mathcal{B} in the Hausdorff distance, although slightly fatter.

Figure 6 is devoted to the models of interest in this paper. The parameters are $\xi = 0.2$ (appearing in the curvature cost (2)), $\theta = \pi/3$ (the current orientation), and $\varepsilon = 0.1$ (tolerance in Proposition 1.1). The offsets $\hat{\mathbf{e}}_k$, $1 \leq k \leq K$, are illustrated on Figure 3 page 7. Comparing with Figure 2, we can confirm that the sets B are close to the corresponding ellipse¹², half ellipse, non-centered ellipse, and triangle \mathcal{B} respectively. However the true control sets \mathcal{B} are flat, with Hausdorff dimension 2, whereas their counterparts B are slightly fatter.

¹²The choice $\xi = 1$ in Figure 2, versus $\xi = 0.2$ in Figure 6, yields a round disk instead of an ellipse

B Convexity of the metric

We prove in this appendix that the metrics $\mathcal{F}_{\mathbf{p}}^{\text{RS}+}, \mathcal{F}_{\mathbf{p}}^{\text{EM}}, \mathcal{F}_{\mathbf{p}}^{\text{D}} : \mathbb{E} \rightarrow [0, \infty]$ are convex, for any fixed $\mathbf{p} \in \Omega$, due their construction (3) and to the following two results.

Lemma B.1. *Let $\mathcal{C} : \mathbb{R} \rightarrow [1, \infty]$ be convex and lower semi-continuous, and let $f :]0, \infty[\times \mathbb{R} \rightarrow [0, \infty]$ be defined by $f(n, t) := n\mathcal{C}(t/n)$. Then f is lower semi-continuous, 1-positively homogeneous, everywhere positive, and obeys the triangular inequality.*

Proof. Lower semi-continuity, homogeneity and positivity are obvious. In addition for any $(n, t), (n', t') \in]0, \infty[\times \mathbb{R}$ one obtains

$$\frac{f(n + n', t + t')}{n + n'} = \mathcal{C} \left(\frac{t}{n} \frac{n}{n + n'} + \frac{t'}{n'} \frac{n'}{n + n'} \right) \leq \frac{n}{n + n'} \mathcal{C} \left(\frac{t}{n} \right) + \frac{n'}{n + n'} \mathcal{C} \left(\frac{t'}{n'} \right) = \frac{f(n, t) + f(n', t')}{n + n'}. \quad \square$$

Note that 1-positive homogeneity and the triangular inequality together imply convexity. We recall the notation $\mathbb{E} := \mathbb{R}^2 \times \mathbb{R}$, used in the next result.

Corollary B.2. *Let $\mathcal{C} : \mathbb{R} \rightarrow [1, \infty]$ be convex, lower semi-continuous, and such that $l(\varepsilon) := \lim \mathcal{C}(\varepsilon t)/t$ as $t \rightarrow \infty$ exists and belongs to $]0, \infty]$, for each $\varepsilon \in \{-1, 1\}$. Let $F : \mathbb{E} \rightarrow [0, \infty]$ be defined as $F(\dot{\mathbf{x}}, \dot{\theta}) := \|\dot{\mathbf{x}}\| \mathcal{C}(\dot{\theta}/\|\dot{\mathbf{x}}\|)$ for each $(\dot{\mathbf{x}}, \dot{\theta}) \in \mathbb{E}$ such that $\dot{\mathbf{x}} = \|\dot{\mathbf{x}}\| \mathbf{n}$ and $\|\dot{\mathbf{x}}\| > 0$, where $\mathbf{n} \in \mathbb{S}^{d-1}$ is a fixed direction. Let also $F(0, 0) = 0$, $F(0, \dot{\theta}) = |\dot{\theta}| l(\dot{\theta}/|\dot{\theta}|)$ if $\dot{\theta} \neq 0$, and $F(\dot{\mathbf{x}}, \dot{\theta}) := +\infty$ otherwise. Then F is lower semi-continuous and obeys*

- (1-positive homogeneity) $F(\lambda \dot{\mathbf{p}}) = \lambda F(\dot{\mathbf{p}})$, for all $\lambda > 0$ and all $\dot{\mathbf{p}} \in \mathbb{E}$.
- (Separation) $F(\dot{\mathbf{p}}) = 0$ iff $\dot{\mathbf{p}} = 0$, for all $\dot{\mathbf{p}} \in \mathbb{E}$.
- (Triangular inequality) $F(\dot{\mathbf{p}} + \dot{\mathbf{q}}) \leq F(\dot{\mathbf{p}}) + F(\dot{\mathbf{q}})$, for all $\dot{\mathbf{p}}, \dot{\mathbf{q}} \in \mathbb{E}$.

Proof. By the previous lemma, F obeys the announced properties on the convex set $]0, \infty[\mathbf{n}] \times \mathbb{R}$. These properties are also satisfied on the closure $([0, \infty[\mathbf{n}] \times \mathbb{R}$ since, clearly, F is extended to it by its lower continuous envelope, and since the limits $l(1)$ and $l(-1)$ are positive (for separation). Finally the announced properties hold for the trivial extension of F to $\mathbb{R}^2 \times \mathbb{R}$ by $+\infty$ since the subset $([0, \infty[\mathbf{n}] \times \mathbb{R}$ is closed and convex. \square

References

- [BC10] Fethallah Benmansour and Laurent D. Cohen. Tubular Structure Segmentation Based on Minimal Path Method and Anisotropic Enhancement. *International Journal of Computer Vision*, 92(2):192–210, March 2010.
- [BCD97] M Bardi and I Capuzzo-Dolcetta. Optimal control and viscosity solutions of Hamilton-Jacobi-Bellman equations. Birkhauser, 1997.
- [BCL94] Jean-Daniel Boissonnat, André Cérézo, and Juliette Leblond. Shortest paths of bounded curvature in the plane. *Journal of Intelligent and Robotic Systems*, 11(1-2):5–20, 1994.
- [BCM15] Jean-David Benamou, Francis Collino, and Jean-Marie Mirebeau. Monotone and Consistent discretization of the Monge-Ampere operator. *Mathematics of computation*, September 2015.

- [BCPS10] F Benmansour, G Carlier, G Peyré, and F Santambrogio. Derivatives with respect to metrics and applications: subgradient marching algorithm. *Numerische Mathematik*, 116(3):357–381, May 2010.
- [BE84] M Bardi and L C Evans. On Hopf’s formulas for solutions of Hamilton-Jacobi equations. *Nonlinear Analysis. Theory, Methods and Applications. An International Multidisciplinary Journal. Series A: Theory and Methods*, 8(11):1373–1381, 1984.
- [BK10] Jean-Benoît Bost and Klaus Künnemann. Hermitian vector bundles and extension groups on arithmetic schemes. I. Geometry of numbers. *Advances in Mathematics*, 223(3):987–1106, February 2010.
- [BOZ04] J Frederic Bonnans, Elisabeth Ottenwaelter, and Hasnaa Zidani. A fast algorithm for the two dimensional HJB equation of stochastic control. Technical report, 2004.
- [BR06] Folkmar Bornemann and Christian Rasch. Finite-element Discretization of Static Hamilton-Jacobi Equations based on a Local Variational Principle. *Computing and Visualization in Science*, 9(2):57–69, June 2006.
- [CCM14] Da Chen, Laurent D. Cohen, and Jean-Marie Mirebeau. Vessel Extraction Using Anisotropic Minimal Paths and Path Score. In *IEEE International Conference on Image Processing (ICIP 2014)*, paris, France, 2014. IEEE.
- [CMC15] D Chen, Jean-Marie Mirebeau, and L D Cohen. Global Minimum for Curvature Penalized Minimal Path Method. *BMVC*, 2015.
- [CMC16] Da Chen, Jean-Marie Mirebeau, and Laurent D. Cohen. A New Finsler Minimal Path Model With Curvature Penalization for Image Segmentation and Closed Contour Detection. *Computer Vision and Pattern Recognition (CVPR)*, pages 355–363, June 2016.
- [CS92] J H Conway and N J A Sloane. Low-Dimensional Lattices. VI. Voronoi Reduction of Three-Dimensional Lattices. *Proceedings of the Royal Society A: Mathematical, Physical and Engineering Sciences*, 436(1896):55–68, January 1992.
- [DMMP16] Remco Duits, Stephan P L Meesters, Jean-Marie Mirebeau, and Jorg M Portegies. Optimal Paths for Variants of the 2D and 3D Reeds-Shepp Car with Applications in Image Analysis. *arXiv.org*, December 2016.
- [Dub57] L E Dubins. On curves of minimal length with a constraint on average curvature, and with prescribed initial and terminal positions and tangents. *American Journal of Mathematics*, 79:497–516, 1957.
- [Eul44] L Euler. Methodus inveniendi Lineas curvas maximi minive proprietate gaudentes. *Lausanne/Geneva: Bousquet*, 1744.
- [Féj33] L Féjer. On the infinite sequences arising in the theories of harmonic analysis, of interpolation, and of mechanical quadratures. *Bulletin of the American Mathematical Society*, 1933.
- [FM13] Jérôme Fehrenbach and Jean-Marie Mirebeau. Sparse Non-negative Stencils for Anisotropic Diffusion. *Journal of Mathematical Imaging and Vision*, pages 1–25, 2013.

- [KBKh94] Ron Kimmel, Alfred M Bruckstein, Nahum Kiryati, and Tekhniyon Makhon tekhnologi le-Yisra'el Fakultah le-handasat hashmal. Multi-valued Distance Maps for Motion Planning on Surfaces with Moving Obstacles, 1994.
- [LRr13] Wei Liao, Karl Rohr, and Stefan W o rz. Globally Optimal Curvature-Regularized Fast Marching For Vessel Segmentation. *Medical Image Computing and Computer-Assisted Intervention-MICCAI 2013. Springer Berlin Heidelberg.*, pages 550–557, 2013.
- [MD17] Jean-Marie Mirebeau and Johann Dreo. Automatic differentiation of non-holonomic fast marching for computing most threatening trajectories under sensors surveillance. *arXiv.org*, April 2017.
- [Mir13] Jean-Marie Mirebeau. Efficient fast marching with Finsler metrics. *Numerische Mathematik*, pages 1–43, 2013.
- [Mir16] Jean-Marie Mirebeau. Minimal stencils for discretizations of anisotropic PDEs preserving causality or the maximum principle. *SIAM Journal on Numerical Analysis*, 54(3):1582–1611, 2016.
- [Mir17] Jean-Marie Mirebeau. Anisotropic fast-marching on cartesian grids using Voronoi's first reduction of quadratic forms. April 2017.
- [Mon06] Richard Montgomery. *A Tour of Subriemannian Geometries, Their Geodesics and Applications*. American Mathematical Soc., August 2006.
- [Mum94] David Mumford. *Elastica and Computer Vision*. pages 491–506. Springer New York, New York, NY, 1994.
- [Ngu04] P Nguyen. Low-dimensional lattice basis reduction revisited. *Algorithmic Number Theory*, 2004.
- [Obe06] A M Oberman. Convergent Difference Schemes for Degenerate Elliptic and Parabolic Equations: Hamilton–Jacobi Equations and Free Boundary Problems. *SIAM Journal on Numerical Analysis*, 44(2):879–895, January 2006.
- [PPKC] Gabriel Peyré, Mickael Péchaud, Renaud Keriven, and Laurent D. Cohen. *Geodesic Methods in Computer Vision and Graphics*.
- [Ran41] Gunnar Randers. On an Asymmetrical Metric in the Four-Space of General Relativity. *Physical Review*, 59(2):195–199, January 1941.
- [RS90] J A Reeds and L A Shepp. Optimal paths for a car that goes both forwards and backwards. *Pacific Journal of Mathematics*, 145(2):367–393, 1990.
- [RT92] Elisabeth Rouy and Agnès Tourin. A Viscosity Solutions Approach to Shape-From-Shading. *SIAM Journal on Numerical Analysis*, 29(3):867–884, July 1992.
- [SBD⁺15] Gonzalo Sanguinetti, Erik Bekkers, Remco Duits, Michiel H J Janssen, Alexey Mashtakov, and Jean-Marie Mirebeau. Sub-Riemannian fast marching in SE(2). In *Progress in Pattern Recognition, Image Analysis, Computer Vision, and Applications*, pages 366–374. Springer, Cham, Cham, 2015.

- [Sch09] A Schürmann. Computational geometry of positive definite quadratic forms. *University Lecture Series*, 2009.
- [Sel74] Eduard Selling. Ueber die binären und ternären quadratischen Formen. *Journal für die Reine und Angewandte Mathematik*, 77:143–229, 1874.
- [SUKG13] Petter Strandmark, Johannes Ulen, Fredrik Kahl, and Leo Grady. Shortest Paths with Curvature and Torsion. In *2013 IEEE International Conference on Computer Vision (ICCV)*, pages 2024–2031. IEEE, 2013.
- [Tsi95] J.N. Tsitsiklis. Efficient algorithms for globally optimal trajectories. 40(9):1528–1538, September 1995.
- [WDB⁺08] Ofir Weber, Yohai S Devir, Alexander M Bronstein, Michael M Bronstein, and Ron Kimmel. Parallel algorithms for approximation of distance maps on parametric surfaces. *ACM Transactions on Graphics (TOG)*, 27(4):104–16, October 2008.

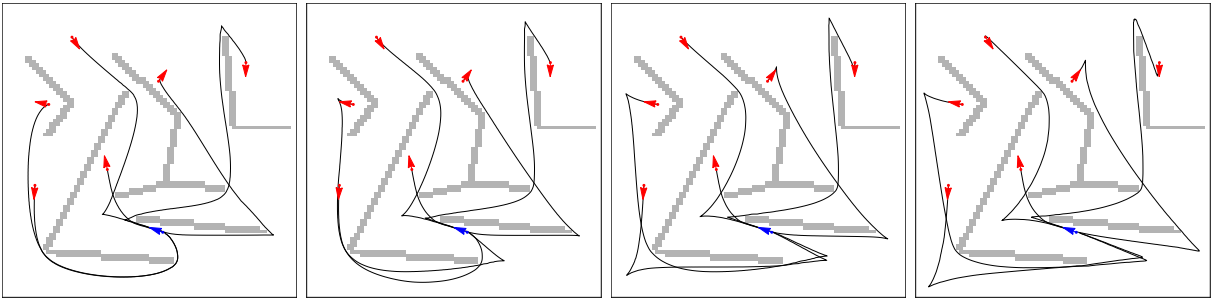


Figure 7: Reeds Shepp reversible model, $\xi \in \{0.1, 0.2, 0.4, 0.8\}$. $\varepsilon = 0.1$, CPU time $\approx 0.3s$

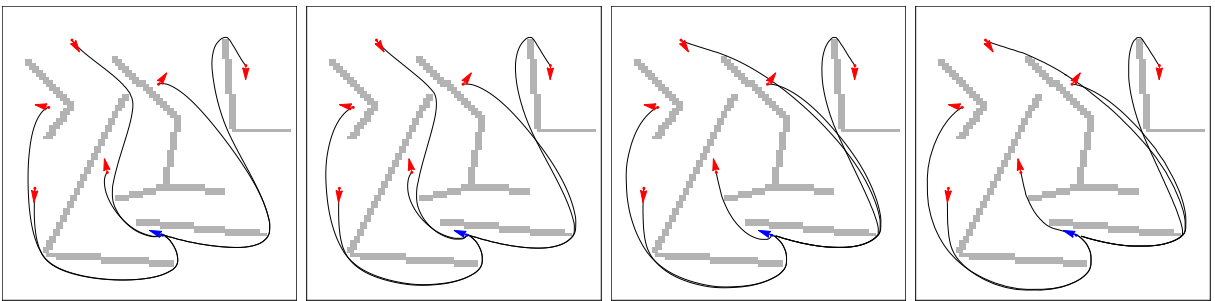


Figure 8: Reeds Shepp forward model, $\xi \in \{0.1, 0.2, 0.4, 0.8\}$. $\varepsilon = 0.1$, CPU time $\approx 0.2s$

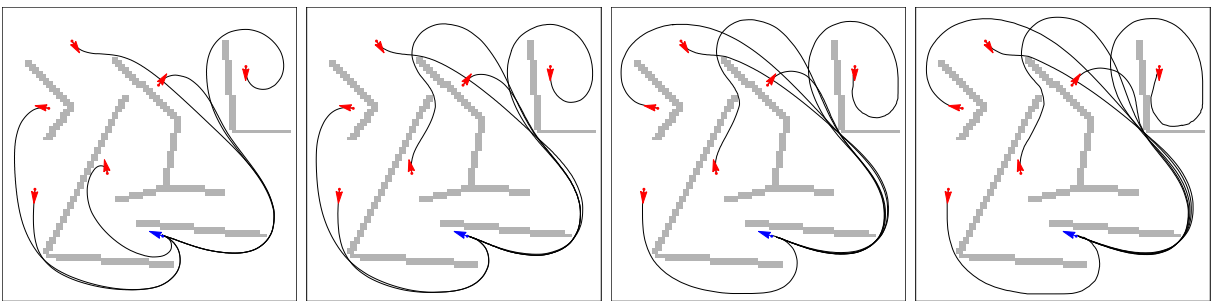


Figure 9: Euler-Mumford elastica, $\xi \in \{0.1, 0.2, 0.3, 0.4\}$. $\varepsilon = 0.1$, $K = 5$, CPU time $\approx 1.2s$

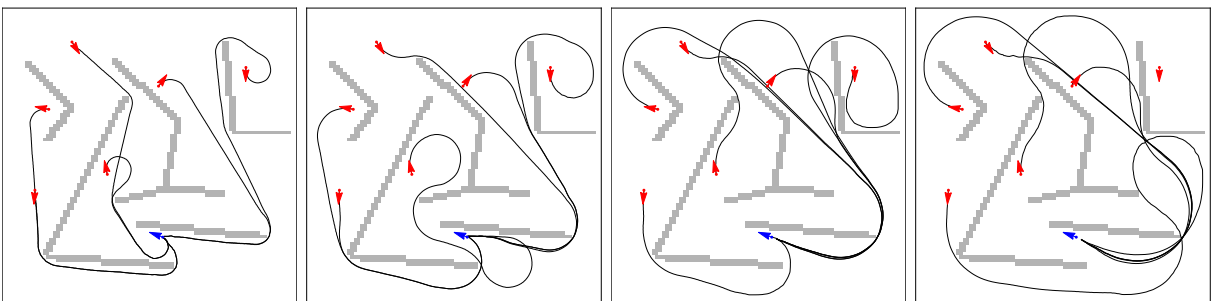


Figure 10: Dubins model, $\xi \in \{0.05, 0.1, 0.15, 0.2\}$. $\varepsilon = 0.1$, CPU time $\approx 0.6s$

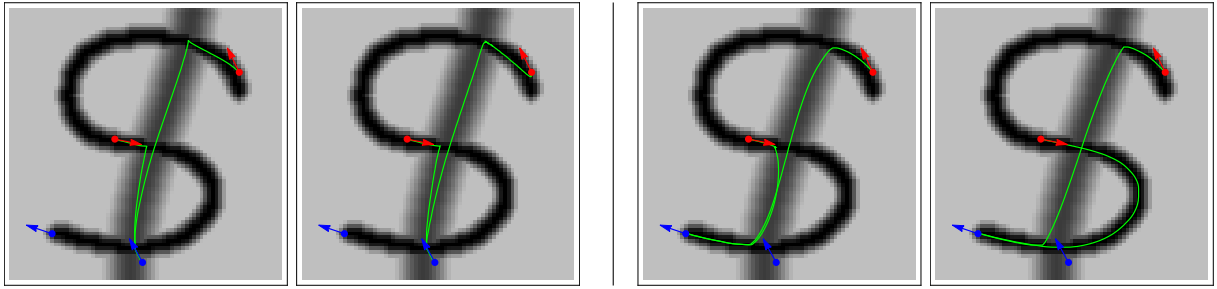


Figure 11: Tubular segmentation test with the Reeds-Shepp models, reversible (left), and forward (right). First image $\xi = 0.2$, second $\xi = 0.8$. This segmentation test is mostly “failed”, on purpose, for different reasons, see §5.3. CPU time $\approx 0.3s$.

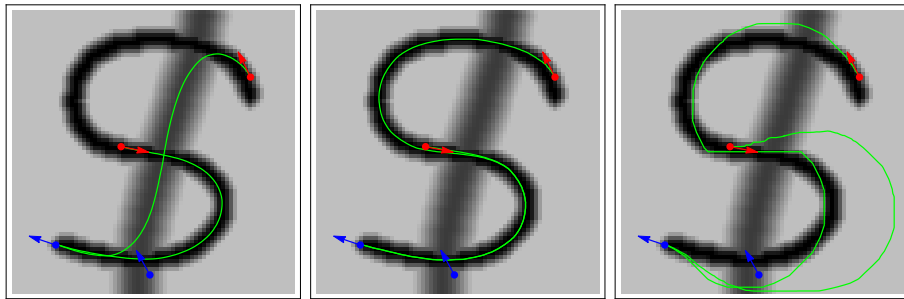


Figure 12: Tubular segmentation using Euler-Mumford elasticas. Curvature penalization is left: insufficient ($\xi = 0.2$), middle: adequate ($\xi = 0.6$), right: exaggerate ($\xi = 1.5$). CPU time $\approx 1.2s$.

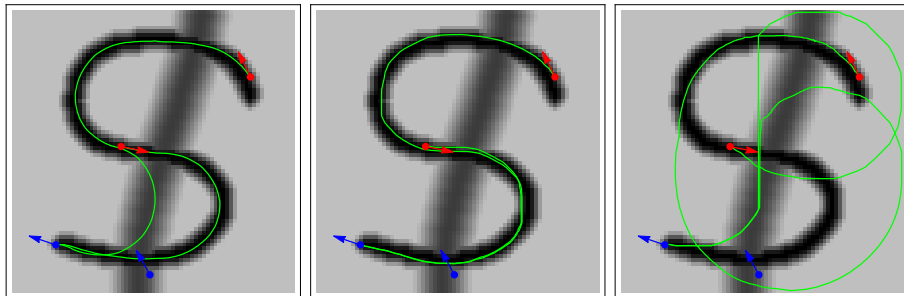


Figure 13: Tubular segmentation using the Dubins model. Curvature penalization is left: insufficient ($\xi = 0.2$), middle: adequate ($\xi = 0.35$), right: exaggerate ($\xi = 0.5$). CPU : $\approx 0.5s$.

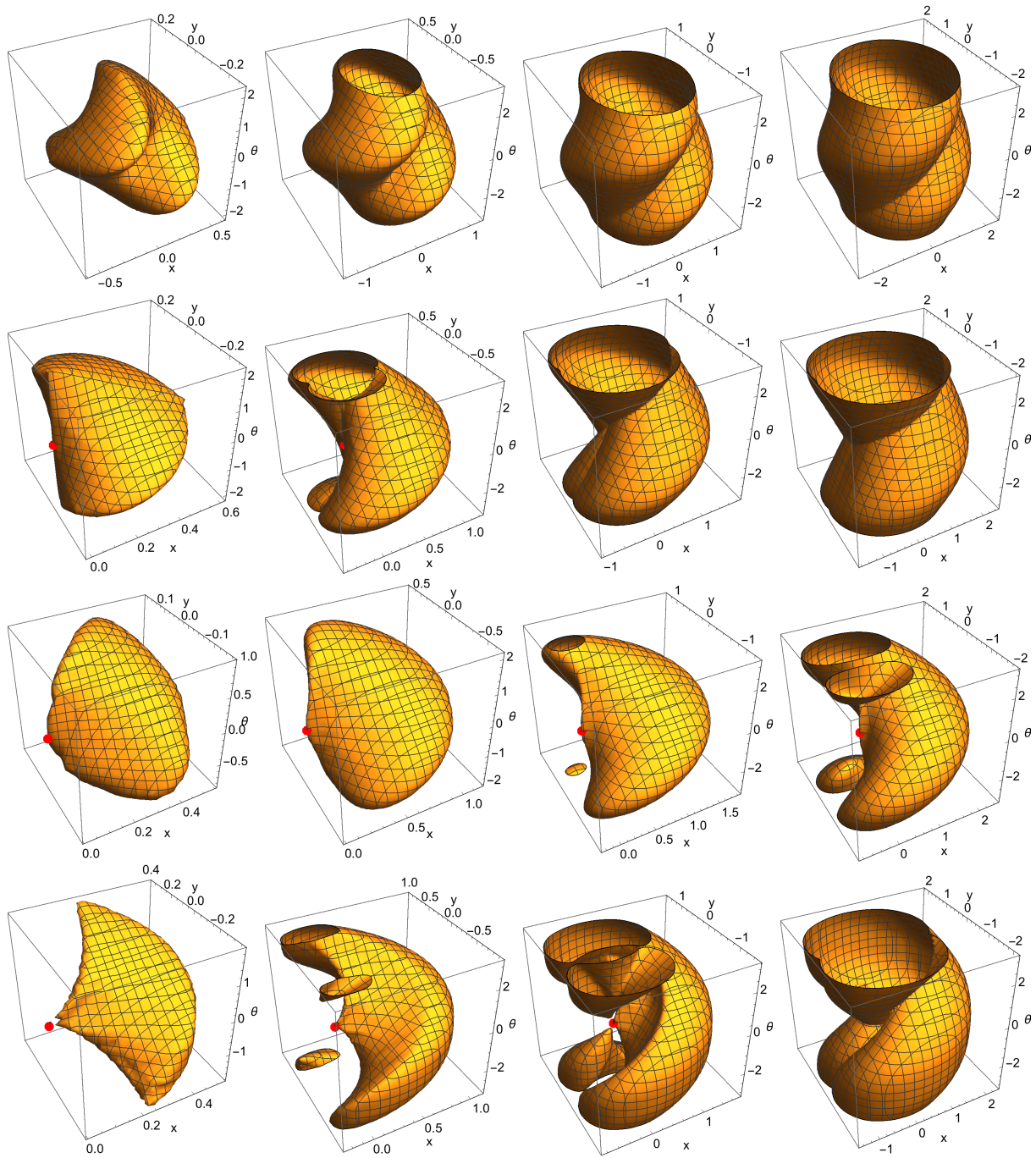


Figure 14: Level sets, $\xi = 0.14$, at time 0.3, 0.6, 0.9, 1.2. Origin shown as red point.